Doctoral Dissertation

EXPLORATION OF MOBILE ROBOTS FOR MULTIPLE RADIATION SOURCE ESTIMATION

Nantawat Pinkam

Supervisor: Professor Chong Nak-Young

School of Information Science
Japan Advanced Institute of Science and Technology

September 2020

Abstract

In this work, we consider the localization problem of multiple unknown radiation sources with measurement uncertainty by using robotic systems in a geometric environment. The goal is to give an accurate map of radiation which contains a number of sources, locations, and intensities. Furthermore, the exploration cost must be minimized. We proposed the scheme for the localization of multiple radioactive sources using the particle filter. In a normal circumstance, a robot will estimate the source location by pursuing the intensive intensity site. However, a low radiation area has little information which makes an unpredictable estimation. Thus, an exploration algorithm must be utilized. In consequence, the exploration cost must be minimized because the exploration time might be restricted. We propose the exploration method using frontier-based exploration which involves the target point selection algorithm by considering the minimum distance from a robot to an unexplored region, and the increasing gradient direction. In addition, the area pruning algorithm is introduced to further decrease the exploration time by overlooking less important areas and applying Bayesian estimation to further eliminate the potentially no source area. After every source is discovered, we proposed the sources intensity separation algorithm to further raise the estimation accuracy. The proposed method has been verified by the simulations using MATLAB in both ideal environment and SLAM dataset of a real building. In addition, the uncertainty in the robot self-localization was introduced and experimented. The effect of environment attenuation that decreases the radiation measurement is also investigated and the robot is successfully localized the radiation source inside a single entrance room. The proposed strategy can incredibly decrease the exploration cost compared to the regular techniques and increment the accuracy of multiple sources localization.

Keywords: Bayes' theorem, source localization, information theory, exploration and path planning, mobile robot

Acknowledgment

The author would like to thank my supervisor, Professor Chong Nak-Young who guides me through the research, for the continuous support of my Ph.D. study and related research, for his patience, motivation, and immense knowledge. His guidance helped me in all the time of research and writing of this thesis. I could not have imagined having a better advisor and mentor for my Ph.D. study.

Besides my advisor, I would like to thank the rest of my thesis committee: Prof. Nguyen Le Minh, Assoc. Prof. Ikeda Kokolo, Prof. Capi Genci, and, Assoc. Prof. Lee Geunho, for their insightful comments and encouragement, but also for the hard questions which incented me to widen my research from various perspectives.

I am highly indebted of Ministry of Education, Culture, Sport, Science and Technology, for the financial support thourgh MEXT scholarship. Lastly, I would like to thank my family and friends who always give me a support when I need.

List of Figures

List of Tables

Contents

Chapter 1

Introduction

The environmental hazard is an important threat where chemical substance damages the environment, which has an unfavorable effect on living organisms. One of the causes that contaminate surroundings is radioactive material leakage, which is an increasing concern in national security [5, 6]. This emerging threat can be either induced by a malicious attack or accidental release of radioactive material. Thus, the radiation source estimation can be a valuable tool in order to plan a counter-measure to the problem, including saving human life and clean up the leakage material [7, 8].

Nowadays, the existing technologies in radiation detection mainly operate manually or stationary [9,10]. The first method is to use human as an explorer by manually waving the radiation detection device in the possible area of radioactive leakage [11]. In this method, the gathered information may not provide the complete visual or statistic data map. In the worst case, the operators may be exposed to the radiation themselves, which can later cause a serious radiation sickness [12]. Another method to detect the radioactive material is to use a stationary portal monitor. This method is mainly used in the port to scan the shipping container or cargo. The drawback of this method is the lack of mobility.

Autonomous robotic systems have become increasingly interested by researchers around the world [13]. The replacement of human force to perform dangerous task such as nuclear radiation detection is the advantage of the robotic systems. In addition, the mobility given by robots can surpass human in the process of data gathering in an inaccessible area by human. Moreover, robots can work together as a team to quickly accomplish the task objective with either centralized or decentralized way. Thus, using robots in the task of radiation intensity mapping is a better choice.

This thesis is divided into 6 chapters. Chapter 1 consists of the introduction. Chapter 2 is the literature review. Next, chapter 3 explains the recursive bayesian estimation and particle filter. Chapter 4 talks about the exploration algorithms for robots. Chapter 5 shows the experimentation and analysis of this research. Lastly, chapter 6 is the conclusion of all works.

1.1 Problem Statement

The main problem of exploration in the radiation field is the measurement uncertainty [14–16]. Each sensor measurement of the robot at the same position does not guarantee to have the same value. In a particular case, it is based on Poisson distribution. The particle filter is one of the tools that give flexibility over the non-linear system. One way to navigate through the exploration field to locate the radiation source is to follow the estimated source location of the particle filter [17,18]. However, that does not guarantee to be the optimum path, or the result may be a failure in the worst case due to the distance between the robot and the source. If the location of the robot is far away from the source or in low radiation area, the particle filter does not guarantee to give an accurate result due to lack of information. This work proposed the method for both exploration and multiple sources localization using robotic systems. The minimum cost in exploration can be achieved by moving a robot to the appropriate position. We proposed the algorithm for selecting the next best position by considering several conditions, such as, the minimum distance from the current position of the robot to the available target position and the largest gradient direction. Furthermore, the area pruning algorithms are employed to decrease the exploration cost by avoiding the possibly low intensity area using recursive Bayesian estimation pruning and low priority flag. In addition, for single source case, information gain based exploration has been investigated. The robot will use the information gain-based exploration, which can calculate the best possible action for the robot by using the particles information (weight, intensity, and location). Finally, after the sources localization is finished, unknown sources intensity separation algorithm will be applied to further increase the measurement accuracy.

Chapter 2

Literature Review

2.1 Basic Knowledge of Radioactivity

Radioactivity is a process of an unstable atom emits ionization radiation. The atom loses a nucleus in the process. Radioactivity is also known as radiation decay, or nuclear decay. The material which emits radiation is consider a radioactive [19–21].

2.1.1 Type of Radiation

The types of energy that emit from an unstable atom are alpha particle (α), beta particle (β), and gamma ray (γ). Fig. 2.1 shows those particles and their penetration properties.

2.1.1.1 Alpha Particle

Alpha particle is the weakest type of radiation. It consists of two neutrons and two protons which weight about 8,000 times of an electron. It can be shielded by a piece of paper which means it is completely harmless to human when a body get exposed. However, it is only harmful when it is inside the body.

2.1.1.2 Beta Particle

Beta particle is an electron particle which has very light weight around 1/2000 the mass of single proton or neutron. It can be shielded by a wall of wood or aluminium. It is able to penetrate the human skin a little which is not harmful to human in a small dose.

2.1.1.3 Gamma Ray

Gamma ray is the third kind of radiation which is not particle. It is a high energy form of light which has no mass. It has high penetration property

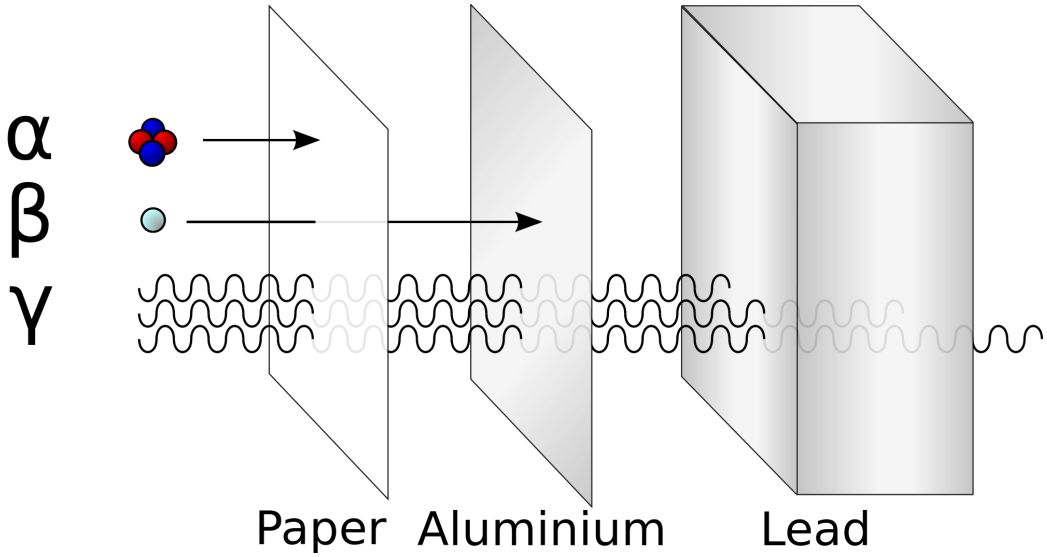

Figure 2.1: Alpha particle (α), beta particle (β), and gamma ray (γ) with their penetration properties [1].

which mean it can penetrate through almost everything including human body. However, it can be blocked by a thick wall of lead. It is very hazard to living organisms [22].

2.1.2 Radioactivity Measurement

The most common radioactivity measurement is a Geiger counter. It consists of a metallic tube which is filled with a gas. Fig. 2.2 shows how a Geiger counter works. When the device is exposed to the radiation, The atom inside the tube will be ionized by the radiation. The negatively charged electrons (blue particle) are attracted the positively charged anode (red wire) while the positively charged protons (red particle) are attracted to the side of the tube which is a negatively charged cathode (blue wall). A Geiger counter will count the electron that passed the anode wire. The unit of a Geiger counter is count per second (count/s) [22].

2.1.3 Radiation Model

The radiation reading from a measurement device follows the inverse square relationship. The intensity of the radiation source is inversely proportional to the distance relatively to the instrument according to the following equation

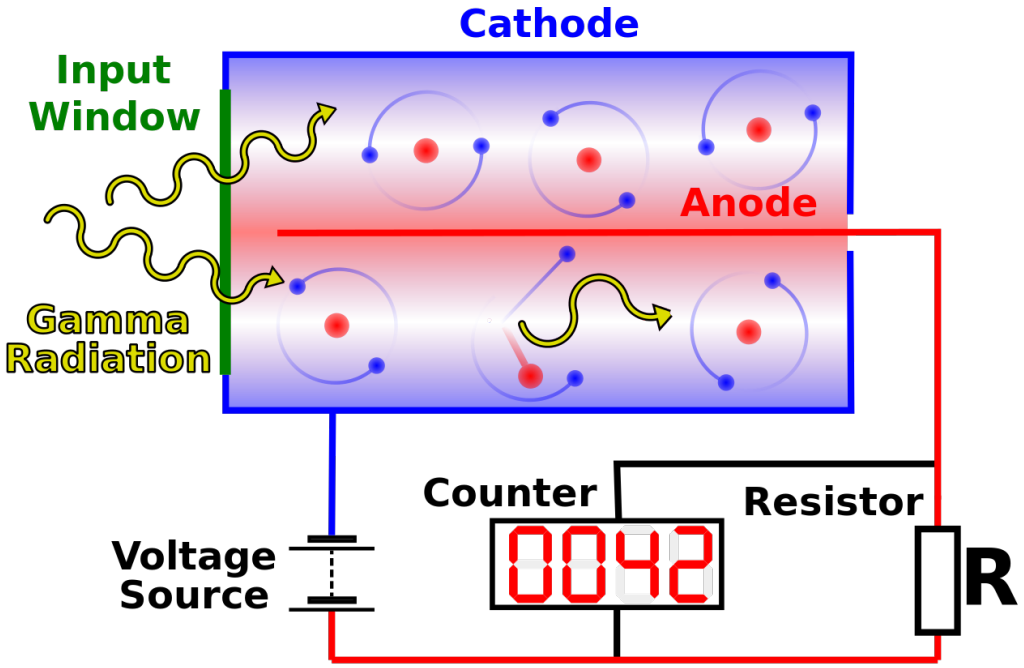

Figure 2.2: The operation inside a Geiger counter [2].

[23]:

$$\lambda_k = \frac{I}{(x_k - x_0)^2 + (y_k - y_0)^2 + (z_k - z_0)^2} + \lambda_b \tag{2.1}$$

where λ_k is the intensity at the measurement device. I is the intensity of the source, (x_k, y_k, z_k) is the position of the measurement device, (x_0, y_0, z_0) is the position of the source, and λ_b is the background intensity at the measurement point. In our case, we use a ground mobile robot and we assume that the intensity source is on the ground. Therefore, the altitudes z_k, z_0 are zero. However, from the experiment, if the robot moves closer to the source point, the reading becomes near infinity because the different between (x_k, y_k) and (x_0, y_0) is near zero. To solve this problem, we set the altitude different z to be 1. The new equation is as follow:

$$\lambda_k = \frac{I}{(x_k - x_0)^2 + (y_k - y_0)^2 + 1} + \lambda_b \tag{2.2}$$

The example plot of the radiation using Eq. 2.2 is shown in Fig. 2.3. For multiple sources case, since there are two or more sources, the intensity model

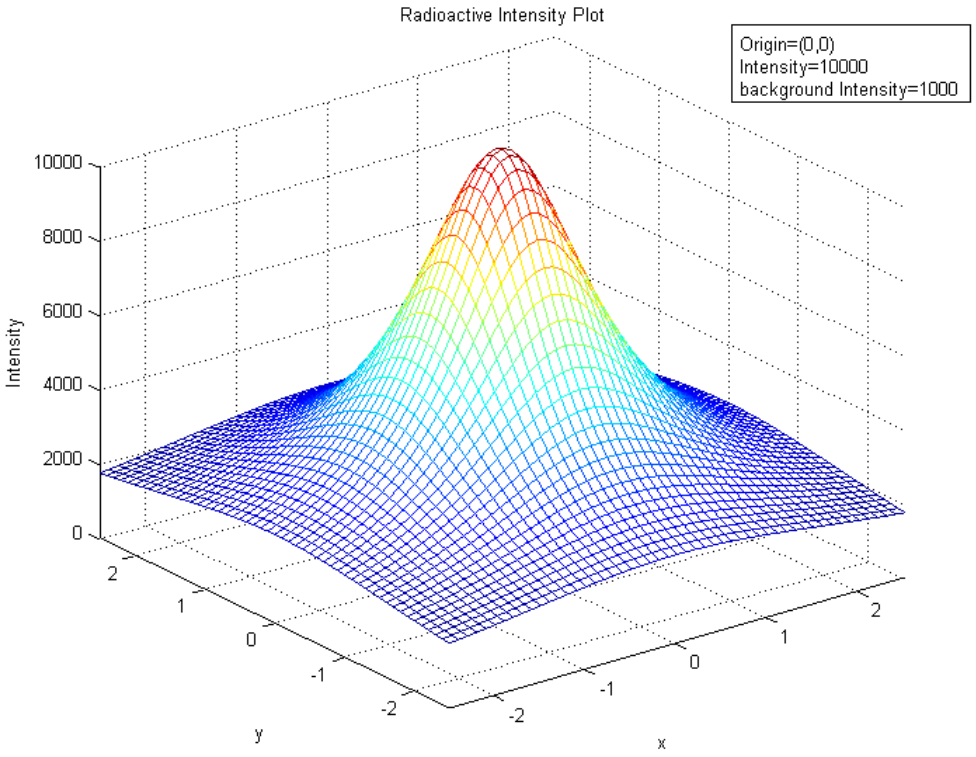

Figure 2.3: The example plot of the radiation of the source intensity of 10,000 at the location (0,0). The background intensity is set to 1,000.

equation (Eq. 2.2) cannot be applied to map the source. In this case, we adopt the new intensity model by combining every sources using the following equation:

$$\lambda_k = \left\{ \sum_{i=1}^{\mathcal{M}} \frac{I_i}{(x_k - x_i)^2 + (y_k - y_i)^2 + 1} \right\} + \lambda_b \tag{2.3}$$

where λ_k is the k^{th} measurement at (x_k, y_k). $\mathcal{M}$ is the maximum number of the source. I_i is the i^{th} intensity at (x_i, y_i). λ_b is the background radiation. The example plot of the radiation using Eq. 2.3 is shown in Fig. 2.4. However, each decay event of radioactive is random, independent and occurs at a fixed mean rate λ. [24] describes the model of radioactive decay using Poisson statistics as the following equation:

$$f(k, \lambda) = \frac{\lambda^k e^{-\lambda}}{k!} \tag{2.4}$$

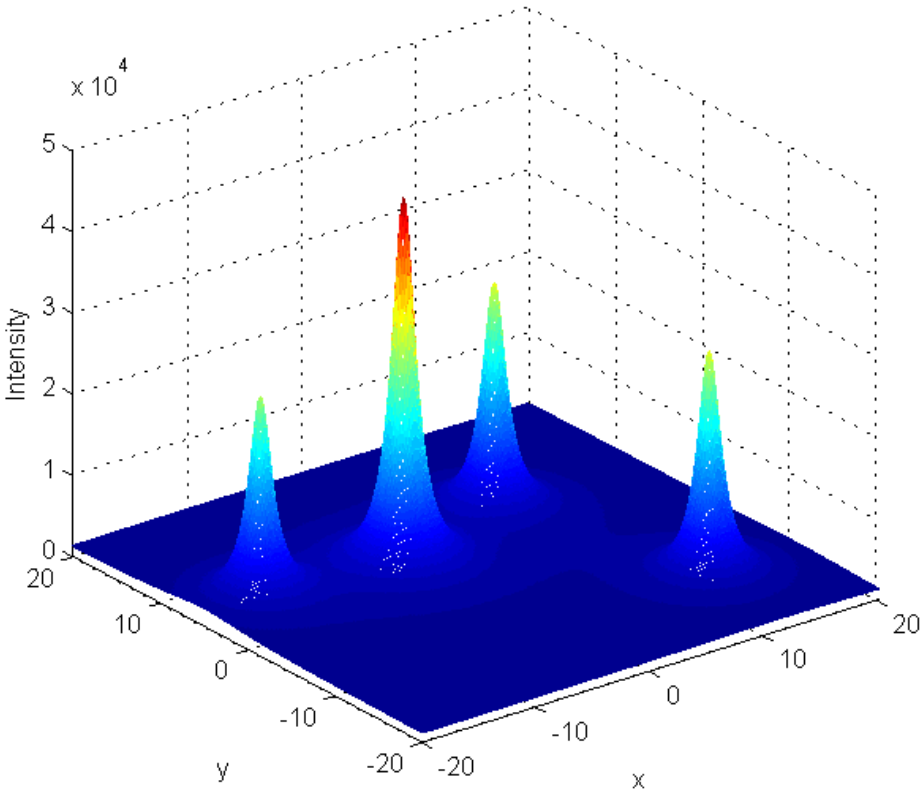

Figure 2.4: The example plot of the radiation of 4 sources with random intensities. The background intensity is set to 1,000.

where $\lambda = I$ is the average number of count for that period of time. k is the exact measurement reading from the source. Gaussian distribution can be used to approximate Poisson distribution when λ becomes large (with $\lambda = \mu = \sigma^2$). Fig. 2.5 shows the uncertainty of measurement vary with distances and graph fitting using Poisson and Gaussian distribution.

We assume that the radiation detector attached to the robot location (x_k, y_k) is uniformly directional response and neglect the air attenuation. The measurement by a robot is independently distributed and the exposure time τ of all measurement is constant. The radioactive are separable point sources and have a finite number of points in a known geometric area without obstacle. However, the number of sources is unknown by the robot.

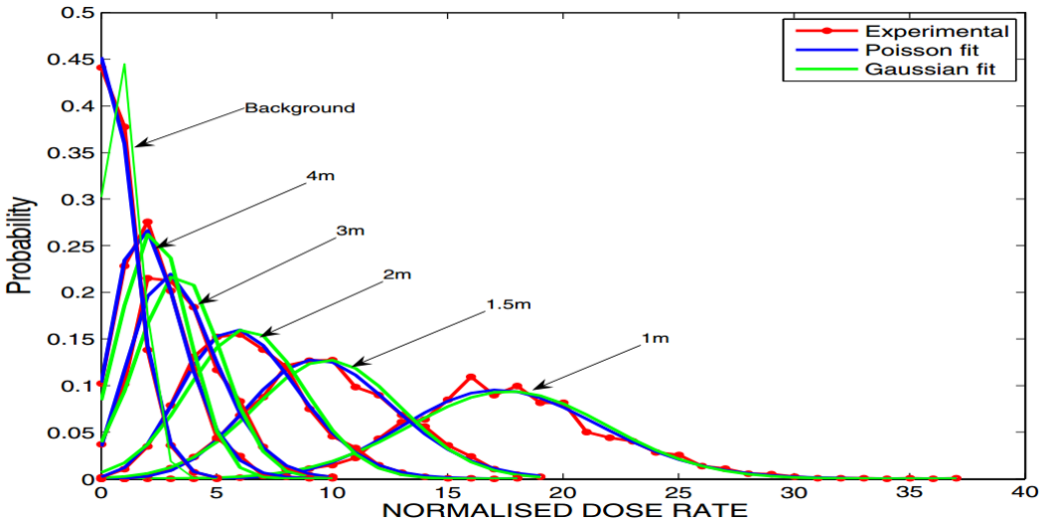

Figure 2.5: A measurement uncertainty of radioactive vary with distances with the graph fitting using Poisson and Gaussian distribution [3].

2.2 Related Works

The radioactive measurement gives a non-linear output [25,26], yet introduces uncertainty in measurement [24]. In order to handle these issues, there are several studies addressing the problem of source localization and estimation.

The radioactive source localization can be achieve using several techniques. The main categories for localizing the radiation source lies in the single source and multiple sources localization. For a single source localization, the common method is to use radiation reading as signal strength in different locations to determine the possible source in a certain area. [3], [27] utilize this approach by measurement the radiation circularly around the possible intensity source. The author applied three estimation techniques: maximum likelihood estimator (MLE), the extended Kalman filter (EKF), and the unscented Kalman filter (UKF). The Cramér-Rao lower bound was used to find the lower bound for estimation algorithms. The MLE gave the best result among other methods, but the computational intensive is the problem of this algorithm. It is unlikely that MLE can be used in real-time application. The EKF and UKF gave inaccurate result. The EKF, moreover, diverged from the CRLB. The test was done on both simulated source and trial data.

Similar technique of MLE was used in [28] to detemine multiple sources by measuring the source from the distance which the number of source, intensity strength and location are unknown. The author managed to estimate the source location using MLE and use generalize maximum likelihood to find the

number of souces. Another technique is to estimate the sources parameters using particle filter using important sampling with a progressive correction. The author successfully estimates 0-2 sources but from three sources onward, it was not very good using MLE. Bayesian estimation perform well in both cases.

[29] use the concept similar to global positioning system calculation by finding the level curves of the sources using the detector placed in the corner of the room. Thus, they said the intersection point has the highest probability that the source exist. The recursive least square optimization was used to estimate the sources from different sensors. However, the source intensity is claimed to be known as a *priori*. They successfully utilized realtime tracking of the source with some error in an indoor environment.

One of the interesting approaches is to use a vehicle to carry a detection device for measuring the intensity. [4] used a helicopter to carry a detector and flew over the area to localize the radiation source. The particle filter was used as the localization technique with a prior knowledge of the intensity of the source type of $1/R^2$. [30] used a mobile ground robot equipped with a detector to localize a source. There are obstacles in the environment and the author used the artificial force field algorithm with the control vector to avoid them. As a result, the smooth path was generated and the robot successfully located the source.

The multi sensor approach is presented in [31]. The author used a group of mobile robots with detectors to map the radiation over a given polygonal area. Each robot is capable to share the measurement information and its location with another robot using wireless communication. The search environment was divided into a grid map. The robots will follow the information gradient and map the radiation by measure every grid cell. The test was done using a red LED as a simulated source.

For multiple radiation sources localization, [32] presents glowworm algorithm for a swarm of robots for multiple sources localization. The glowworm optimization is a well-known algorithm for localize the local optima of function. The agents in the algorithm carry a luminescence quantity called luciferin, which used to for information sharing. The agent will vary its sensor range parameter in order to compute its movement and move toward the one that has higher luciferin then its own. The author adapted the glowworm optimization for the case of radiation sources localization. It is successfully run with a swarm of 100 agents. The achieve minimum distance between two sources is 0.39m.

Another interesting technique for multiple sources localization is the contour tracking technique as in [23]. The author used a helicopter that equipped with the measurement device. The helicopter flew in the radiation

field by tracking its contour at low intensity measurement. Since the shape of the radiation that emits from the source is a circular shape. The contour of a single source is circle. For multiple sources, the Hough transform is used to determine multiple circles, in order to find the centers of the circles, which leads to the source locations. The limitation of the helicopter is that the fuel burns very fast. The author managed to swiftly tracking contour and provided a rough estimation of the radioactive sources.

In an intense radiation field, it is possible to locate the radioactive source by letting a robot follows the intensity gradient. However, if the robot is a long distance from the radiation source, the intensity measurement will be weak. Thus, a robot needs an exploration algorithm to efficiently locate the strong measurement which will lead it to the source. In addition, the exploration time might be constrained since there is limited measure of battery and limit evacuation time. Thus, an efficient exploration scheme for a robot must be utilized, which should minimize the exploration cost (*e.g.* traveling distance, time) but maximize the information for a robot. For exploration strategy, [33] presented the frontier-based exploration algorithm by directing robots to a region, called frontier cells, which lies between known and unknown areas. The algorithm is able to fully explore a reachable workspace and generate a reachability map [34, 35]. A robot will use appropriate criteria for choosing the best frontier for the best performance. The common criterion is the minimum distance from a robot to the frontier cell. However, it depends on the environment that additional criteria may be applied (*e.g.* terrain type, path cost, input measurement).

Chapter 3

Radiation Estimation Algorithm

Due to the fact that the reading of a measurement device is uncertain as discuss in Section 2.1.3, the gradient-based methods may not work because they do not consider sensor uncertainty [36]. Thus, the estimation algorithm is needed to tackle the problem of noisy measurement.

3.1 Recursive Bayesian Estimation

Recursive Bayesian estimation (RBE) or Bayes filter is an excellent method to deal with sensor uncertainty [37, 38]. It also provide the real-time computational feasibility with localization accuracy [9, 39]. Most recursive Bayesian estimations have the same concept which is to predict the system behavior by using the measurement to correct the prediction following Bayes theorem:

$$P(x \mid z_1, \ldots, z_n) = \frac{P(z_n \mid x, z_1, \ldots, z_{n-1}) P(x \mid z_1, \ldots, z_{n-1})}{P(z_n \mid z_1, \ldots, z_{n-1})} \tag{3.1}$$

where x is the estimated state. z is the observation as the measurement. The left hand side of the equation is $P(x \mid z_1, \ldots, z_n)$ which is the posterior belief. It is the product of the measurement model $P(z_n \mid x, z_1, \ldots, z_{n-1})$ and the prior belief $P(x \mid z_1, \ldots, z_{n-1})$ divided by the normalization constant $P(z_n \mid z_1, \ldots, z_{n-1})$.

Recursive Bayesian estimation start with the initial state. Next step is the prediction step, it will update the belief space. Then the measurement step, the prediction is corrected using the measured data [40]. The process will repeat at the prediction step and will converge when the prediction is close to the measurement. Fig. 3.1 shows the basic of recursive Bayesian estimation operation. There are two kinds of belief space in recursive Bayesian estimation. The first one is the bell-shape belief space called Gaussian belief space as in Fig. 3.2. The Kalman filter utilizes this kind of belief space due to the fact that it has only two parameters; mean and covariance. Another one is the non-Gaussian belief space which has an arbitrary shape [41, 42].

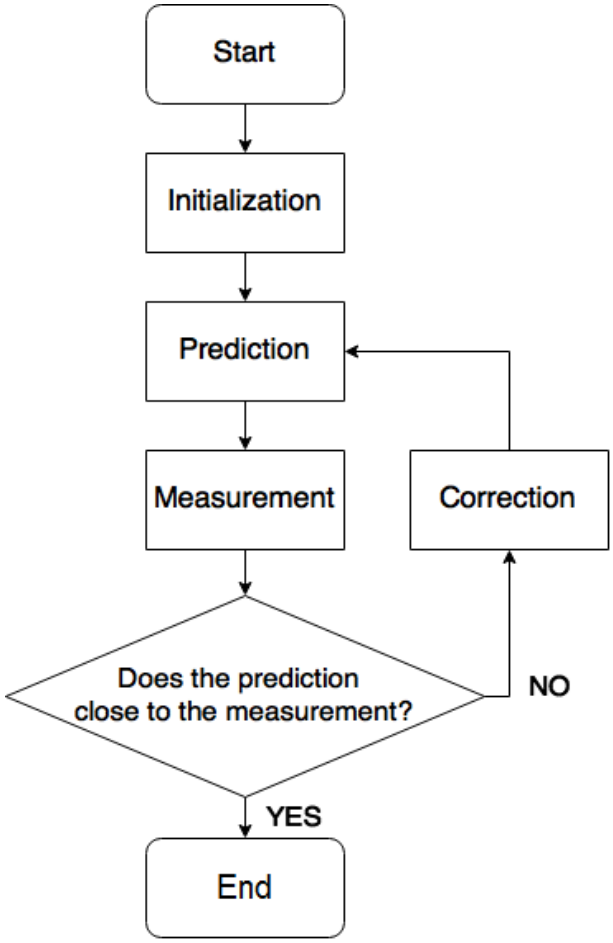

Figure 3.1: Overall process of the recursive Bayesian estimation algorithm.

This belief space suits for recursive Bayesian estimation algorithms like the particle filter because the filter has particles which have random attributes and each of them represent a single belief. The plot of these beliefs can be any shape, for instance in Fig. 3.3. The grid-based method and element-based method are also suit non-Gaussian belief space. the In this work, we use the non-Gaussian belief space because a single static sensor measurement of a source intensity cannot be used to determine the source location directly. The non-Gaussian belief space would provide a ring-like shape which tells us where the source may locate.

Each recursive Bayesian estimation algorithms comes with different performance in efficiency, ability for non-Gaussian, and ability for non-linearity as in Fig.3.4. The simplest algorithm of recursive Bayesian estimation is the Kalman filter (KF). It is the most efficient but perform poorly in non-Gaussian

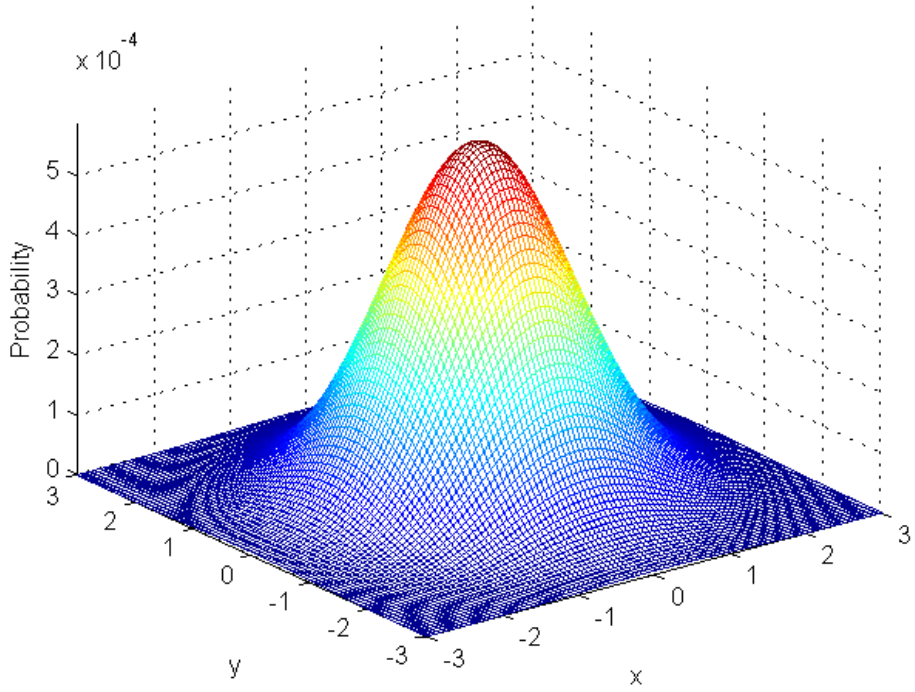

Figure 3.2: A Gaussian belief space.

system and it is a very linear process model [43, 44]. The extended Kalman filter (EKF) uses the Jacobian matrix to relax the linear constraint but it still suffer from non-Gaussian distribution [45, 46]. The unscented Kalman filter (UKF) allows some non-Gaussian belief space but does not work well with highly non-linear and non-Gaussian system [3, 47]. The grid-Based method (GM) has the performance depends on the selection of grid mesh or the number of elements and it suffers from computational complexity because the convolution of motion and measurement update e.g. the 3-D grid update requires 6-D operation [48–50]. The same reasons go for element-based method (EM). The most compromise of efficiency and performance for non-linear and non-Gaussian system is the particle filter (PF) [51]. In addition, the particle filter is non-parametric, thus it provides heuristic and more flexibility than other algorithms [52–55]. Therefore, it is used for intensity mapping algorithm in this work.

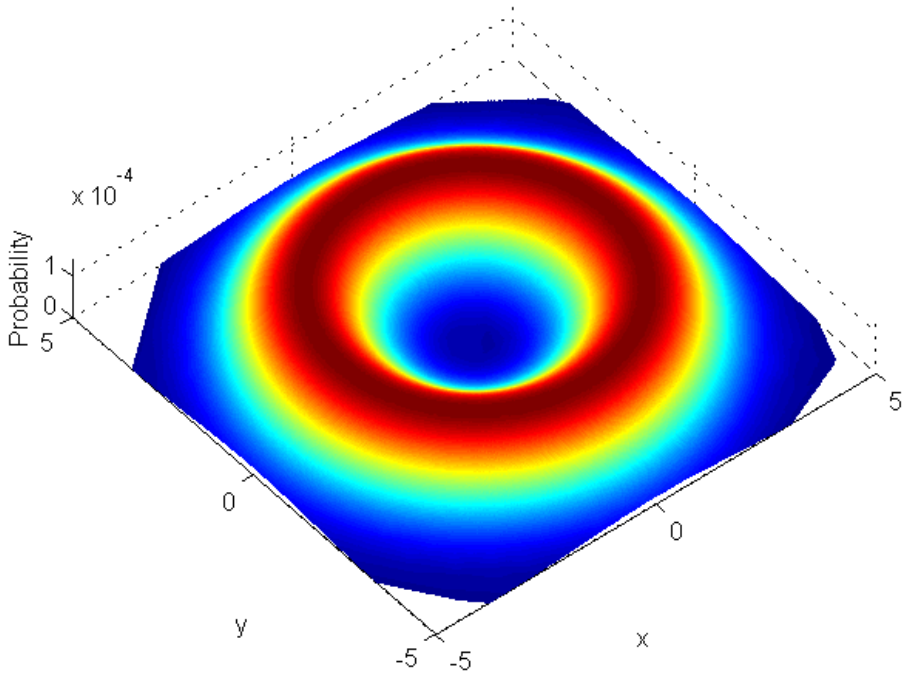

Figure 3.3: A non-Gaussian belief space.

3.2 Particle Filter

In this work, we choose the particle filter as the mapping algorithm since it compromises efficiency and performance for the non-linear and non-Gaussian systems [56, 57]. In addition, the particle filter is non-parametric. Thus, it provides heuristic, and it is more flexible than other algorithms [58, 59]. The particle filter or Sequential Monte Carlo (SMC) is the method representing the posterior belief using a set of random state samples as particles [60]. Each particle is basically a hypothesis of the real state at time t with an associate weight to represent the accuracy of the hypothesis based on the state measurement. The detail of the particle filter algorithm is in Algorithm 3.1. The particle filter starts with initialization of random hypothesis states as initial particles with equally associated weights. Then, the error model is used to find the error between measurement and prediction. The weight of each particle will be updated by the product of the weight of previous time step and the likelihood function. The likelihood function comes in the form of the normal distribution of the error with mean μ and variance σ. The

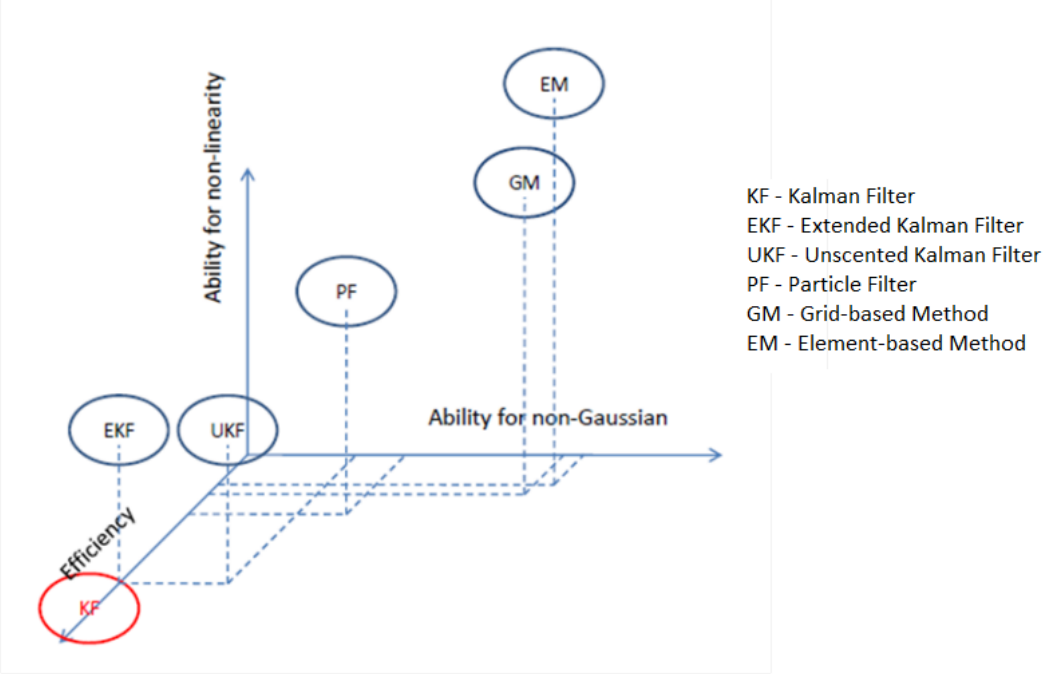

Figure 3.4: Recursive Bayesian estimation algorithms comparison [4].

weight must be normalized so they sum up to 1. The estimated state will be calculated by state estimate model. Some of the lowest weight particles will be resampled at the high weight particles at resampling step. Finally, the particles and the weights will be updated to be used in the next time step.

3.2.1 Target State

We use mobile robots to explore and map the radiation. The estimation state $\mathbf{x}$ for each particle requires the location (x, y) of the source and its intensity I as:

$$\mathbf{x} = \begin{bmatrix} x & y & I \end{bmatrix} \tag{3.2}$$

3.2.2 Intensity Estimation of Particles

We can use Eq. 2.2 to calculate the particle expected intensity I at the location (x, y) as we have a k^{th} measurement z_k at the robot location (x_k, y_k). However, it may introduce an estimation accuracy problem since we only use the current measurement that only provides the information at a specific location. If we combine the previous measurements, which include measurement locations

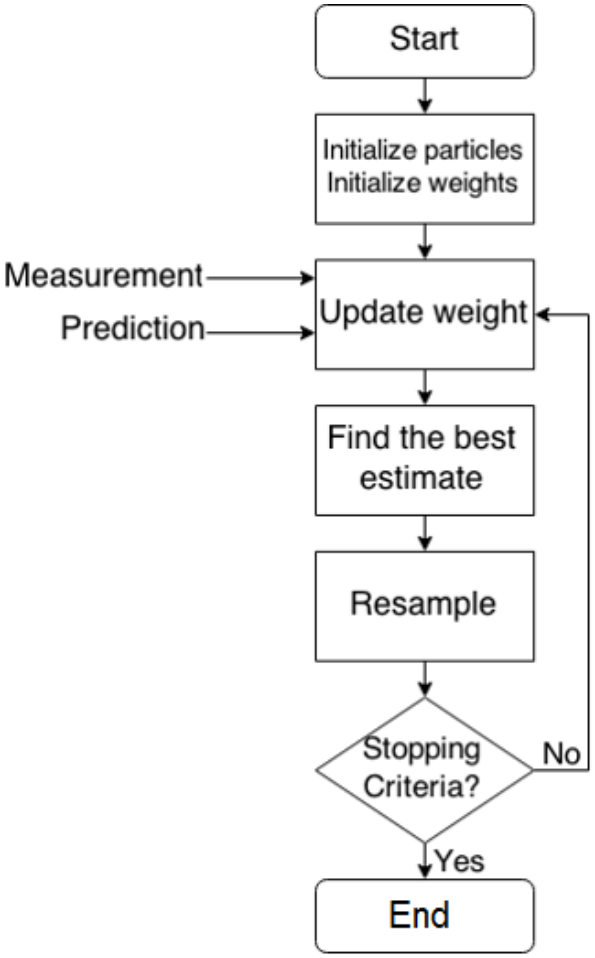

Figure 3.5: Overall process of the particle filter.

$(x_{1:k}, y_{1:k})$ and intensity measurement $\lambda_{1:k}$, the particles' intensity estimation will be more accurate.

3.2.2.1 Single Landmark Intensity Estimation

From Eq. 2.2, we can estimate the particle's intensity I^i at (x^i, y^i) using the current measurement z_k by:

$$\frac{I^i}{d_k^2} + \lambda_b = z_k \tag{3.3}$$

where $d_k = \sqrt{(x_k - x^i)^2 + (y_k - y^i)^2}$. However, the drawback of single landmark intensity estimation is that, the current measurement does not estimate the intensity quite well. The reason is because the measurement

Algorithm 3.1 Particle Filter

1: Initialize particles: $x_0 = rand(N, 1)$
2: Initialize particles' weights: $w_0 = 1/N$
3: **while** Not converge **do**
4: $error^i = error\_model(measurement^i, prediction^i)$
5: **for** $i = 1$ to N **do**
6: Update weight: $w_k^i = w_{k-1}^i \cdot likelihood\_function(error^i)$
7: **end for**
8: Normalize weights: $w = \frac{w}{\sum_{i=1}^{N} w^i}$
9: Calculate state estimate: $\hat{x} = state\_estimate\_model(w, x)$
10: Resampling process
11: Update particles: $x_{k+1} = x_k$
12: Update weights: $w_{k+1} = w_k$
13: **end while**

error from sensor worsen the estimation. Thus, using multiple estimation points can improve the measurement drastically.

3.2.2.2 Multiple Landmarks Intensity Estimation Algorithm

Optimization method To get more accurate estimation of the intensity point I^i is to use all n measurement $z_{k-n}, \ldots, z_k$. Optimization algorithm is one of the method to achieve this goal. In this work, we want to show you the example of using an optimization algorithm to determine the estimation intensity. The algorithm that we choose is the nonlinear program solver in MATLAB called *fmincon*, which specify the constrains and function by:

$$\min_x f(x) \text{ such that } \begin{cases} c(x) < 0 \\ ceq(x) = 0 \\ A \cdot x \leq b \\ Aeq \cdot x = beq \\ lb \leq x \leq ub, \end{cases}$$

where $c(x)$ and $ceq(x)$ are the subject of minimization of inequality and equality of nonlinear function respectively. $A \cdot x \leq b$ and $Aeq \cdot x = beq$ subject to the minimization of linear inequality. lb and ub are lower bound and upper bound of x. For this work, we only require lb and ub parameters for intensity I^i. The rest of the parameters are empty. The objective function is the likelihood function equation (Eq. 3.14) in section 3.2.3.

However, the drawback of the optimization method is the computational time. Since it requires intensive calculation from the lower bound lb to upper bound ub of every particle, the computation time increases directly proportional to the number of particles.

Calculation method From section 3.2.2.1, consider the previous measurements from the first measurement to measurement n, they also can estimate the intensity I^i by:

$$\frac{I^i}{d_k^2} + \lambda_b = z_k \tag{3.4}$$

$$\frac{I^i}{d_{k-1}^2} + \lambda_b = z_{k-1} \tag{3.5}$$

$$\frac{I^i}{d_{k-n}^2} + \lambda_b = z_{k-n} \tag{3.6}$$

combining those terms, we have:

$$\frac{I^i}{d_k^2} + \lambda_b + \frac{I^i}{d_{k-1}^2} + \lambda_b + \cdots + \frac{I^i}{d_{k-n}^2} + \lambda_b = z_k + z_{k-1} + \cdots + z_{k-n} \tag{3.7}$$

$$\frac{I^i}{d_k^2} + \frac{I^i}{d_{k-1}^2} + \cdots + \frac{I^i}{d_{k-n}^2} = \sum_{j=0}^{n} (z_{k-j} - \lambda_b) \tag{3.8}$$

$$I^i \cdot (d_k^{-2} + d_{k-1}^{-2} + \cdots + d_{k-n}^{-2}) = \sum_{j=0}^{n} (z_j - \lambda_b) \tag{3.9}$$

$$I^i \cdot \sum_{j=0}^{n} d_{k-j}^{-2} = \sum_{j=0}^{n} (z_{k-j} - \lambda_b) \tag{3.10}$$

$$I^i = \frac{\sum_{j=0}^{n} (z_{k-j} - \lambda_b)}{\sum_{j=0}^{n} d_{k-j}^{-2}} \tag{3.11}$$

Thus, Eq. 3.11 can be used to estimate the particle's intensity I^i using previous and current measurements.

3.2.3 Likelihood Function

By using Eq. 2.4, we can calculate the likelihood $\mathbf{x}_i$ of particle i by using the k^{th} measurement z_k and the predicted intensity λ_k^i from Eq. 2.2, in the case of single landmark estimation. Here, we approximate the Poisson distribution to the Gaussian distribution to reduce the computational complexity [3]:

$$p(z_k; \mathbf{x}^i) = \mathcal{P}(z_k; \lambda_k^i) \tag{3.12}$$
$$\approx \mathcal{N}(z_k; \lambda_k^i, \lambda_k^i) \tag{3.13}$$

In the case of multiple landmarks estimation using the previous and current measurements $z_{1:k}$ at $(x_{1:k}, y_{1:k})$, the new likelihood function is the product of all likelihoods from all measurements as:

$$p(z_{1:k}; \mathbf{x}^i) \approx \prod_{j=1}^{k} \mathcal{N}(z_j; \lambda_j^i, \lambda_j^i) \tag{3.14}$$

where z_k is the measurement update from the robot at time step k. $\mathbf{x}^i$ is the current state of the particle i which is used to calculate the predicted intensity λ_k^i at the robot location using Eq. 2.2 as follow:

$$\lambda_k^i = \frac{I_i}{(x_k - x_i)^2 + (y_k - y_i)^2} + \lambda_b \tag{3.15}$$

where (x_k, y_k) is the robot position at time step k. I_i is the intensity of the particle i. (x_i, y_i) is the location of the particle i. λ_b is the background radiation. The Poisson distribution is approximated as the Gaussian distribution by $\mu = \sigma^2 = \lambda_k$.

The state estimation of the particle filter is usually the average state of the particles with the highest weights. If the portion of the top particles is too high, the algorithm may not converge. If the portion is too low, the algorithm may converge to the wrong location.

3.2.4 Resampling Process

The resampling process is on how to remove the lowest weight particles and resample them elsewhere in order to avoid the problem of degeneracy [61]. The degeneracy problem is the usual problem in the particle filter, which is a few highest weight particles dominate the distribution while most particles will have weights close to zero [62]. The resampling process will remove a portion of the lowest particle weights and resample them at the high weight particles using the roulette wheel selection [63, 64]. In addition, the particles that have zero weight will be resampled as well. It is to ensure that some of the high weight particles will be selected and also add diversity to the

population from lower weight particles. The newly born particles $x_{k+1}^{index_L^j}$ will have the a uniform weight as:

$$w_k^{index_L} = \mathcal{U}(1/N) \tag{3.16}$$

where $w_k^{index_L}$ is the low weight particles with index $index_L$, and N is the number of particles. The Gaussian noise is applied to the portion of those which are resampled near the high weight particles x_k^{target} to increase the diversity as in the following equation:

$$x_{k+1}^{index_L^j} = x_k^{target} + \mathcal{N}(\mu, \sigma^2) \tag{3.17}$$

where $x_k^{index_L^j}$ is the low weight particle j. x_k^{target} is the selected target of high index using the roulette wheel selection. $randn$ is the Gaussian noise with the mean $\mu = 0$ and the standard deviation σ is mag. However, as the process continues, the standard deviation of the noise mag becomes linearly lower overtime to make the algorithm converge. When the measurement is higher than the detection threshold, the robot will pretty much know which area contains the source. Thus, resample the particle at the estimated states will accelerate the convergence process.

3.2.5 Termination Criteria

The algorithm will converge when the termination criteria are met. In this case, we set the termination criteria as: if the root mean square error of the estimated intensity is less than 5% for 5 iterations and if the robot has visited the area within 1.5m around the estimated location, the algorithm has converged. The reason why the robot has to visit the estimated location is to prevent the algorithm from ending too soon, which may lead to the false location of the radiation source.

Chapter 4

Exploration Algorithms

4.1 Frontier-base Exploration

In order to explore the environment, the robot needs to know which part of the area is not visited and which part is visited. By knowing visited and unvisited area, the robot will not have to move to the same location, thus it gives an efficient exploration [65]. Frontier-based exploration is the excellent tool for a robot exploration. It uses a grid map to determine visited and unvisited area. The cells between visited and unvisited area are called frontier cells, which the robot uses to determine where to go next [33, 66–69].

Fig. 4.1 shows how a robot creates grid map. The white area is the area that has already been visited by the robot. The green area is the area that has not been visited by the robot yet. The blue asterisks are the frontier cells.

4.1.1 Target Point Selection

To determine the direction of a robot, an algorithm for choosing an appropriate frontier cell is needed. We will use a cost function to determine the for the robot using the following criteria:

1. Intensity gradient: the robot will choose the frontier in which the intensity measurement tends to be higher by following the direction of increasing intensity gradient.
2. Distance: the robot will calculate the Euclidean distance from itself to the frontier.

The minimum-cost path is computed using the following equation:

$$V_t^i = \alpha||i - t|| + (1 - \alpha)D(ax_0 + by_0 + c, (t_x, t_y)) \tag{4.1}$$

where V_t^i is the cost of a robot $i_{x,y}$ to reach frontier position $t_{x,y}$. α is the importance weight of the distance and the intensity gradient which set between $[0, 1]$. From experiment, we set $\alpha = 0.8$. The intensity gradient

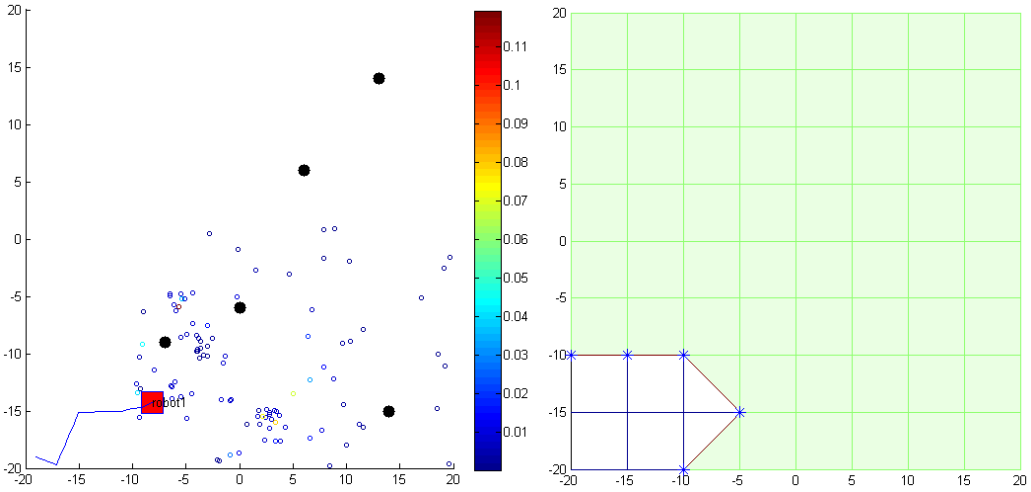

Figure 4.1: Left side, the simulated environment with a robot represented by a square. Radiation sources are represented by black dots. Small dots with color indicate the particles with associate weights. Right side, The robot grid map with visited area (white), unvisited area (green) and frontier cells (asterisks).

can be achieved by using the past and current measurements of a robot. $D(ax_0 + by_0 + c, (x, y))$ is the distance from a frontier position (x, y) to the gradient line $ax_0 + by_0 + c$ as in Eq. 4.2.

$$D(ax_0 + by_0 + c, (t_x, t_y)) = \frac{|at_x + bt_y + c|}{\sqrt{a^2 + b^2}} \tag{4.2}$$

where $ax_0 + by_0 + c$ is the line equation of the gradient direction and (t_x, t_y) is the position of a frontier cell.

4.1.2 Area Pruning

To create an accurate map, the robot needs to visit every cell in the grid map. However, a small isolated unvisited cell that is surrounded by explored cells with low intensity can be ignored because it gives low exploration gain. In addition, a source is unlikely located in that area because the surrounding cells are examined. We can apply Eq. 2.2 to find the possible intensity of that cell, if it is lower than the detection threshold, it can be ignored, thus, explored. The situation like this usually happen by chance. In our case, we will assume that some frontier cells are not worth to visit. We intentionally skip some frontier cells and flagged them as low priority cells in order to

examine the surrounding area. The flagged frontier cells are not adjacent to each other. As a result, we can increase the chance that the cells are automatically avoided as we explored.

Every unvisited cells in the grid map can still potentially be ignored. We introduce the cells' weight by applying recursive Bayesian estimation (RBE). The intention of this algorithm is not to find the radioactive sources, but it determines which cells has low value as a robot travel and measure the intensity along the way. RBE uses the same technique as PF (Eq. 3.13) to determine the weight of each cell. Thus, if the measurement is decreasing as the robot moves toward one cell, that cell could be ignored because the probability of finding a source in that cell is low. However, the low weight cells can only be remove when the robot moves close to that cells, to prevent the problem of over pruning, since a single measurement cannot determine the whole weight of all cells. In addition, the algorithm will not work in the high intensity area (*e.g.* near the sources) because it will be come a source searching algorithm instead, which is the task of the particle filter. Fig. 4.1 also shows the cells those are marked with low priority flags ($\diamond$) and all unexplored cells are assigned with weights.

4.1.3 Multi-robot Systems Extension

From a single robot, we can extend our work to muti-robot systems by adding one or more robots to the workspace. Each robot can communicate to exchange information, including grid map, partial intensity map, and the current source estimation. However, in some cases, two or more robots choose the same frontier cell which is not the optimal solution. To prevent this, robots will compute the utility of frontier cells U_t [70]. Initially, each frontier cell t will have the utility U_t set to 1. Once a robot choose a frontier cell t', the utility of that frontier cell and adjacent frontier cells in distance d from t' are reduced by $P(d)$. Thus, the utility $U(t_n|t_1, ..., t_{n-1})$ of a frontier cell t_n given that the frontier cells $t_1, ..., t_{n-1}$ are assigned to the robots $1, ..., n-1$ is computed by

$$U(t_n|t_1, ..., t_{n-1}) = U_{t_n} - \sum_{i=1}^{n-1} P(||t_n - t_i||) \tag{4.3}$$

If there are many robots which choose the frontier cell t_n, the utility of that cell tends to be low. In our case, the environment is known and has no obstacles. $P(d)$ is set to be the normal distribution with $\mu = 0$ and $\sigma = 0.4$, so the utility of the target frontier cell t_n will be close to 0.

Algorithm 4.1 Target Point Selection

1: Determine frontier cells of all robots
2: Compute the cost V_t^i for each robot
3: Set the utility $U_t = 1$ for all frontier cells
4: **while** there is a robot without a target point **do**
5: Determine a robot i and a frontier t that satisfy: $(i, t) = \text{argmax}_{(i',t')} U_t - \gamma V_t^i$
6: Reduce the utility of the selected frontier cell and adjacent frontier cells by $U_{t'} \leftarrow U_{t'} - P(||t' - t_n||)$
7: **end while**

By considering a trade-off between the cost of moving to the target frontier cell V_t^i and the its utility U_t, the target point selection can be calculated using Algorithm 4.1.

From Algorithm 4.1, $U_t - \gamma V_t^i$ is used to find the robot i and the frontier t which give the best evaluation. The process continues iteratively until all robots choose their frontier cells. $\gamma \in [0.01, 50]$ gives the importance of cost versus utility. It is set to 1 in this case.

When any robots discovers any neighbors, they will start sharing information to each other. The exchange information process aims to reduce the exploration time. Thus, there are several crucial information to be shared, which are the current source estimation, exploration map, and partial intensity map. The current source estimation is shared among neighbors in order to increase the converging process. When two or more robots have the same source estimation, the robot will accelerate the termination process. To reduce the exploration time, the unvisited grid maps of robots will intersect and the intersection part could be where both robots have not visited. Another piece of information to share is the partial map of the sources discovered by each robot. The partial intensity maps of each robot will be merged so each robot knows the locations of the sources that have already been discovered. The merging process is to compare discovered sources with each other. If there are any new sources from other robots, the sources will be added. If there are sources which are already discovered, the position and intensity of any duplicate sources will be averaged.

4.2 Information Gain-based Exploration

The entropy is the tool to measure the uncertainty of a random variable [71,72]. In this case, we want to evaluate the uncertainty of the map using the entropy

to model this in the probabilistic manner [73].

$$H[P(\mathbf{x})] = -\int_{\mathbf{x}} p_i \log p_i \tag{4.4}$$

$$\approx -\sum_{i=1}^{n} p_i \log p_i \tag{4.5}$$

where, $p_i = P(\mathbf{x} = \mathbf{x}_i)$. In our case, the particle filter entropy is as the following equation:

$$H[P(\mathbf{x}|z_t)] = -\sum_{i=1}^{\#particle} w_i p(x_i|z_t) \log p(x_i|z_t) \tag{4.6}$$

where, $\mathbf{x}$ is the distribution of the particles. w_i is the weight of each particle i. z_t is the observation that we obtain at the time step t. Then, the action of the robot a_t can be evaluated using the expected information gain. It is the change of the entropy for the particle filter when we apply the action as:

$$I(\hat{z}, a_t) = H[P(\mathbf{x}|z_t)] - H[P(\mathbf{x}, \hat{\mathbf{x}}|a_t, \hat{z})] \tag{4.7}$$

where $\hat{z}$ is the observation to be obtained when action a is taken. This value can be calculated by Eq. 2.2, using the estimated intensity value from the current particle filter time step t. $\hat{x}$ is the new distribution of particles introduces by the action a_t. The expected information gain can be obtained by integrating all the possible measurements $\hat{z}$ when the robot takes action a_t.

$$E[I(a_t)] = \int_{\hat{z}} p(\hat{z}|a_t, z_t) I(\hat{z}, a_t) dz \tag{4.8}$$

However, to compute the expected information gain is usually a complicated task. Instead, the utility function using the greedy aspect of the maximum information gain I when the robot takes action a as:

$$\mathbf{a}^* = \underset{a}{\operatorname{argmax}}\, H[P(\mathbf{x}|z_t)] - H[P(\mathbf{x}, \hat{\mathbf{x}}|a, \hat{z})] \tag{4.9}$$

The utility function becomes:

$$U(a) = I(a) - \alpha \text{cost}(a) \tag{4.10}$$

where α is the weight of the cost of the action a that the robot has to take. We choose the best action, *i.e.*, the action that gives the highest utility as the robot action. The robot will evaluate the available adjacent cells around

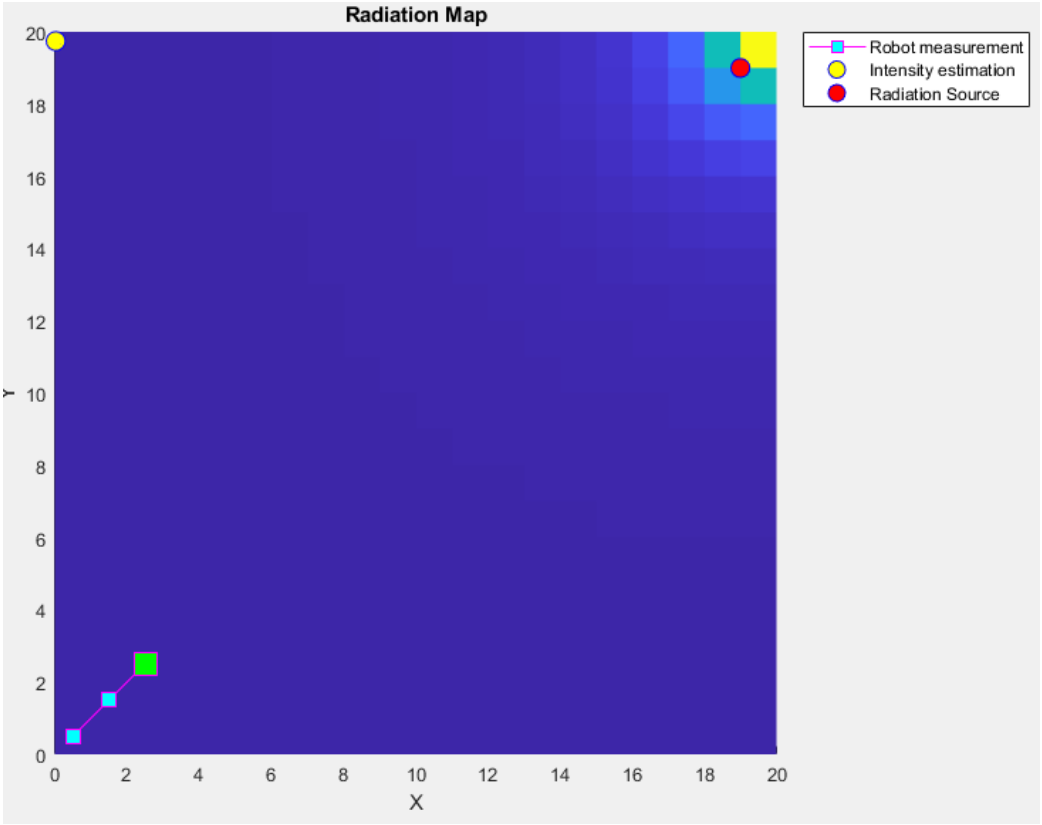

Figure 4.2: The simulated environment with a robot represented by a green square. The small squares that follow the robot are the previous reading in the last two time steps $(k-1, k-2)$. The real location of the source represented by the red circle and the background of the map represents its corresponding radiation level. The estimated location of the radiation source by particle filter represented by the yellow circle.

the robot, at most 8 cells, to calculate the utility of those cells and choose the highest utility as the next action.

Fig. 4.2 shows the overall radiation map that the robot has to explore. The radiation map is the map with different radiation levels corresponding to the radiation source. According to Eq. 2.2, radiation intensity will reduce inversely proportional to the distance from the radiation source. Fig. 4.3 shows the particles of the robot that are the possible location of the source.

However, as the robot progress through the area, the entropy of the map becomes less and less significant, according to Fig. 4.4. On the opposite, when the robot is getting closer to the radiation source, the particle filter estimation becomes more accurate. Thus, in order to get an accurate result,

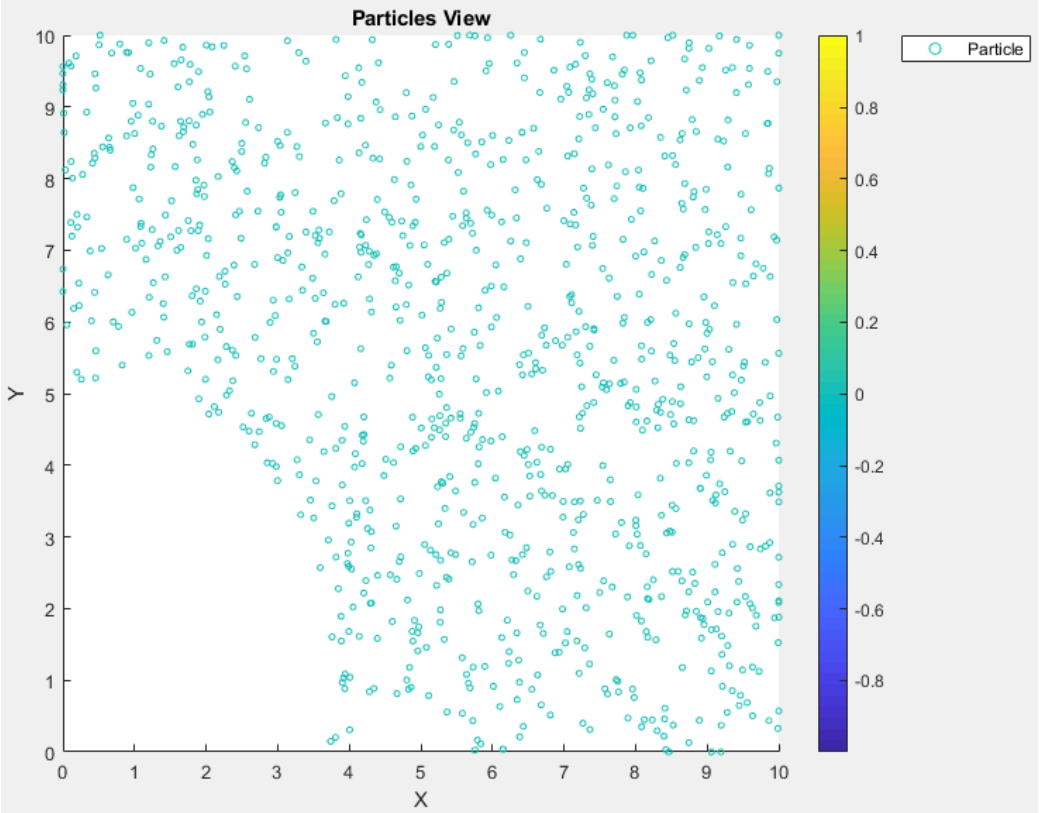

Figure 4.3: The particles of the robot that represents the hypothesis of the source. The white area with no particle is the area that the robot already visited with low information, so the particles in the particular area are resampled elsewhere on the map.

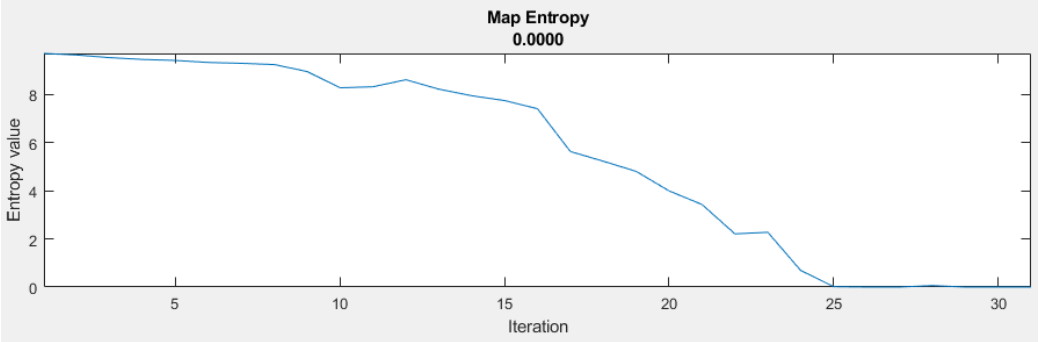

Figure 4.4: The entropy value vs iteration when the robot explores the radiation field. The entropy value decreases as the iteration increases, which means the information that we gain from the map is lower after each iteration.

the robot should switch to use the particle filter estimation as the target, and takes the action that makes the robot get closer to the target.

4.3 Unknown Sources Intensity Separation

A robot will move to the target frontier until the measurement is higher than a certain threshold. Then, a robot will use the particle filter to estimate the source. The source will be determined sequentially and a robot will use discovered sources to create a partial intensity map using Eq. 2.3. Then, a robot will subtract the intensity of sources of the partial map from the measurement in the real world, using the following formula:

$$z'_k = z_k - \sum_{i=1}^{\mathcal{M}'} \frac{I_i}{(x_k - x_i)^2 + (y_k - y_i)^2} \tag{4.11}$$

where z'_k is the k^{th} measurement subtracted by the partial map. z_k is the original k^{th} measurement at (x_k, y_k). $\mathcal{M}'$ is the number of source that the robot has discovered so far. I_i is the i^{th} discovered source at (x_i, y_i).

From Eq. 2.3, a source is created and summed with other sources of different location and intensity. Thus, each source will add some intensity to each other according to this equation:

$$I'_i = \left\{ \sum_{j=1}^{\mathcal{M}} \frac{I_j}{(x_i - x_j)^2 + (y_i - y_j)^2} \right\} + \lambda_b \tag{4.12}$$

where I'_i is the i^{th} output intensity source at (x_i, y_i). $\mathcal{M}$ is the number of intensity points. I_j is the intensity point at (x_j, y_j). The estimated intensity

from particle filter is the measurement of I'_i. If the robot uses the direct measurement, the intensity map created by the robot will be inaccurate. To solve this, we need the intensity correction algorithm. We know that:

$$I'_1 = I_1 + \frac{I_2}{d^2_{1,2}} + \cdots + \frac{I_{\mathcal{M}}}{d^2_{1,\mathcal{M}}} + \lambda_b \tag{4.13}$$

$$I'_2 = \frac{I_1}{d^2_{2,1}} + I_2 + \cdots + \frac{I_{\mathcal{M}}}{d^2_{2,\mathcal{M}}} + \lambda_b \tag{4.14}$$

$$\vdots$$

$$I'_{\mathcal{M}} = \frac{I_1}{d^2_{\mathcal{M},1}} + \frac{I_2}{d^2_{\mathcal{M},2}} + \cdots + I_{\mathcal{M}} + \lambda_b \tag{4.15}$$

where $I'_1, I'_2, \ldots, I'_{\mathcal{M}}$ are the sources which have influence from other sources. $I_1, I_2, \ldots, I_{\mathcal{M}}$ are the original sources without influence from other sources. $d_{i,j}$ is the Euclidean distance from point i to point j. We know $I'_1, I'_2, \ldots, I'_{\mathcal{M}}$ from the measurement and also the location of each source which can be used to calculated $d_{i,j}$. Only $I_1, I_2, \ldots, I_{\mathcal{M}}$ are unknown. Thus, there will be $\mathcal{M}$ unknown variables with $\mathcal{M}$ equations which are linear equations. The Gauss-Jordan elimination can be used to solve this as:

$$\left[\begin{array}{cccc|c} I_1 & \frac{I_2}{d^2_{1,2}} & \cdots & \frac{I_{\mathcal{M}}}{d^2_{1,\mathcal{M}}} & I'_1 - \lambda_b \\ \frac{I_1}{d^2_{2,1}} & I_2 & \cdots & \frac{I_{\mathcal{M}}}{d^2_{2,\mathcal{M}}} & I'_2 - \lambda_b \\ \vdots & \vdots & \ddots & \vdots & \vdots \\ \frac{I_1}{d^2_{\mathcal{M},1}} & \frac{I_2}{d^2_{\mathcal{M},2}} & \cdots & I_{\mathcal{M}} & I'_{\mathcal{M}} - \lambda_b \end{array}\right] \tag{4.16}$$

Chapter 5

Experimentation and Analysis

5.1 Overall Process

The flowchart of our proposed method is in Fig. 5.1. A robot starts with the initialization of particles. The particles are always initialized randomly in the unvisited region of exploration grid because there is no point to place the particle in the visited region. Next, the robot will determine an appropriate frontier cell and move accordingly until the sensor pick up a high intensity reading. Now, the robot will use the particle filter to determine a source by moving closer to the expected stat. When a robot discover the source, it will create a partial intensity map using Eq. 2.3. The measurement of a robot will now subtract the intensities of the sources in the partial map. For multi-robot systems extension, a robot will check for its neighbors when it moves toward the frontier cell and estimation point. When any robots discovers any neighbors, they will start sharing the information to each other. We assume that each robot broadcasts their findings in the circular area around itself. For simplicity, the information is always transmitted without delay and no data loss. After one robot receive the piece of information, it will update their own information immediately. The exchange information process aims to reduce the environment exploration and source intensity estimation time. Two robots will exchange information including visited and unvisited regions, discovered locations and intensities of sources, and the current estimation of the source. The process will be restarted in the initialization again until there is no frontier cell left, which means all the area is explored and all intensity sources should be found.

The illustrated example is in Fig. 5.2. A robot starts with the initialization of particles together with the Bayesian pruning algorithm. The particles are always initialized randomly in the unvisited region of exploration grid. There are two type of maps which are real map and robot's map (Fig. 5.2a). The robot will explore the real map to locate intensity sources. When the robot has discovered a source, it will create its own intensity source in separate map. Next, the robot will determine an appropriate frontier cell and move

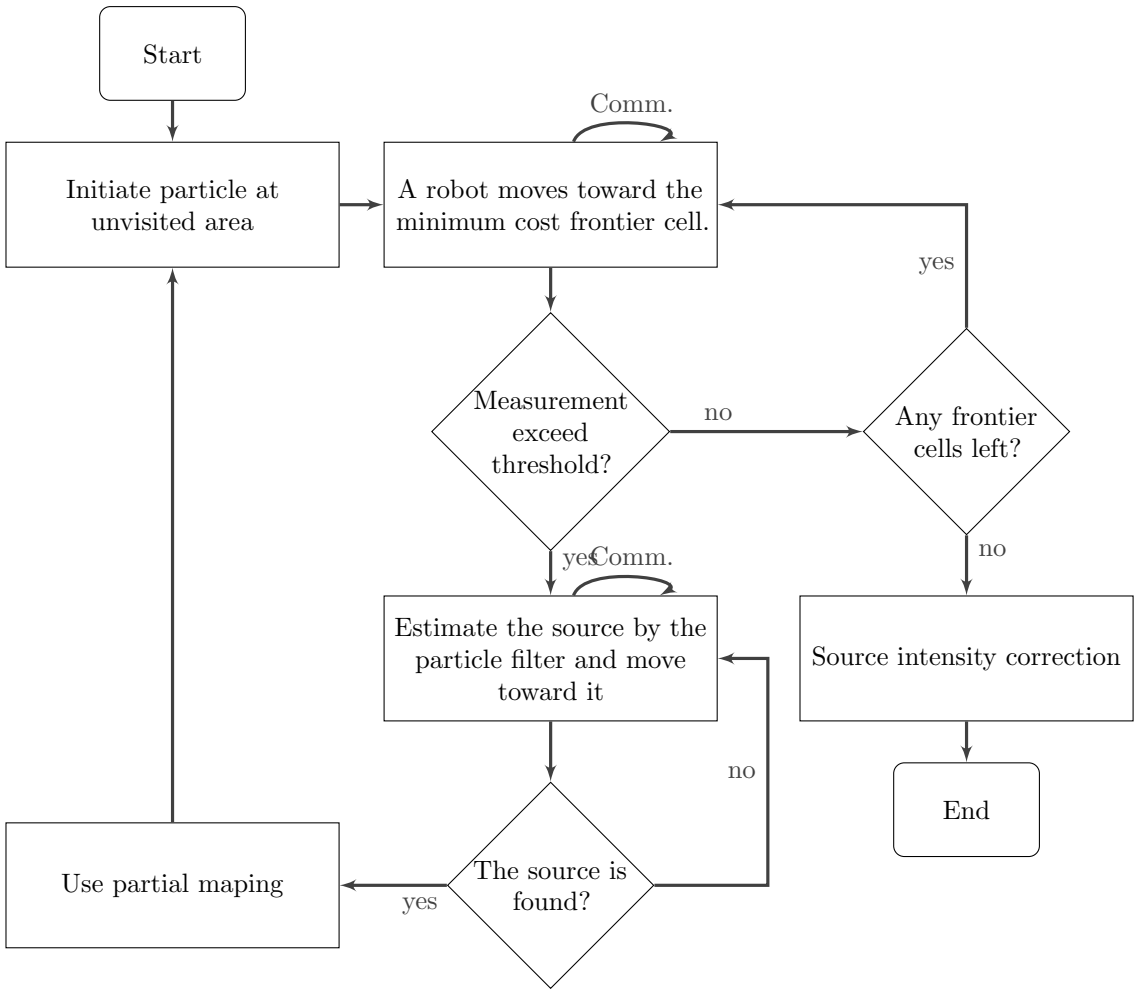

Figure 5.1: Overall process of the proposed method for a single robot which involves exploration and intensity sources estimation.

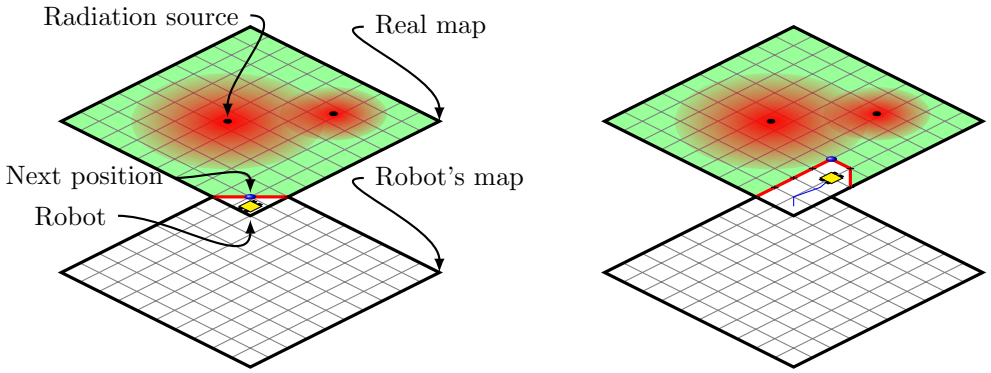

(a) $t = 1$

(b) $t = 4$

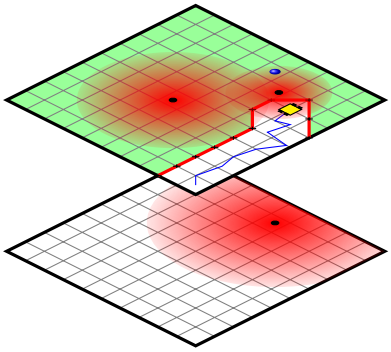

(c) $t = 11$

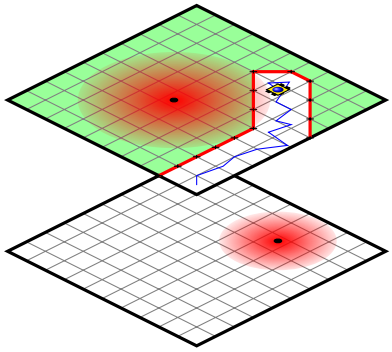

(d) $t = 14$

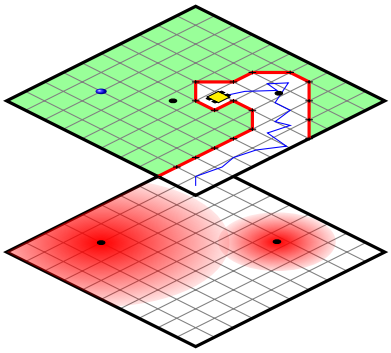

(e) $t = 16$

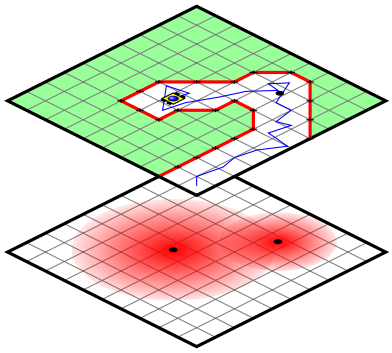

(f) $t = 21$

Figure 5.2: The robot operation in different time step. The black dots with faded red color are radiation sources. The robot is the yellow square. The real map will be explored by the robot where the unexplored area fills with green color and the explored area is white. The cells between those two areas are frontier cells which form the red line. The blue dot is the next best position for the robot and also serves as the best intensity estimation location. The blue line is the robot trajectory.

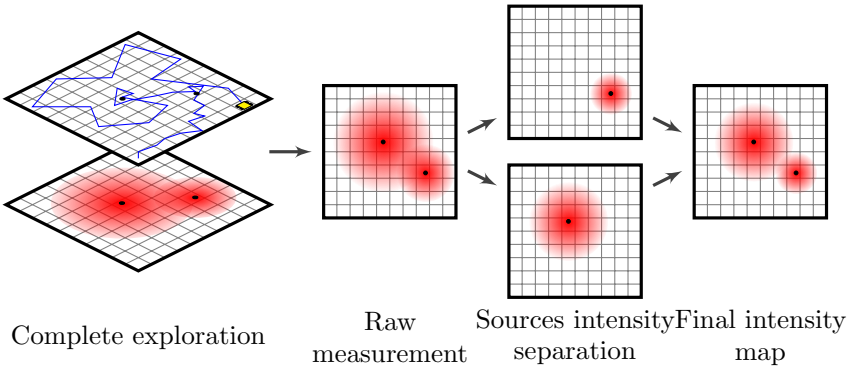

Figure 5.3: Apply sources separation algorithm by isolating and determining true strength of each source and recombine them to increase the map accuracy.

accordingly (Fig. 5.2b) and prune out any possibly low intensity frontier cells until the sensor picks up a high intensity reading. Now, the robot will use the particle filter to determine a source by moving closer to the estimate source location and use disperse resampling algorithm to ensure the location of the source (Fig. 5.2c). When a robot discover the source, it will separate the source by creating a partial intensity map in the robot's map using Eq. 2.3. The measurement of a robot will now subtract the intensities of the sources in the robot's map as in Fig. 5.2d. The process will restart in the initial state again until there is no frontier cell left, which means the area is explored and all intensity sources should be found.

Fig. 5.3 shows the final step of the process. After source localization, the raw measurement at each source location is fused with other sources according to Eq. 2.3. If we use the raw data to recreate the information map, it will not be as accurate as the true map. Thus, the robot will apply the sources intensity separation to find the true strength of the sources and it will increase the accuracy of the estimated sources.

5.2 Cramér-Rao Lower Bound Analysis of a Particle Filter

Cramér-Rao (CR) lower bound is a lower bound on the variance of any unbiased estimator [74]. The bound provides a benchmark which we can compare the performance of any unbiased estimator. The performance is high if the estimator is close to the CR lower bound. However, the performance of the estimator cannot possibly be better than the CR lower bound.

The parameter vector $\mathbf{x}_k$ is estimated as $\hat{\mathbf{x}}_k$ where the index k is the

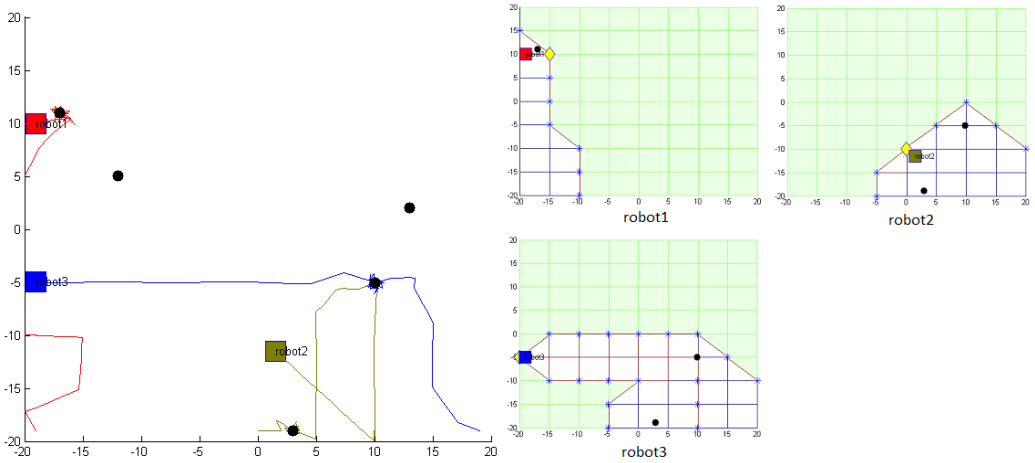

Figure 5.4: The simulation of multiple radiation sources estimation using 3 robots. The main plot shows the environment where the black dots are the radiation sources and the squares are the robots. The side plots show the corresponding exploration grid maps of each robot. Each exploration grid map shows a robot position (square), partial intensity map (black dot), next frontier cell/current estimated point (yellow diamond), visited area (white) and unvisited area (green).

time step. $\mathbf{C}_k$ is the lower bound of the mean-square error (MSE) $\mathbf{\Sigma}_k$ of any unbiased estimator $\hat{\mathbf{x}}_k$ which is defined as:

$$\mathbf{\Sigma}_k = \mathbb{E}\Big\{(\hat{\mathbf{x}}_\mathbf{k} - \mathbf{x})(\hat{\mathbf{x}}_\mathbf{k} - \mathbf{x})^T\Big\}, \tag{5.1}$$

where $\mathbb{E}$ is the expectation operator. The CR lower bound is the inverse of the information matrix $\mathbf{J}_k$:

$$\mathbf{\Sigma}_k \geq \mathbf{C}_k \equiv \mathbf{J}_k^{-1} \tag{5.2}$$

From the Gaussian likelihood model in Eq. 3.13, the information matrix can be calculated using the following formula:

$$\mathbf{J}_k = \mathbf{J}_{k-1} + \frac{1}{\lambda_k(\mathbf{x})}\mathbf{H}_k(\mathbf{x})^T\mathbf{H}_k(\mathbf{x}) \tag{5.3}$$

The formula above is computed in the recursive Bayesian framework by using prior knowledge $\mathbf{J}_0$. $\mathbf{H}_k(\mathbf{x})$ is the Jacobian of the measurement function $\lambda_k(\mathbf{x})$ in Eq. 2.2, which is:

$$\mathbf{H}_k(\mathbf{x}) = \left[\frac{\partial\lambda_k(\mathbf{x})}{\partial x_0} \quad \frac{\partial\lambda_k(\mathbf{x})}{\partial y_0} \quad \frac{\partial\lambda_k(\mathbf{x})}{\partial I}\right], \tag{5.4}$$

where

$$\frac{\partial \lambda_k(\mathbf{x})}{\partial x_0} = -\frac{2I(x_0 - x_k)}{[(x_0 - x_k)^2 + (y_0 - y_k)^2]^2} \tag{5.5}$$

$$\frac{\partial \lambda_k(\mathbf{x})}{\partial y_0} = -\frac{2I(y_0 - y_k)}{[(x_0 - x_k)^2 + (y_0 - y_k)^2]^2} \tag{5.6}$$

$$\frac{\partial \lambda_k(\mathbf{x})}{\partial I} = \frac{1}{(x_0 - x_k)^2 + (y_0 - y_k)^2} \tag{5.7}$$

The prior knowledge $\mathbf{J}_0$ corresponds to the parameter $\mathbf{P}_0$ which is the covariance of the Gaussian prior with mean $\hat{\mathbf{x}}_0$. Thus, $\mathbf{J}_0 = \mathbf{P}_0^{-1}$. The mean $\hat{\mathbf{x}}_0$ and covariance $\mathbf{P}_0$ are acquired based on intelligence information. The covariance matrix $\mathbf{C}_k$ consists of:

$$\mathbf{C}_k = \begin{bmatrix} var(\hat{x}) & cov(\hat{x}, \hat{y}) & cov(\hat{x}, \hat{I}) \\ cov(\hat{y}, \hat{x}) & var(\hat{y}) & cov(\hat{y}, \hat{I}) \\ cov(\hat{I}, \hat{x}) & cov(\hat{I}, \hat{y}) & var(\hat{I}) \end{bmatrix}. \tag{5.8}$$

From the matrix $\mathbf{C}_k$, the standard deviation of estimation error in position is defined as $\sqrt{C_k[1,1] + C_k[2,2]}$ and the standard deviation of estimation error in intensity is $\sqrt{C_k[3,3]}$.

5.2.1 Analysis

The test scenario is a single robot searches for a source. The intensity of the source is fixed at $I = 5 \cdot 10^4$ and the initial covariance is:

$$\mathbf{P}_0 = diag(\begin{bmatrix} \sigma_x^2 & \sigma_y^2 & \sigma_I^2 \end{bmatrix}) \tag{5.9}$$

where $\sigma_x = \sigma_y = 19$ and $\sigma_I = 5 \cdot 10^3$. For the robot, we recorded the walk for 100 time steps and run it 100 times. Then, we find the standard deviation of the error of position and intensity acquire from the robot. However, the particle filter is required to gather at least 20 samples to be reliable. The estimation of the first 20 sample is unreliable, thus omitted. Fig. 5.5 shows the performance of the particle filter and the CR lower bound. The position error is very close to the CR lower bound but the intensity error is pretty noisy. It is because of the reading is uncertain so the estimated intensity at the same position is change every time. Thus, the position is more likely to be used as a stopping criteria than the intensity by the above reason.

5.3 Single Robot Informative-based Exploration

In this case, we want to compare in a single robot case between informative-based exploration using information theory with a common particle filter.

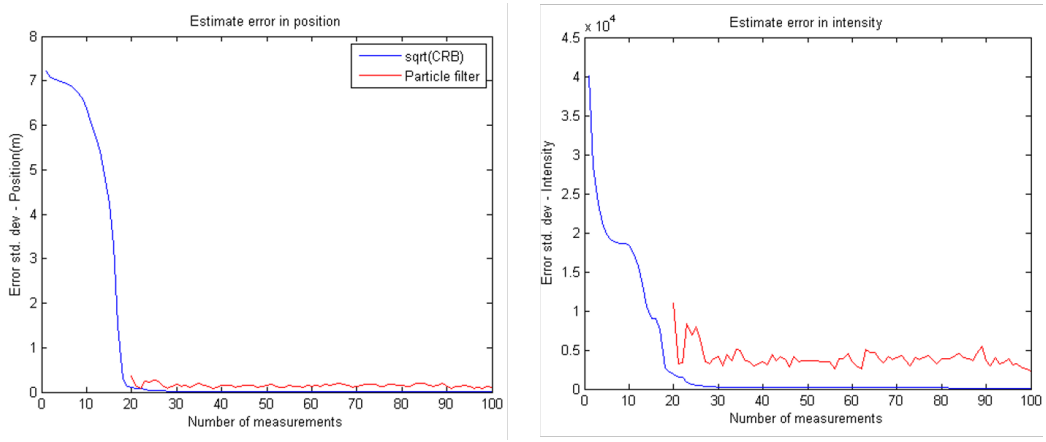

Figure 5.5: Performance of the particle filter compared with the CR lower bound.

5.3.1 Environment Settings

In the experiment, the environment is in a square shape, $20 \times 20\text{m}^2$ with no obstacle. We test each case with the scenario as in Fig.4.1, which the radiation source spawns at the top right corner. The radioactive source has a random intensity between 30,000 to 50,000 counts. The background intensity is set to 1,000 counts [23].

5.3.2 Robots Settings

A robot in the test knows its location using a GPS with the assumption that the GPS reading has no error. The robot will always start at the furthest location away from the source at the bottom left of the map. The background intensity is known by the robot. There are 1000 particles initialized. The map is divided to a small $1 \times 1\text{m}^2$ grid cell. The robot will measure the radiation only one time when they landed on the next exploration cell. It can move in 8 directions. When the robot is further away from the source, the information gain-based exploration will be used. The measurement threshold that the robot will switch to the source estimation seeking is 2000 counts.

5.3.3 Experimentation and Analysis

We run the experiment 100 times with different radiation intensity counts. We notice that the path of the robot of the proposed method is not the optimum path, which is to be expected because of the uncertainty of the measurement.

Table 5.1: Performance comparison of the proposed method vs traditional methods

	Travel distance (unit)	Position Error (m)	Intensity Error (count)
Snake row scan	381.00	0.01	115.05
Snake column scan	381.00	0.03	152.90
Estimation seeking	39.67	0.23	1,661.40
Informative-based	36.16	0.20	1,283.00

We tested our algorithm versus the traditional methods such as the snake scan patterns and source estimation seeking method.

Table 5.1 shows the average travel distance and average error in intensity and position that the robot takes to finish the task. It clearly shows that the traditional method, such as the snake scan that does not rely on a sensor to guide the robot to the next possible best action, gives the highest travel distance. The source estimation seeking method gives a competitive travel distance to the proposed method. However, the proposed method works better because of the selection of the next best action based on the maximum information gain.

In the accuracy aspect, the traditional methods have a lot more measurement points which, result in higher accuracy. The estimation seeking method and the proposed method have a lower number of measurement points, but they give decent accuracy of both intensity and position. Fig. 5.6 gives one example of the route that the robot takes using the proposed method and its corresponding entropy value.

5.4 Particle Filter's Intensity Estimation Methods Comparison

We compare three intensity estimation methods, namely, single landmark intensity estimation, multiple landmarks intensity estimation using optimization function, and multiple landmarks intensity estimation using calculation in different scenarios.

5.4.1 Envinronment Settings

In the experiment, the environment is in a square shape, $10 \times 10\text{m}^2$ with no obstacle. We test each case with a single source on the top right corner $(9, 9)$ in order to see which algorithm can gives the most accurate and fastest

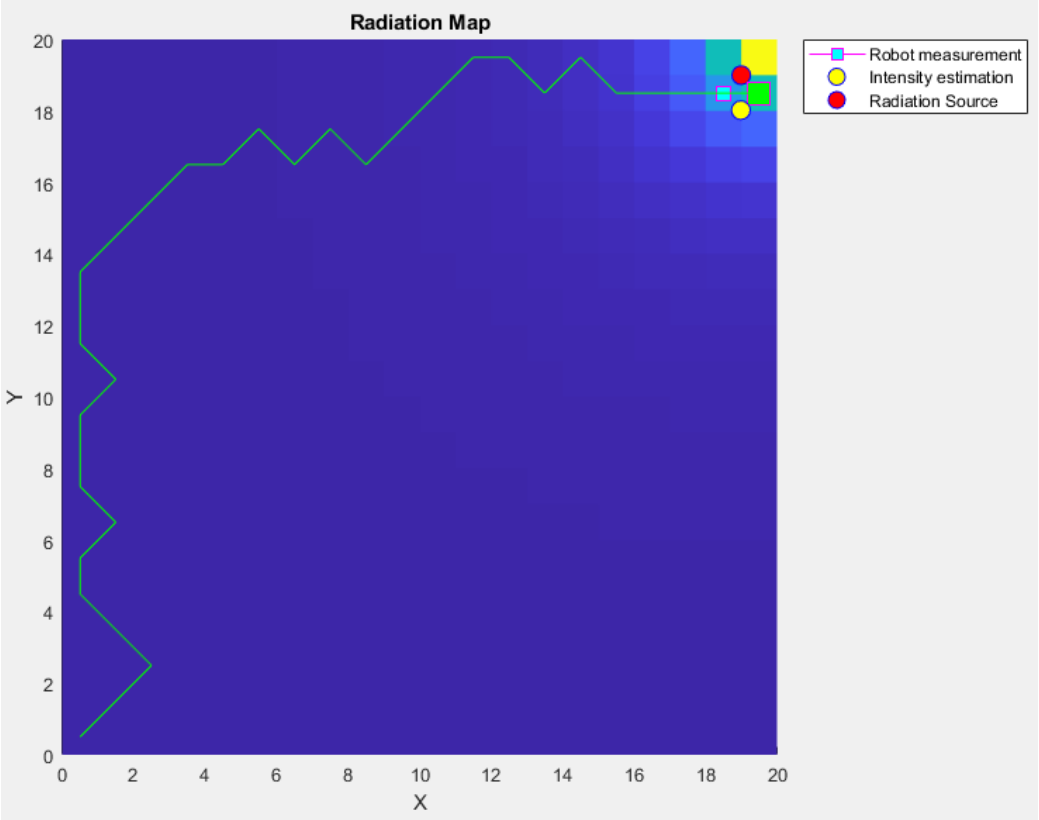

(a) The radiation map.

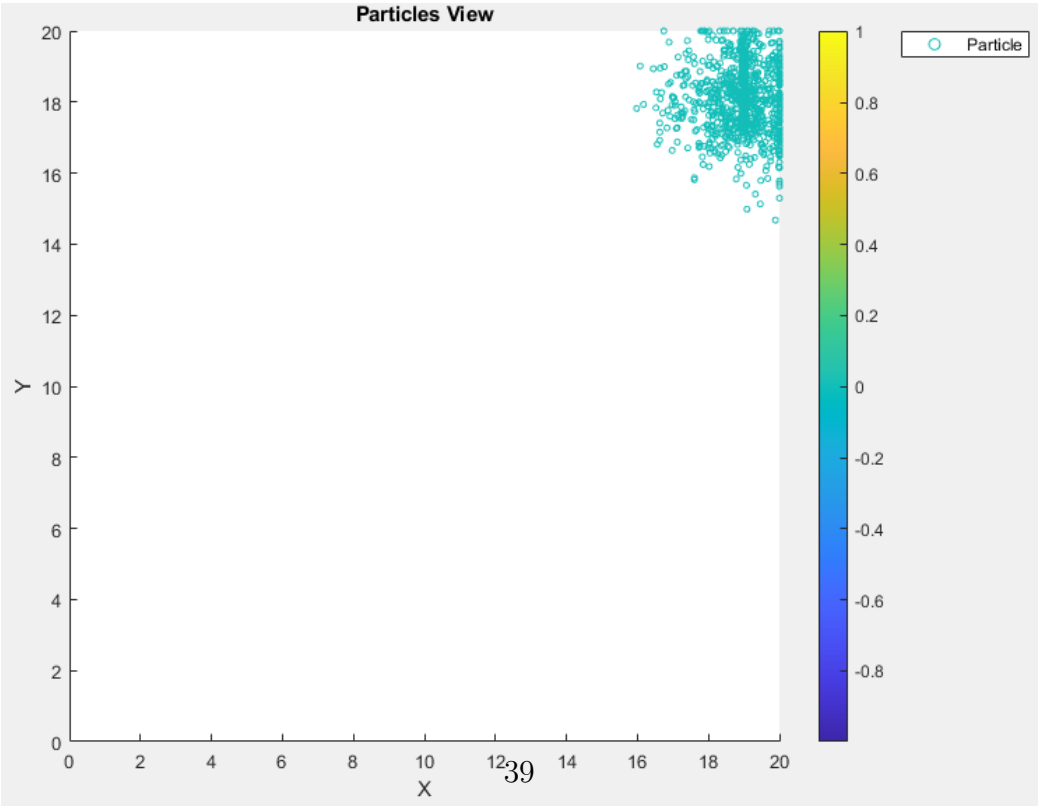

(b) The particle filter view.

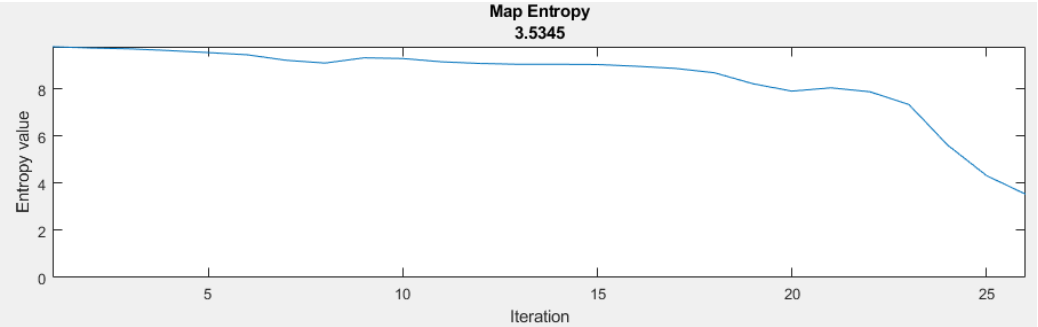

(c) The map entropy value.

Figure 5.6: The green line in the radiation map (a) shows the route that the robot takes to localize the radiation source. The particles in the particles view (b) converges to the source. The map entropy decreases as the iteration increases as expected.

estimation.The intensity point has a fixed radiation level at 30,000 counts. The background intensity is set to 1,000 counts [23]. Fig. 5.7 shows the test environment of this experiment.

5.4.2 Experimentation

We compare these three methods using traditional various intensity sampling methods (realistically and unrealistically) as in Fig. 5.8. We set the stopping criteria as *if the best estimate satisfies less than 5% error of all previous measurement points for 5 iterations. In addition, at least one measurement point must be less than 1.5m from estimation point to prevent early converges which leads to a wrong conclusion.* We tried to stop the algorithm earlier by excluding "at least one measurement point must be less than 1.5m from estimation point", but some results have high error because some incorrect estimate particles can fit to low measurement points.

Different sampling methods have different sampling counts. The algorithms results are shown in Table 5.2 – 5.4 and comparison plots in Fig. 5.9. From the tables and plots, the multiple landmarks method, both optimization and calculation, surpass the single landmark method in terms of position and intensity errors because the effect of adding more measurement points into the calculations. Thus, the calculation and optimization of the estimated intensity point is more accurate. The travel distance of multiple landmarks method is also less then the single landmark method because it use less measurement points to end the algorithm.

The optimization method of multiple landmarks intensity estimation

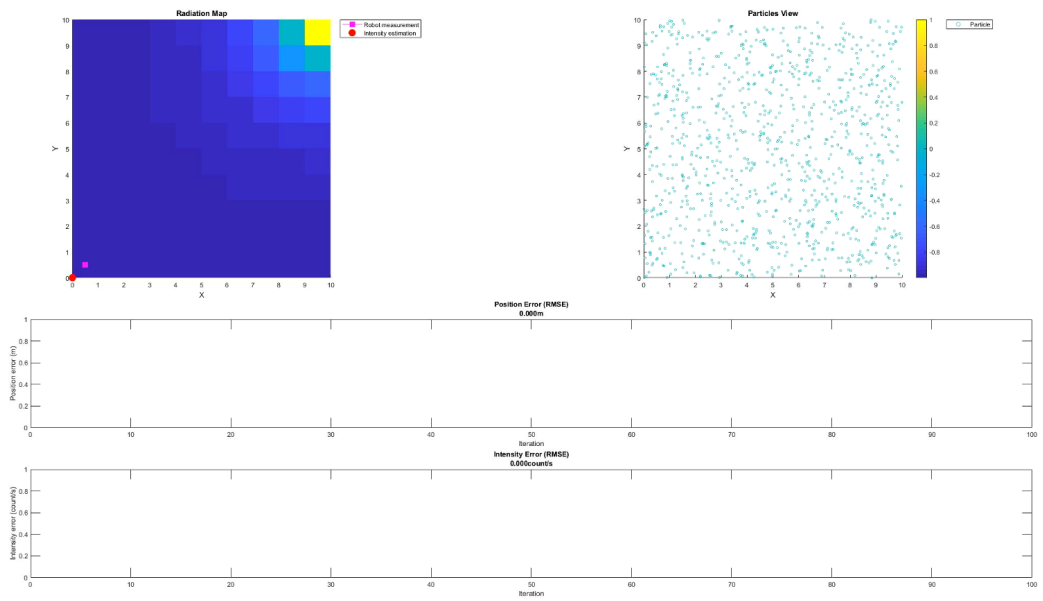

Figure 5.7: Test scenario of intensity estimation algorithms. The top left corner is the robot measurement points in magenta. The environment radiation level is indicated by the color (blue = low radiation, yellow = high radiation). The red dot is the intensity estimation location.

algorithm requires more computational power than the calculation one. Since the calculation can be done at once using matrix operation, it can be calculated quickly. The error in position and intensity of both methods are similar, which is expected. Therefore, the calculation method should be used instead of optimization one.

However, multiple landmarks methods require more memory to store the datapoints for calculation, which may not suit for small robots with limited memory capacity. We can limit the robot to memorize only important landmarks, for example, the newest n points of measurement.

The intensity sampling methods also play the important role. They are the factor of how far the robot travels until the algorithm meets the stopping criteria. From the tables and figures, source seeking movement use the least amount of measurement points but effectively gain the same estimation accuracy compared to other methods. We notice that the useful information is in the high intensity area, especially the measurement points around the intensity point. Thus, this method could be developed further into the realistic algorithm, for example, a robot must try to find the highest gredient direction to meet the intensity point fast.

Now, we want to reduce the memory stored in the robot to make the

Sampling method	Measurement Count	Travel Distance	Position Error (m)	Intensity Error (count)	Computation Time
Snake scan row	95	93	0.01	7.57	33.74
Snake scan column	96	94	0.14	1115.21	33.59
Spiral pattern outter	25	23	0.05	1541.11	8.86
Spiral pattern inner	54	52	0.23	1361.83	17.69
Source seeking	14	16.31	0.09	1204.16	6.25
Max to min	16	25.43	0.17	3148.44	6
Min to max	100	357.52	0.05	278.22	35.73
Random	34	158.56	0.23	1318.75	11.76
All measurement	-	-	-	-	-
		Mean	0.12	1246.91	

Table 5.2: Single Landmark Intensity Estimation

calculation faster and use more efficienly memory capacity. We select the best sampling method, which is the source seeking method, and the efficiency intensity estimation method, which is the multiple landmarks intensity estimation using calculation, then try to experiment with different memory capacity of the robot from maximum of 2 points to 14 points as shown in Fig.5.10. The result shows that 2 measurement points gives highest error. The possible reason is that it gives too little information surround the intensity point. 3 measurement points onward gives a better performance. From the figure, we recommend 4 measurement points which has the lowest memory (4) but the performance is good. More measurement points do not mean the result is better, since their calculation must include low intensity points, which may introduce some errors (9-14). Notice that, the number of measurement counts depend on how particles randomly generate at the intensity points which can effect the computation time.

5.5 Global Map Decomposition Analysis

5.5.1 Environment Settings

In the experiment, the environment is in a square shape, $40 \times 40\text{m}^2$ with no obstacle. We test each case with 3 different scenarios as in Fig.5.11, which are 4 sources at top right, 4 sources at bottom left and 9 sources equally distributed on the map. Each intensity has a random intensity between 20,000 to 50,000 counts. The background intensity is set to 1,000 counts [23].

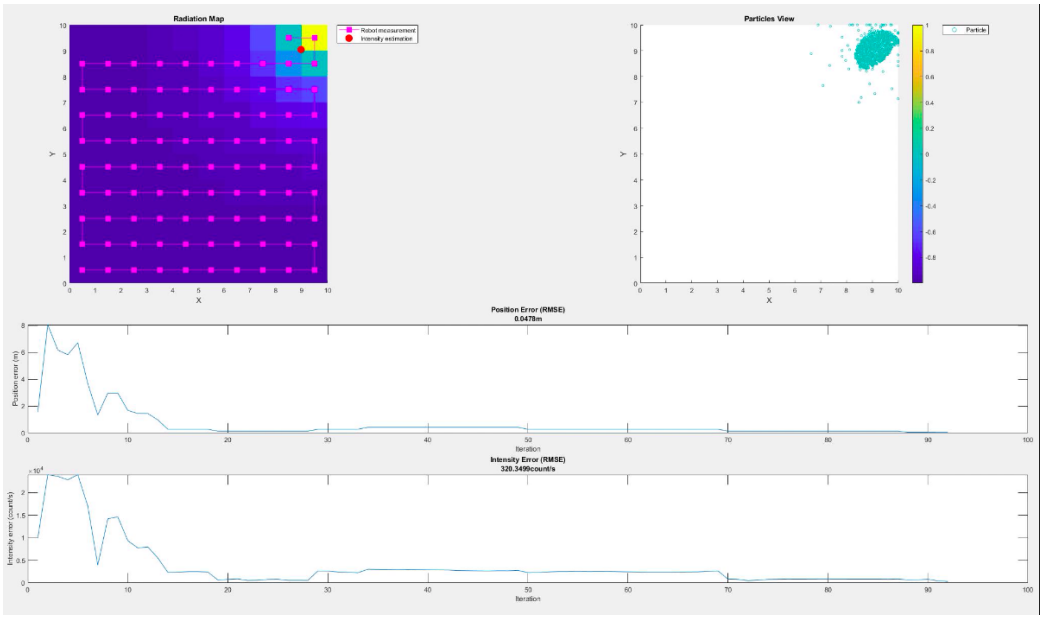

(a) Snake scan row sampling method.

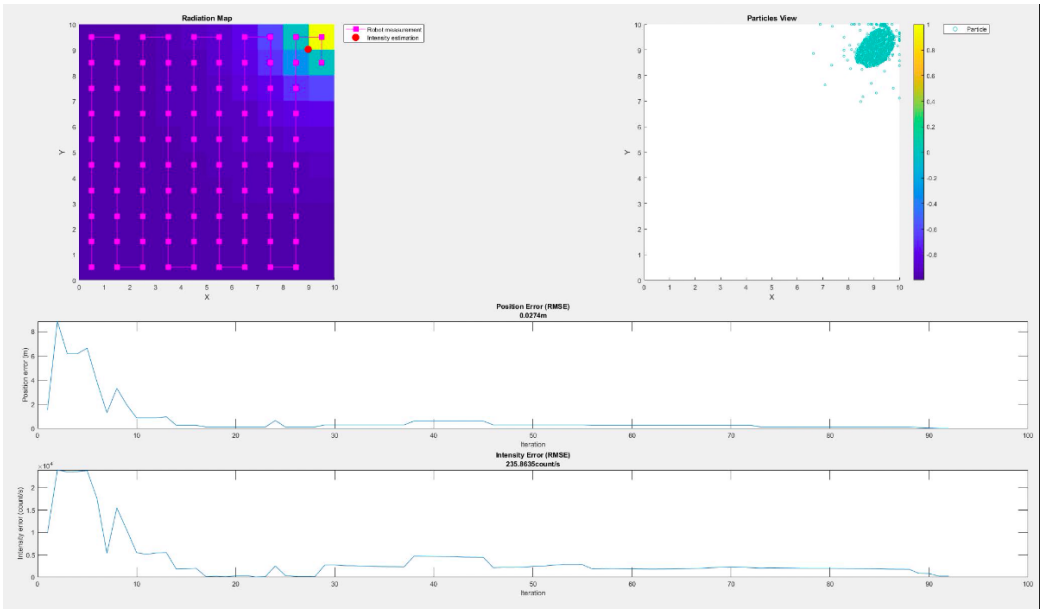

(b) Snake scan column sampling method.

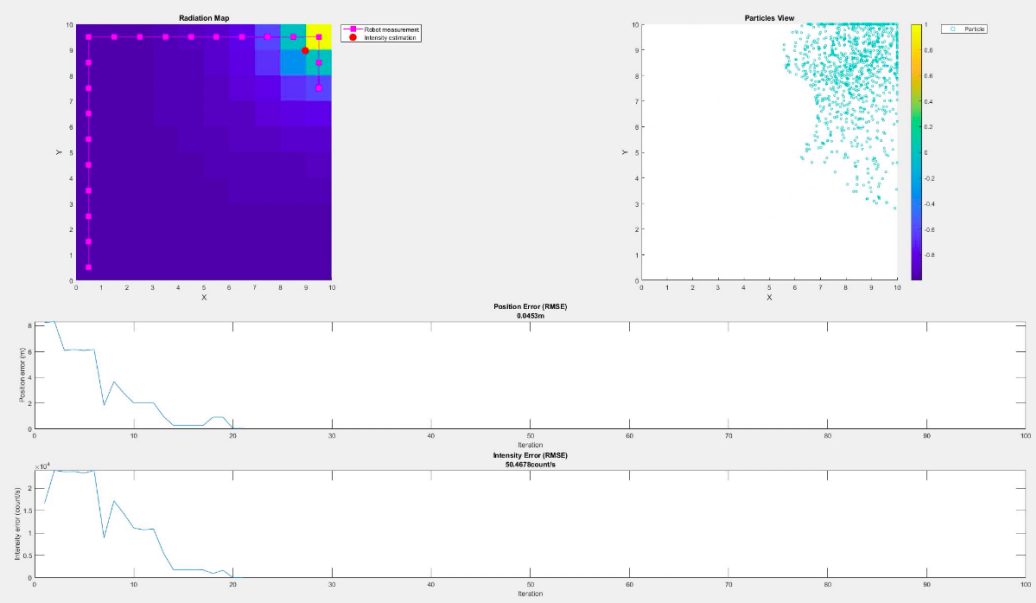

(c) Spiral pattern from outter layer sampling method.

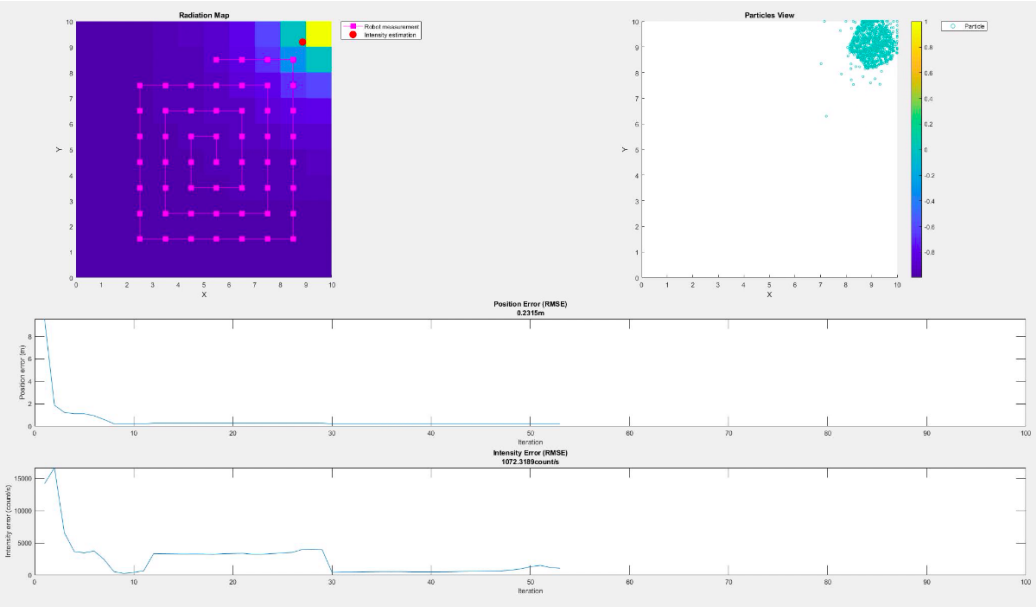

(d) Spiral pattern from inner layer sampling method.

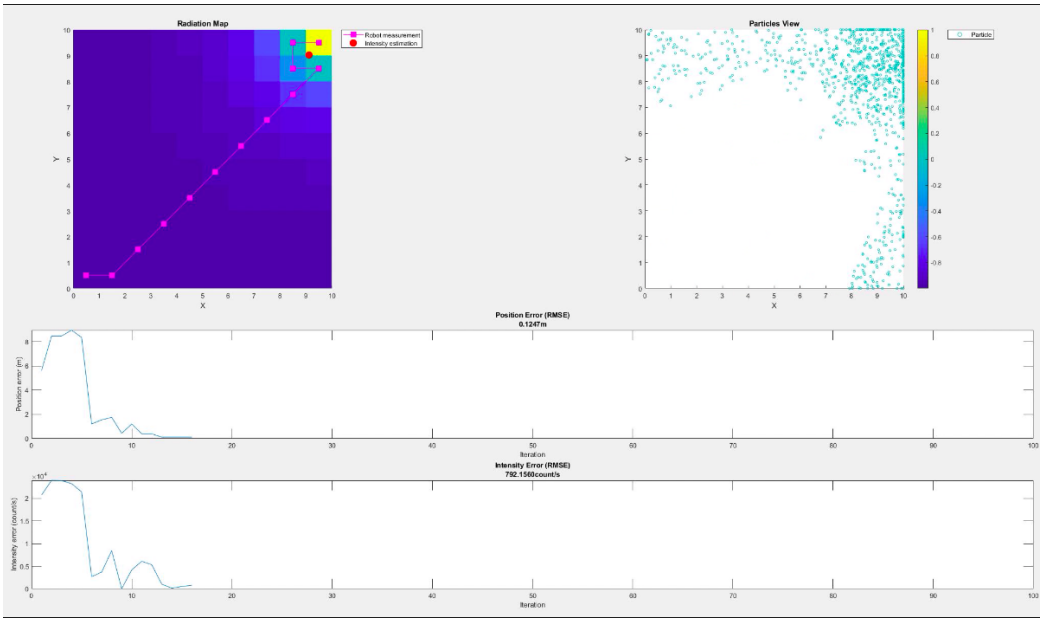

(e) Source seeking sampling method.

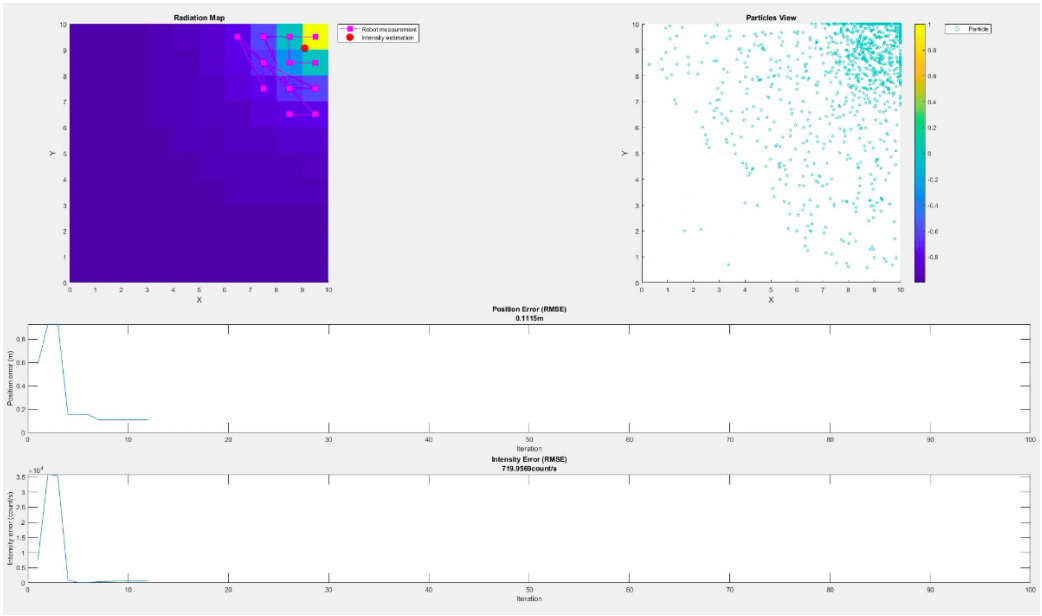

(f) Max to min sampling method.

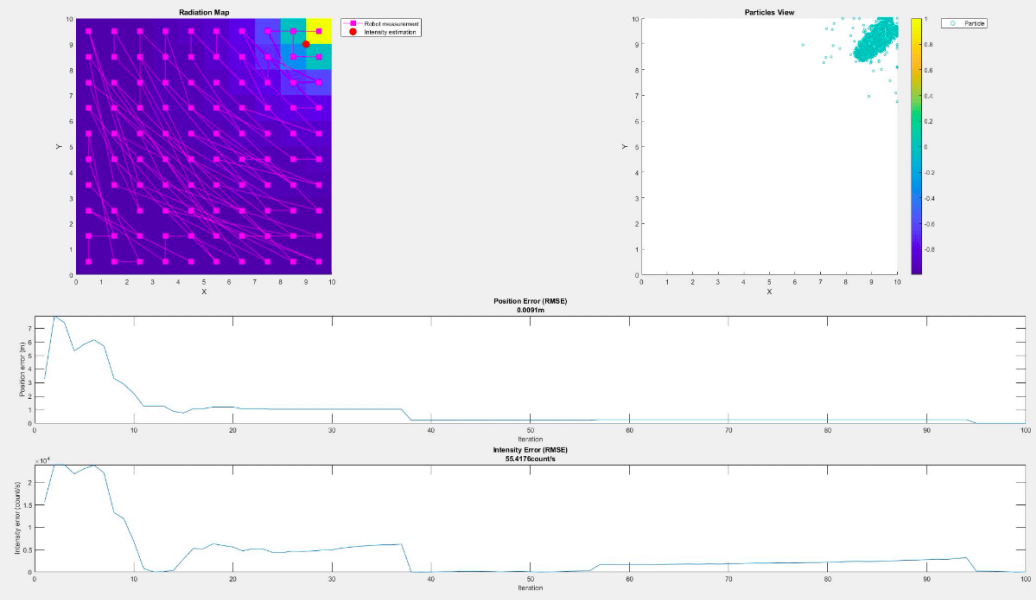

(g) Min to max sampling method.

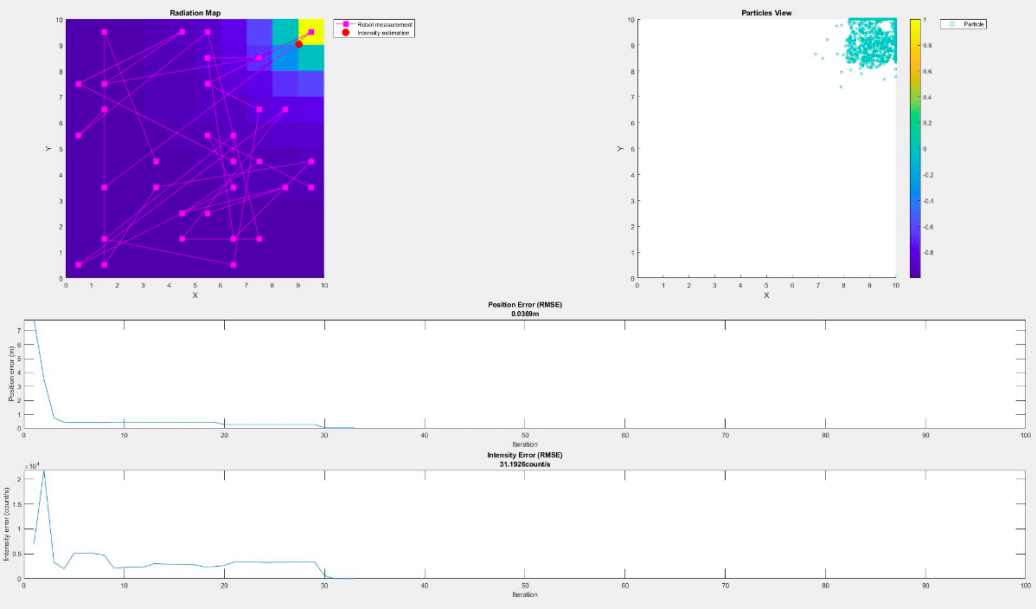

(h) Ramdom sampling method.

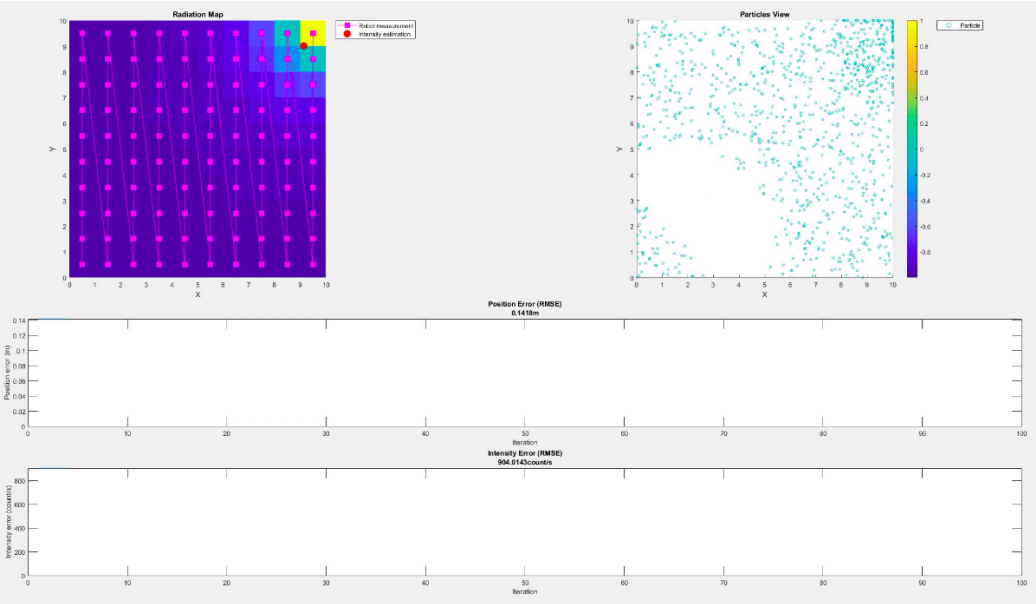

(i) All measurement at once.

Figure 5.8: Sampling methods of radiation estimation algorithms.

Sampling method	Measurement Count	Travel Distance	Position Error (m)	Intensity Error (count)	Computation Time
Snake scan row	93	91	0.05	370.2	864.51
Snake scan column	93	91	0.03	259.3	860.23
Spiral pattern outter	22	20	0.05	10.96	196.01
Spiral pattern inner	54	52	0.23	1223.43	482.68
Source seeking	14	16.31	0.12	870.12	146.26
Max to min	28	61.89	0.14	249.38	130.46
Min to max	100	357.52	0.01	33.29	915.7
Random	34	158.56	0.04	139.34	321.27
All measurement	1	171.5	0.14	962.93	42.64
		Mean	0.09	457.66	

Table 5.3: Multiple Landmarks Intensity Estimation using Optimization

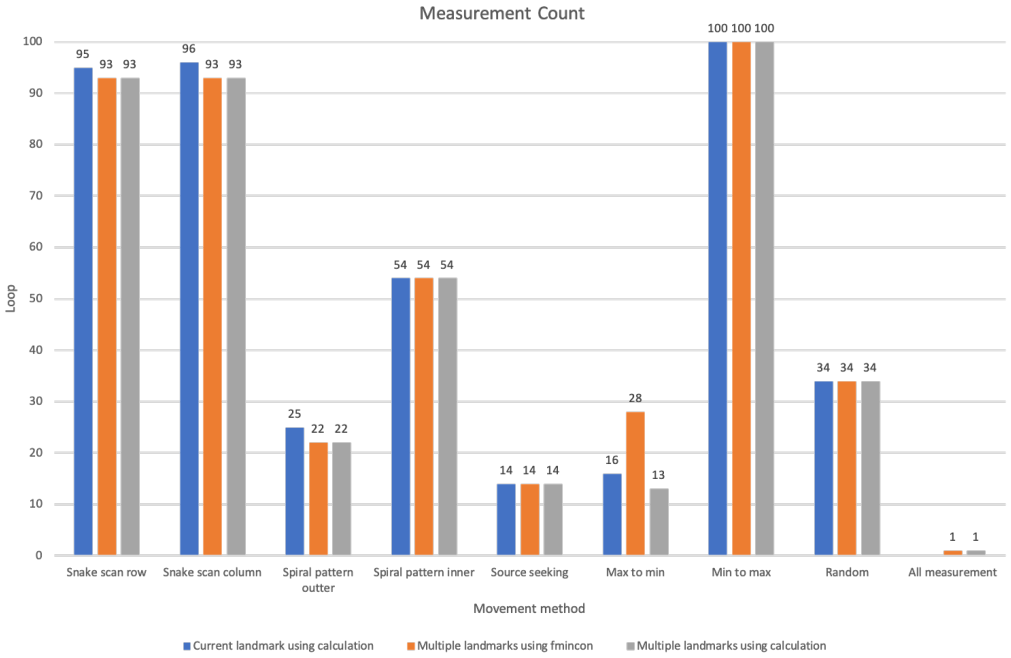

(a) Measurement counts comparison.

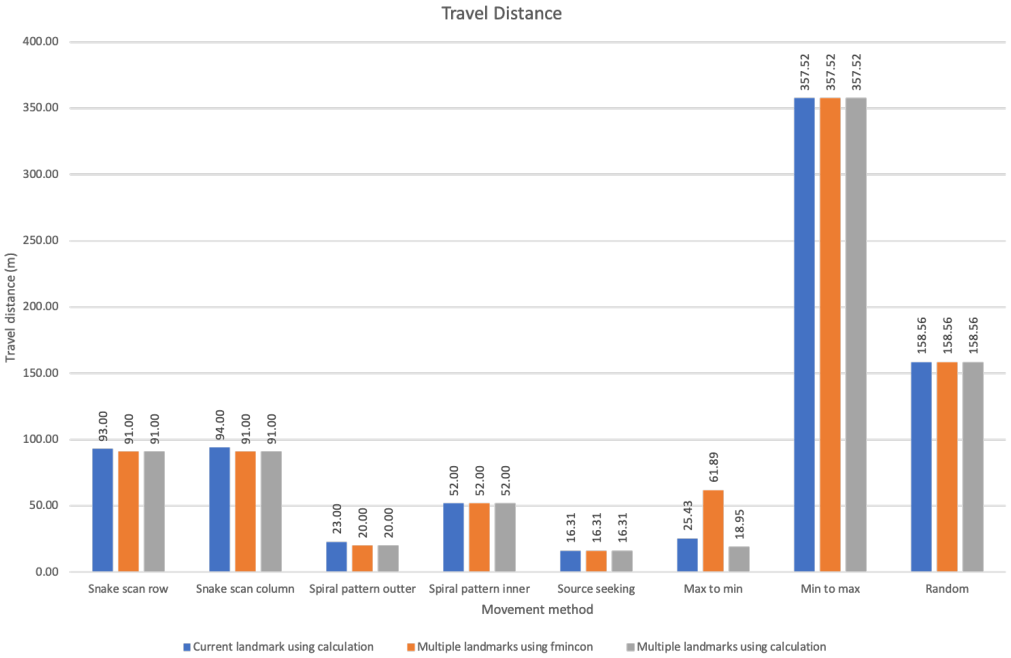

(b) Travel distance comparison.

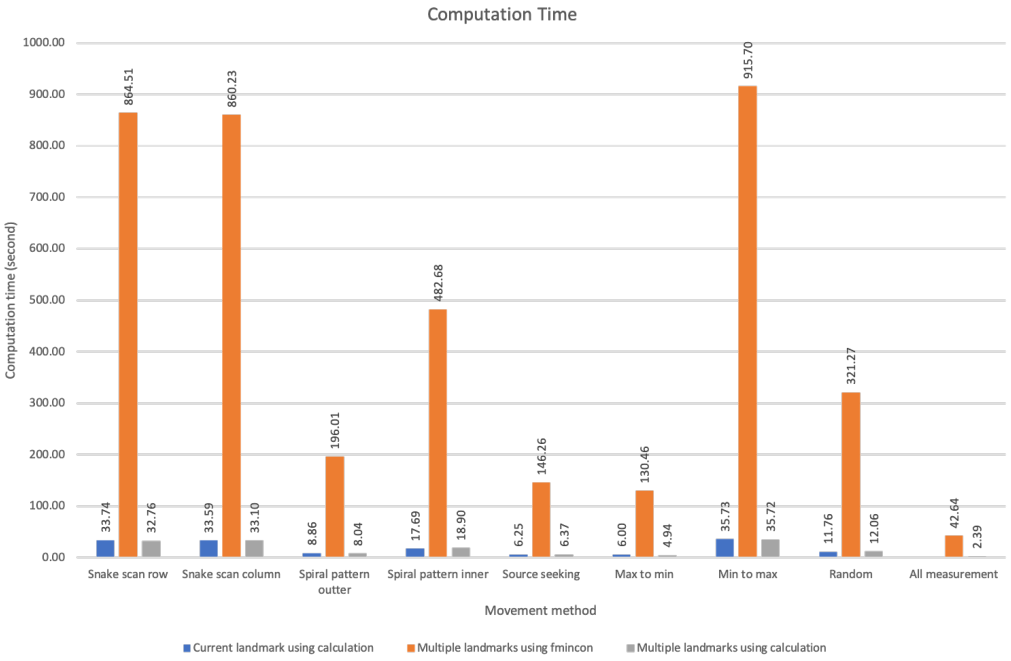

(c) Computation time comparison.

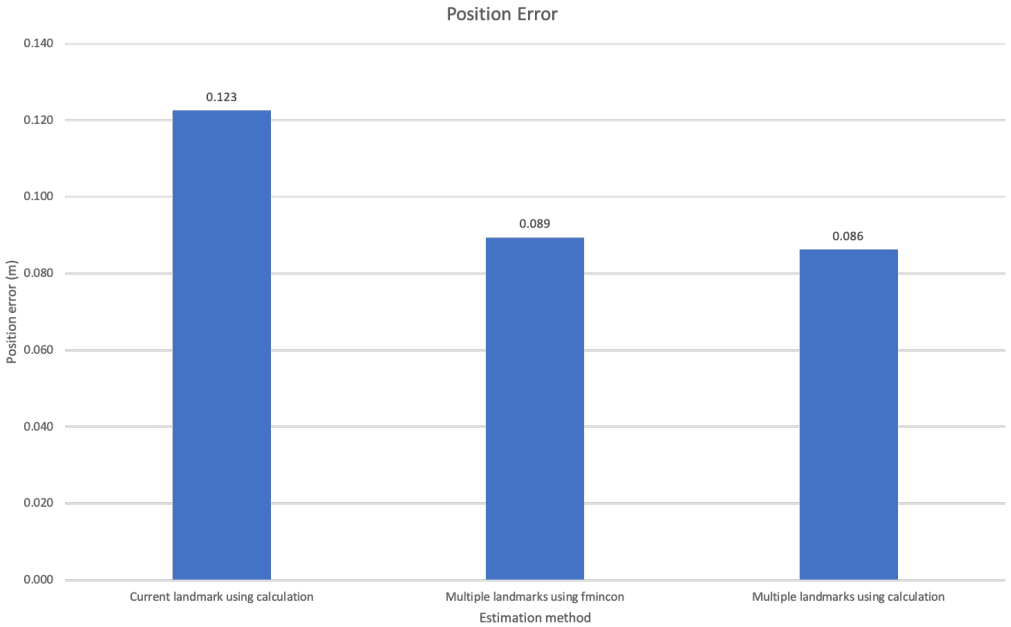

(d) Position error comparison.

Sampling method	Measurement Count	Travel Distance	Position Error (m)	Intensity Error (count)	Computation Time
Snake scan row	93	91	0.05	320.35	32.76
Snake scan column	93	91	0.03	235.86	33.1
Spiral pattern outter	22	20	0.05	50.47	8.04
Spiral pattern inner	54	52	0.23	1072.32	18.9
Source seeking	14	16.31	0.12	792.16	6.37
Max to min	13	18.95	0.11	719.96	4.94
Min to max	100	357.52	0.01	55.42	35.72
Random	34	158.56	0.04	31.19	12.06
All measurement	1	171.5	0.14	904.01	2.39
		Mean	0.09	464.64	

Table 5.4: Multiple Landmarks Intensity Estimation using Calculation

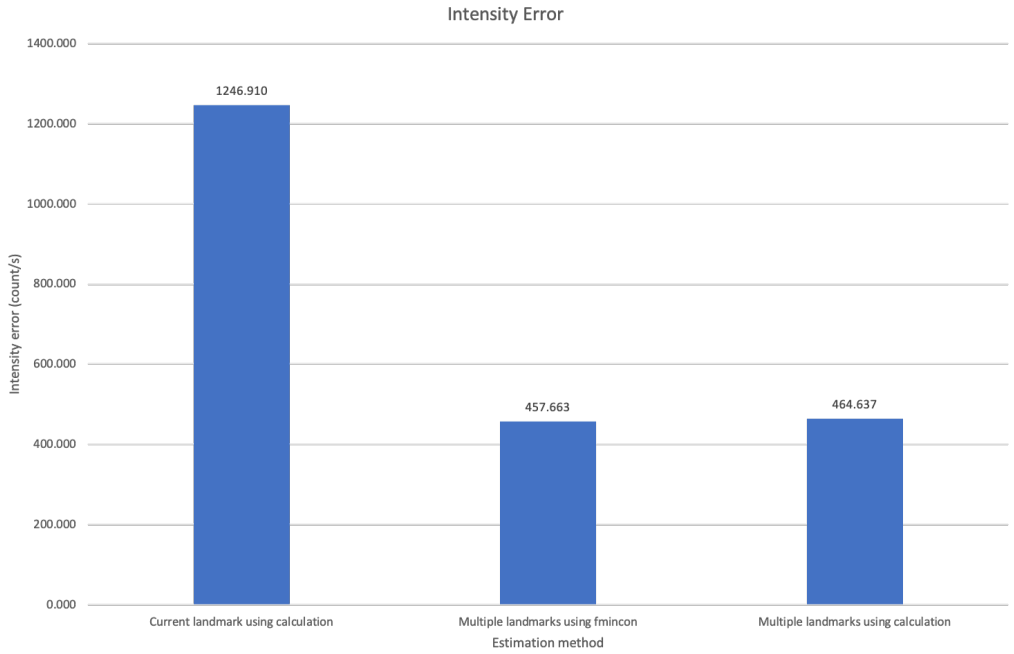

(e) Intensity error comparison.

Figure 5.9: The comparison between estimation methods and measurement sampling methods.

(a) Measurement counts comparison.

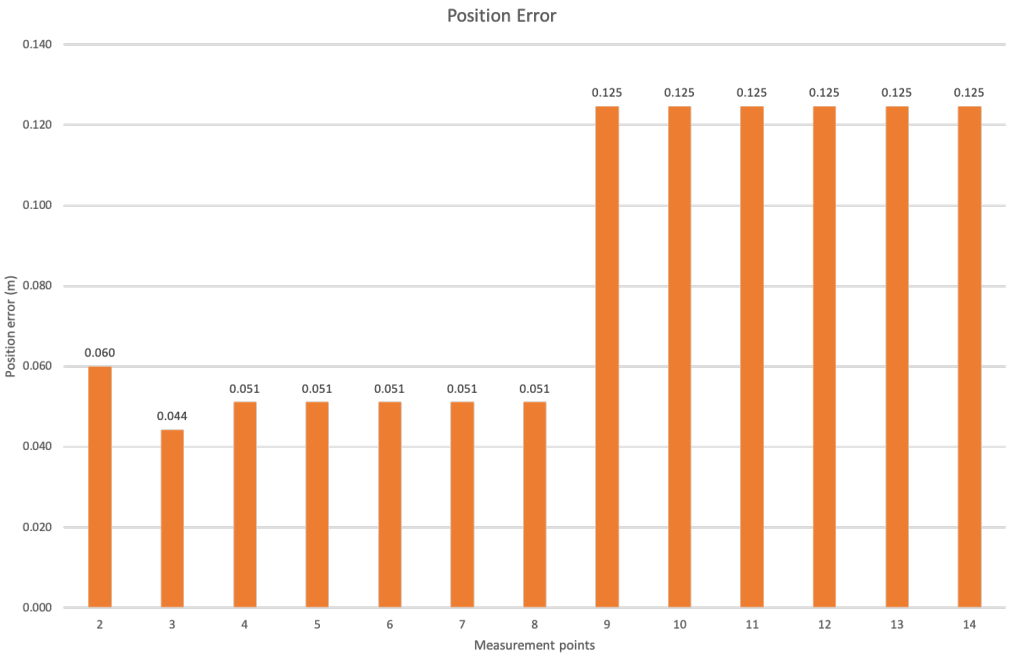

(b) Position error comparison.

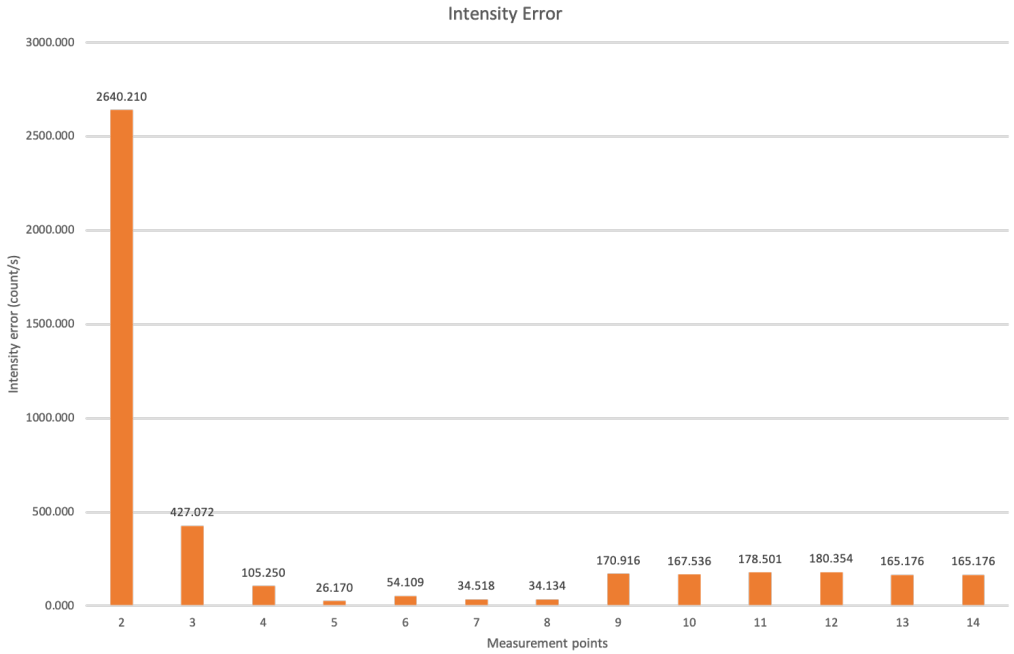

(c) Intensity error comparison.

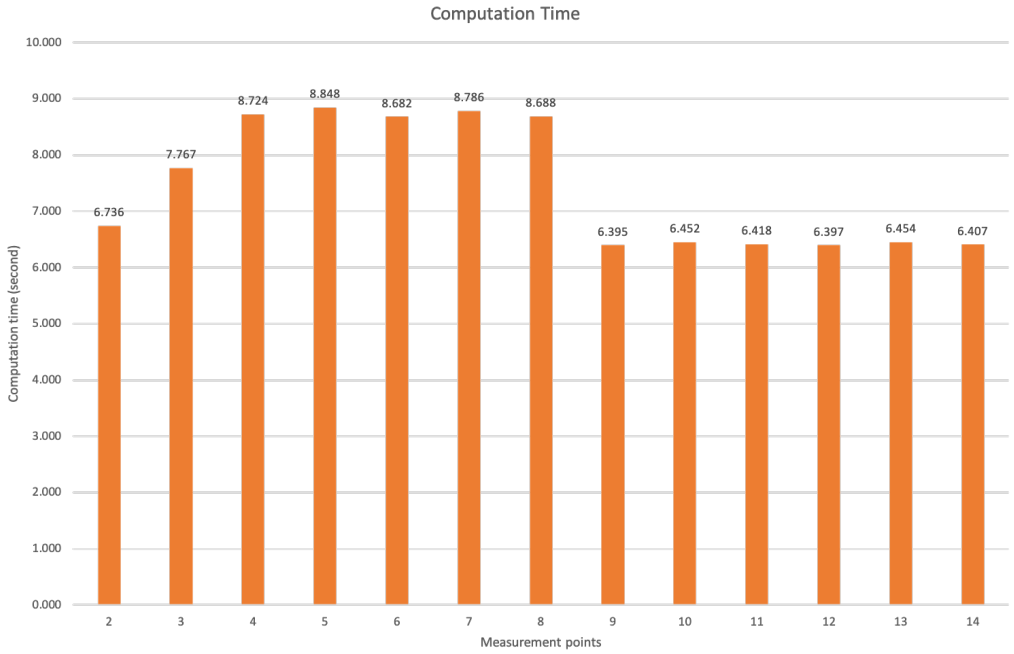

(d) Computation time comparison.

Figure 5.10: Using the source seeking method and multiple landmarks intensity estimation using calculation. We compare between different memory capacity of the robot.

5.5.2 Robots Settings

A robot in the test knows its location using a GPS with assumption that the GPS reading has no error. The background intensity is known by the robot. There are 100 particles initialized. The robot will measure the radiation after it travel for 0.5m. The detection threshold is set to 2,000 counts. If the measurement surpasses the threshold, the particle filter will start to converge to the estimate states. For exploration part, a robot has to explore the environment in order to determine all sources. The area pruning is set to one isolated cell. The minimum weight threshold of RBE pruning is set to e^{-20} within 5m around the robot. For multi-robot systems, robots are able to communicate with a limited distance without delay and packet loss. Fig. 5.4 shows an example of a simulation of multiple radiation sources mapping using 3 robots, together with their correspond exploration grid maps.

5.5.3 Experimentation

At this point, we compare the accuracy of the final intensity map using source separation algorithm and without using one. We use the test scenario in Fig. 5.15 as a ground truth. Table 5.5 shows the comparison at the radiation source. The raw measurements of each source are fused with other sources intensity, thus, the raw measurements are much higher than the ground truth. After we apply the sources separation algorithm, the sources now are closer to the ground truth. In this case, we are able to increase the accuracy from 94.34% to 96.98%.

5.5.4 Indoor Localization Uncertainty Experimentation

To make the experimentation more realistic, the introduction of uncertainty is one of the important factors. In this experiment, we introduce the uncertainty in robot self-localization. The robot will read the current position with some error, according to [75], the error of the practical SLAM-based self localization and mapping is around 0.017-0.047m. In the experiment we will

	Sources Intensity			
Algorithm/Source	1	2	3	4
Ground truth	40000	30000	35000	45000
Raw measurement	42396	32322	36665	46877
Sources separation algorithm	41505	31278	35643	46008

Table 5.5: Source Separation Algorithm Comparison

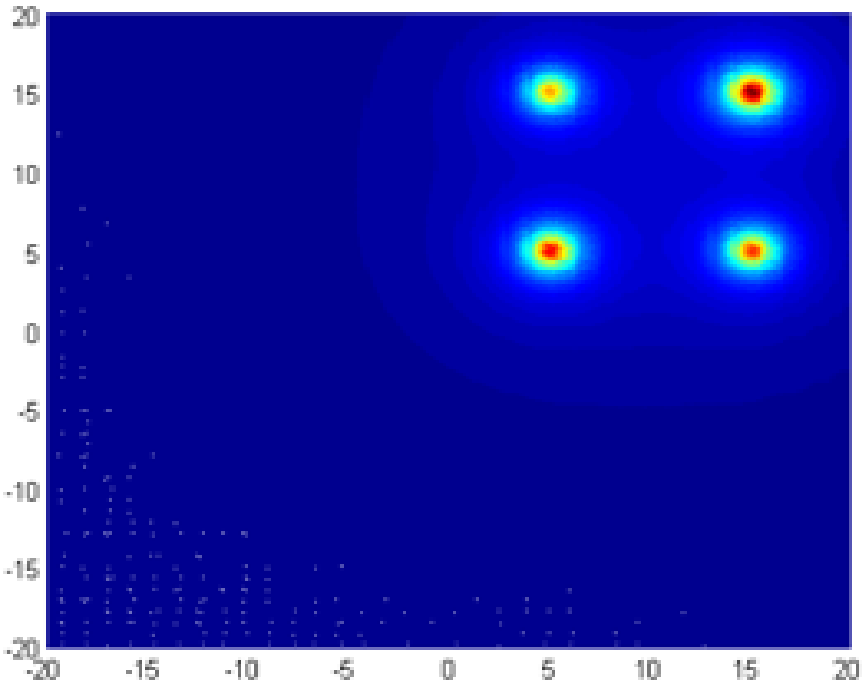
20
15
10
5
0
-5
-10
-15
-20
-20
-15
-10
-5
0
5
10
15
20

(a)

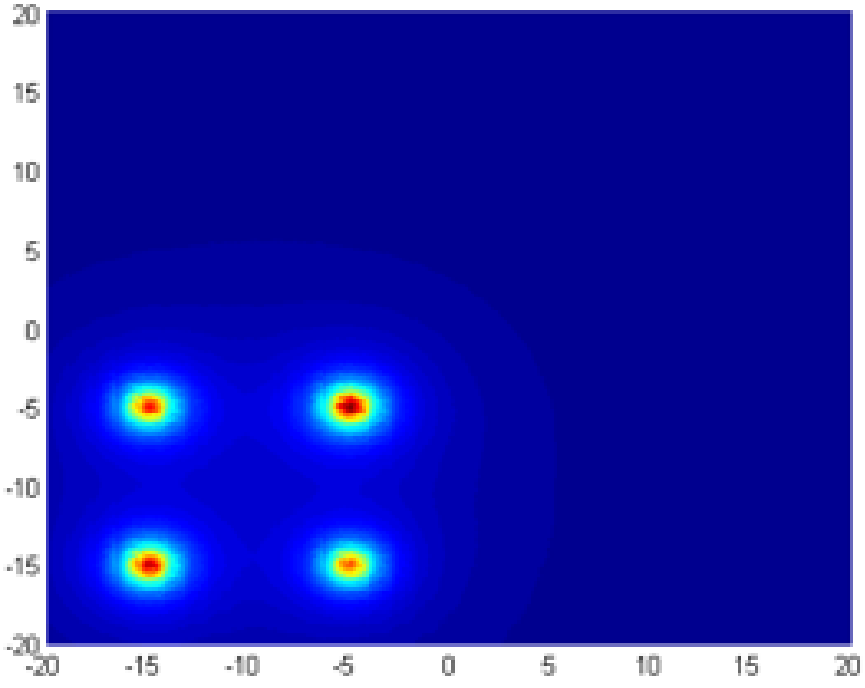
20
15
10
5
0
-5
-10
-15
-20
-20
-15
-10
-5
0
5
10
15
20

(b)

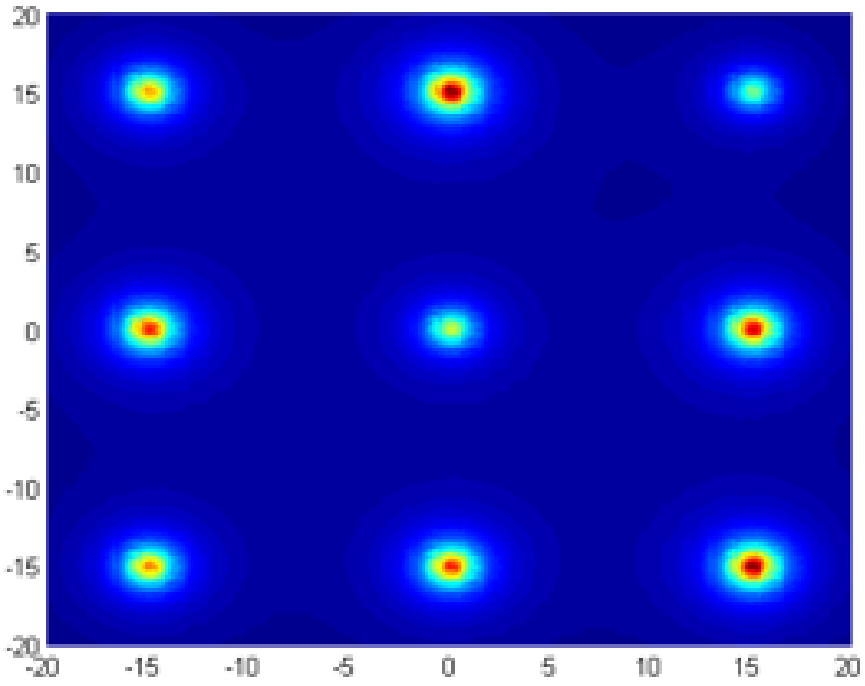

(c)

Figure 5.11: Test scenarios: (a) 4 sources at top right corner, (b) 4 sources at bottom left corner, (c) 9 sources equally distributed.

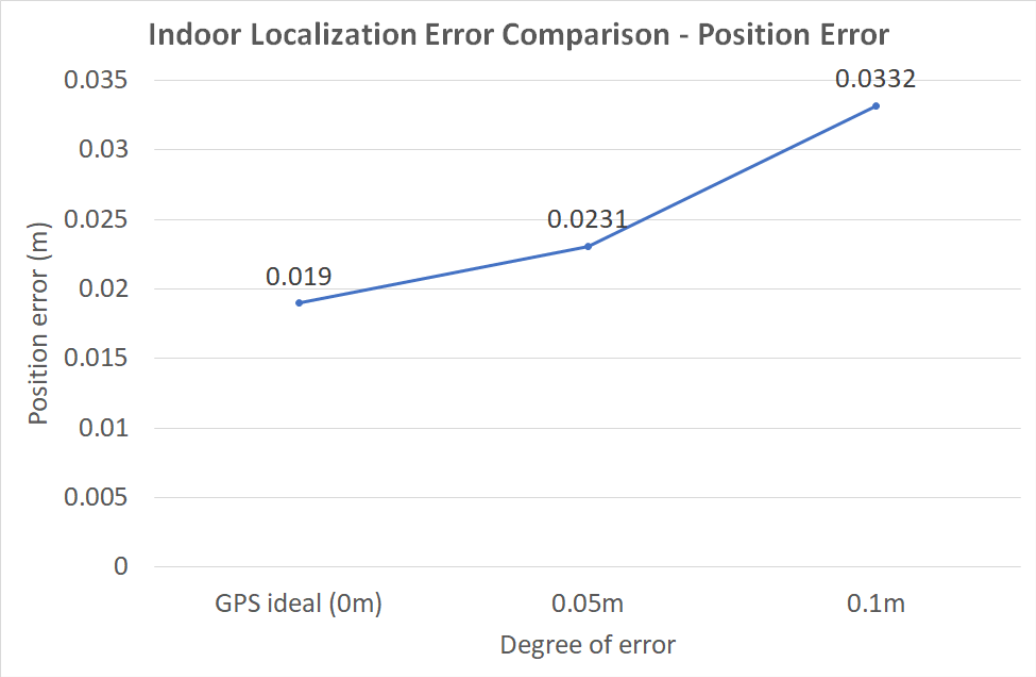

Figure 5.12: The comparison of position error between the ideal case (0m error), 0.05m, and 0.1m error that were introduced to the measurement reading.

compare the result of 0, 0.05, 0.1m error. The error will be added using the normal distribution random function. Fig. 5.12 and 5.13 show the result of the experiment. The ideal case with no error gives the highest accuracy of the location of the source and intensity. When the error is introduced, the accuracy in the intensity estimation decreases. The main reason is that error makes the particle filter function predicts the result with some error which is expected. However, the particle filter function is tolerate to the error of this degree. A dramatic shift in the error value would collaspe the prediction function and not reflect the real world situation.

5.6 Exploration Algorithms Comparison

One of the factors that impact the travel distance of robots is how they select frontier cells. In this proposed method, we use two criteria which are the distance between a robot and frontier cells and the direction of intensity gradient. In addition, pruning processes which are low priority flag and RBE pruning are utilized to further decrease the travel distance.

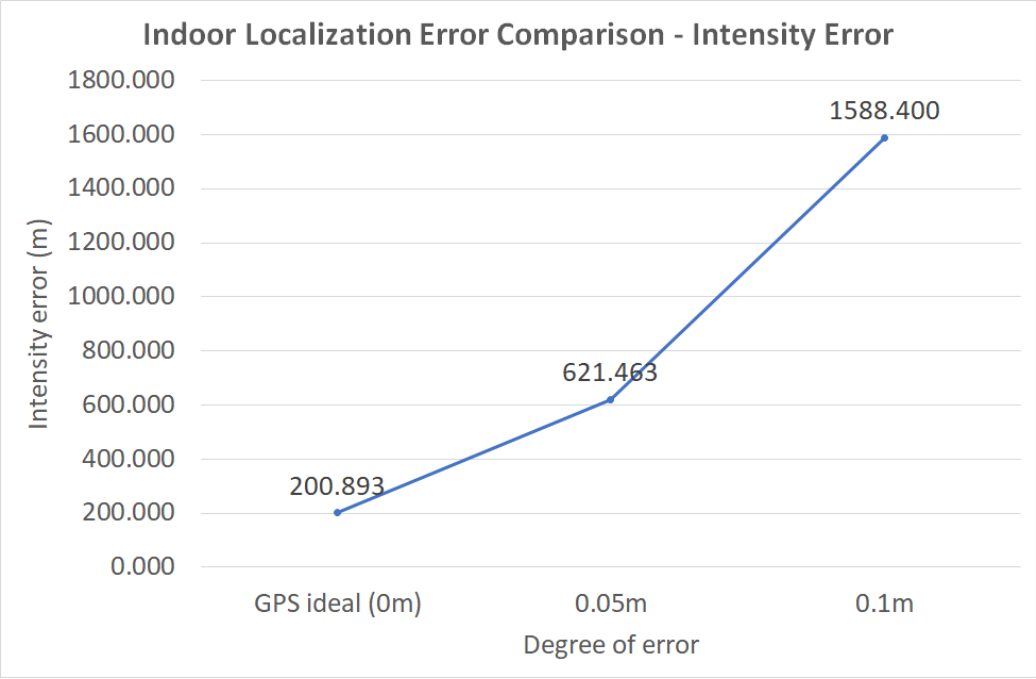

Figure 5.13: The comparison of intensity error between the ideal case (0m error), 0.05m, and 0.1m error that were introduced to the measurement reading.

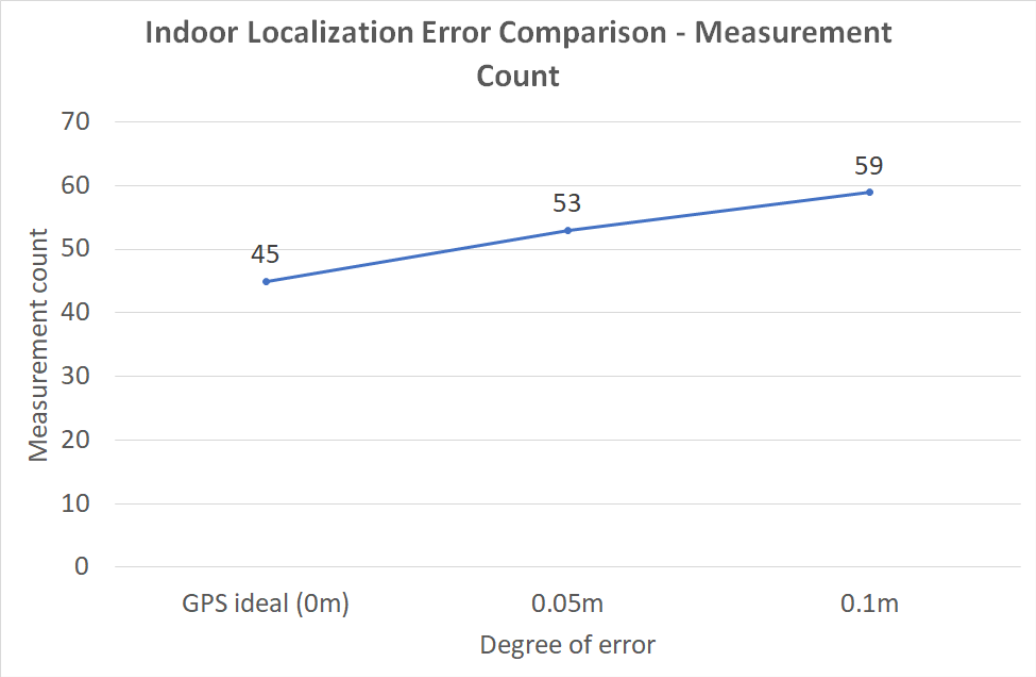

Figure 5.14: The comparison of measurement count between the ideal case (0m error), 0.05m, and 0.1m error that were introduced to the measurement reading.

We compare our proposed method with Frontier-based methods using distance and increase gradient direction as: (1) RBE and random pruning methods, (2) Only random pruning method. The conventional methods as (3) Spiral pattern (4) Frontier-based using only distance as the target point selection (5) Lawn mower pattern. The settings of the environment and robots are the same as 5.5.

We can see that our proposed method surpass all conventional methods (frontier-based exploration using minimum distance only, spiral pattern and lawn mower pattern). It also perform better than RBE and random pruning methods which indicates that the pruning using low priority flag helps decrease the traveling distance drastically.

The frontier-based exploration using increase gradient direction also helps in quickly search the source by comparison between the methods that apply: (1), (2) and (3) with the one that did not apply: (4), (5).

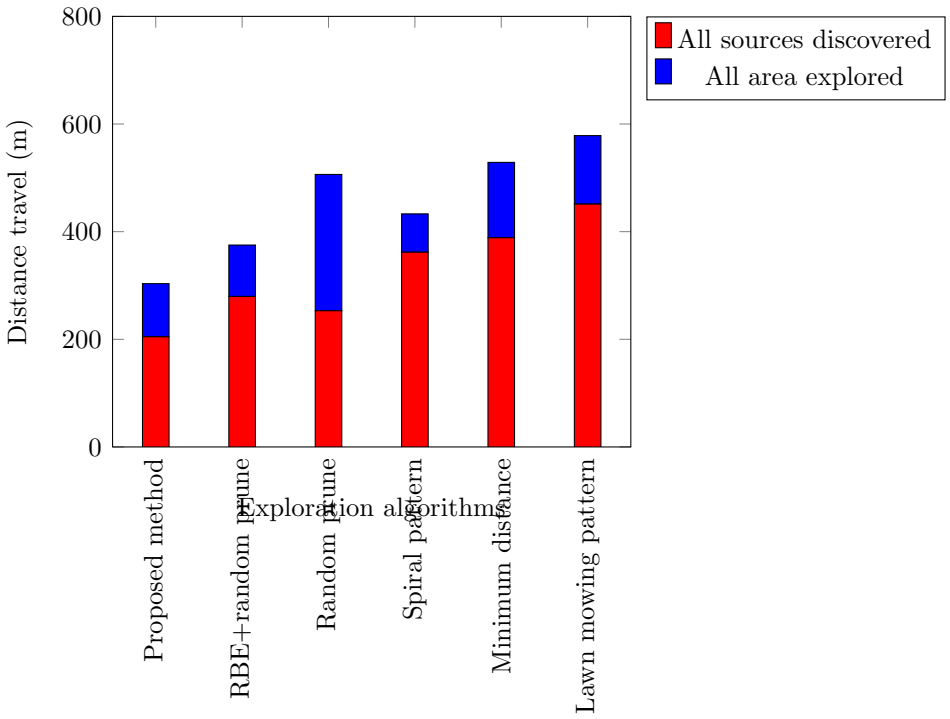

Figure 5.15: Algorithms performance in Scenario I.

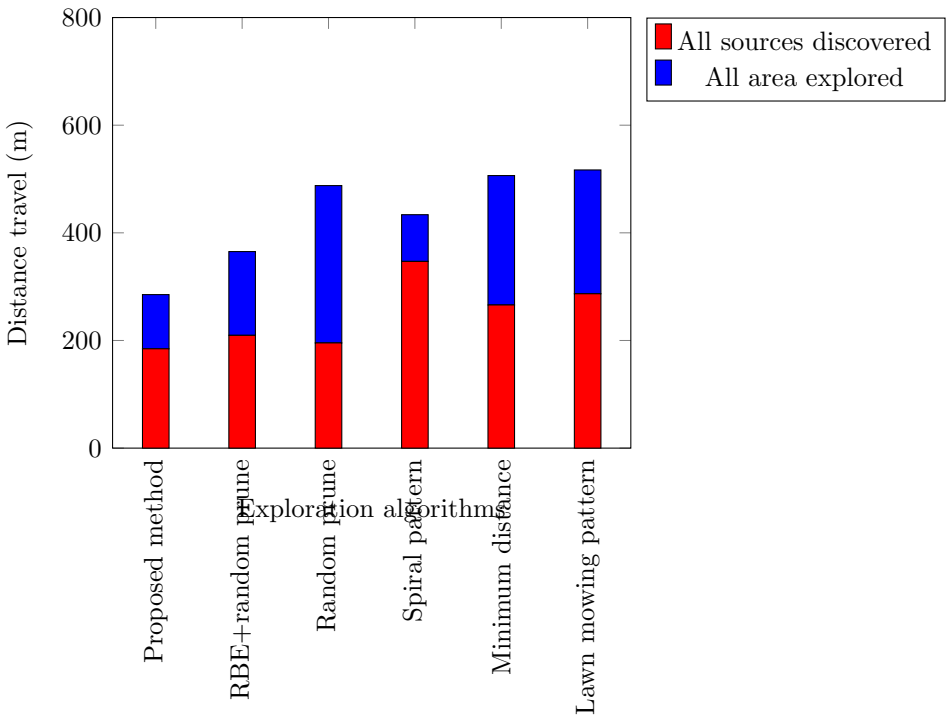

Figure 5.16: Algorithms performance in Scenario II.

5.7 Multi-robot System Extension

The extension of single robot case to multiple robots case is expected to reduce the maximum exploration time. We perform the experiment by increasing the number of robots from single robot up to 7 robots and the communication ranges for all cases are fixed at 5m. The experiment has been performed for 150 times using 5 randomly generated radioactive sources. From Fig. 5.18, the required distance to finish exploration decreases when the number of robots increase as expected. In this case, there information sharing is happens by chance. Thus, the worst case scenario that might happen is each robot explores all area by its own. The mapping errors of all cases are at average of 4.513% in intensity and 0.15m on position.

For the effect of communication range of multiple robot, we compare a single robot case and 3 robots case in the environment that have 5 random generated intensity sources. The experiment has been performed for 150 times. Fig. 5.19 shows the comparison of the distance travel by robots between a single robot and 3 robots with variation in communication range. In conclusion, the more robots, the faster process, and the larger communication

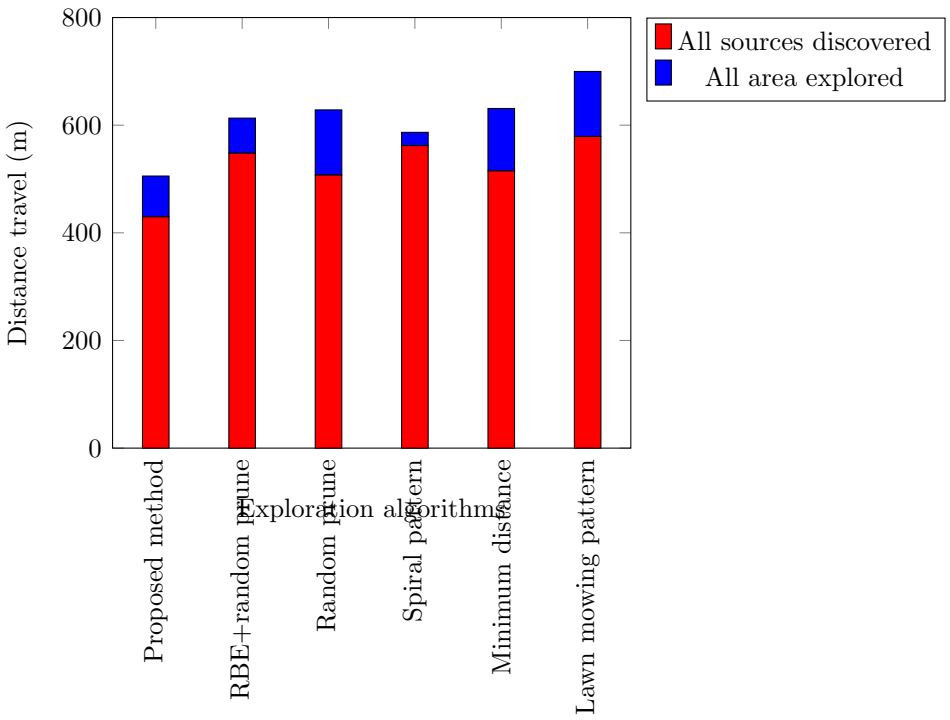

Figure 5.17: Algorithms performance in Scenario III.

range, the lower number of overall travel distance. Notice that at the lowest communication range, the maximum travel distance of the 3 robots case is almost the same as the result of the single robot case. For other cases the number of maximum distance may be larger which depends on how many time robots exchange information.

5.8 Simulation in a Non-geometric Environment

5.8.1 Environment Settings

The geometric environment is a good example of showing how the robot perform in ideal condition. In this case, we experiment with the recorded environment. The major different between geometric environment and real environment is that, robots cannot directly go to the point that they want in a direct path. In this case, we simplify the problem by making no distortion from radiation sources, *i.e.* the radiation sources does not change value when they are inside the simulated building. Fig. 5.21 shows the simulated map of

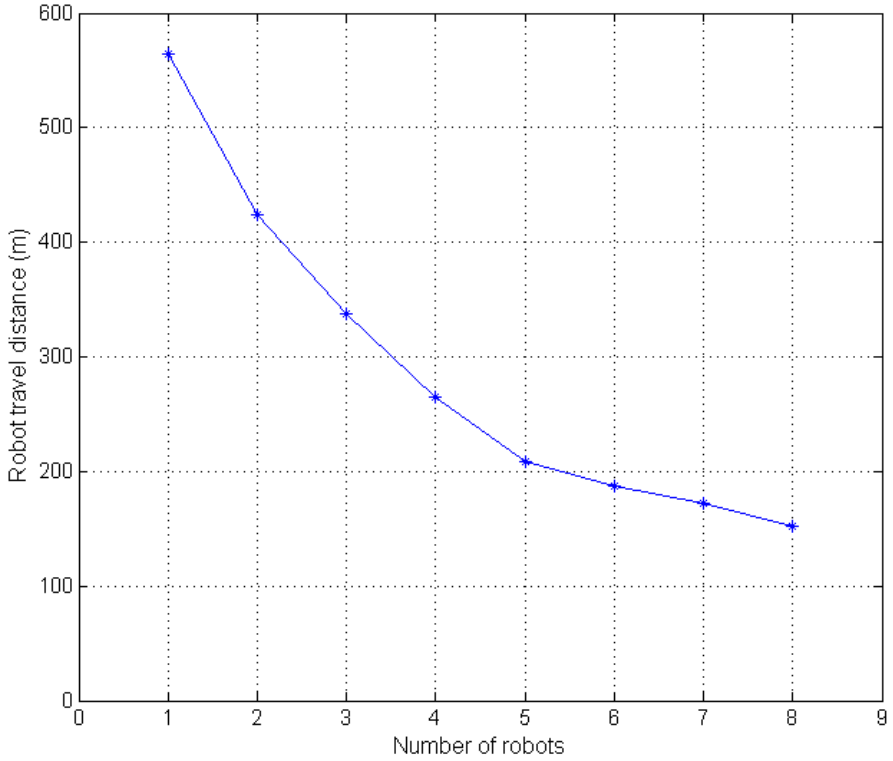

Figure 5.18: Comparison between number of robots.

the Freiburg indoor building 079 that we use as a test map in the experiment. The map was recorded using a robot with SLAM capability [76]. To analyze the map, the white area is a free space, the black area is an occupied space and the grey area is an unknown space. Thus, we can build the map for our robot according to this information. We assume that there are three radiation sources with a random strength between 30,000 to 50,000 counts inside the free space area of the building. The background radiation is set to 1,000 counts.

5.8.2 Robot Settings

A robot in the test knows its location using a GPS with assumption that the GPS reading has no error. The background intensity is known by the robot. There are 1000 particles initialized. The robot will measure the radiation after it travel for 1m. The detection threshold is set to 2,000 counts. If the measurement surpasses the threshold, the particle filter will start to

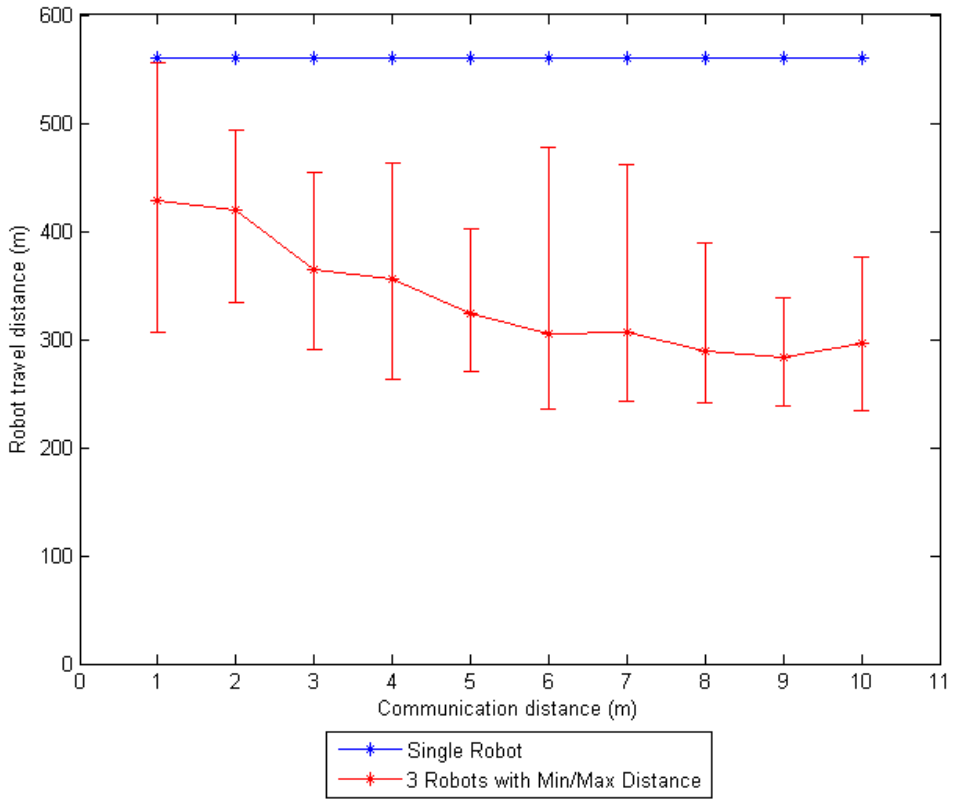

Figure 5.19: Multiple sources experiment: comparison between travel distance vs number of robot with variation in communication range. The vertical bars in the 3 robots case indicate the maximum and the minimum number of travel distance.

converge to the estimate states. For exploration part, a robot has to explore the environment in order to determine all sources. For multi-robot systems, robots are able to communicate with a limited distance without delay and packet loss.

5.8.2.1 Probabilistic Roadmap (PRM)

However, the robot cannot move directly from point A to point B like they can in a geometric environment. We apply a path planning algorithm for the robot to find the way from point A to point B inside the building. A probabilistic roadmap (PRM) is employed to help the robot navigation in the simulated environment.

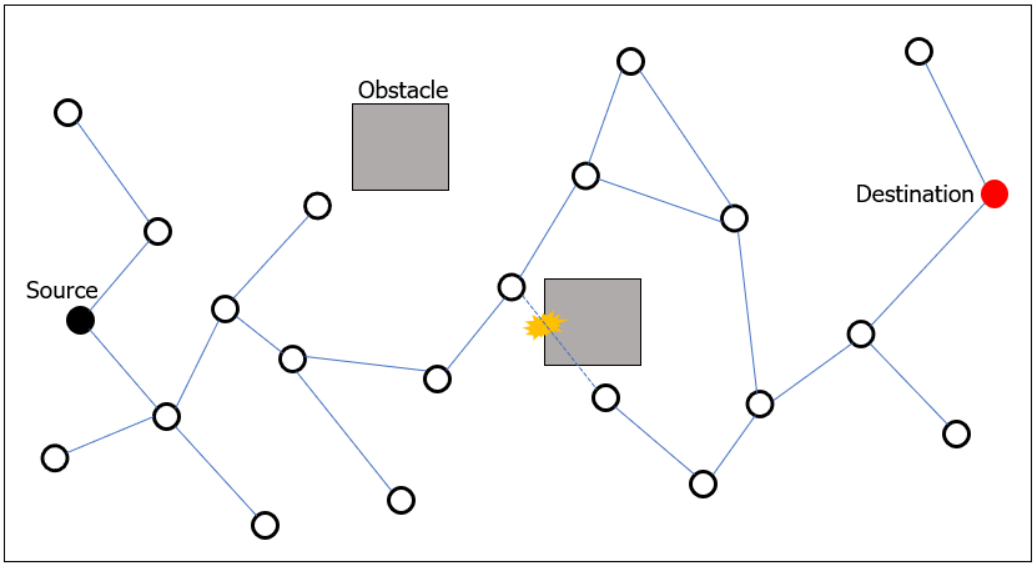

Figure 5.20: Inside a configuration space $\mathcal{C}$, the algorithm samples nodes in a free space $\mathcal{C}_{free}$. Then, the algtorithm will try to connect these nodes to form a graph. The obstacle $\mathcal{C}_{obs}$ is the area that the nodes cannot be connected.

Given the configuration space $\mathcal{C}$ as a space of all possible placement of any objects. The degree of movement of an object corresponds to a dimension of $\mathcal{C}$. Obstacles are consider a forbidden area which the robot cannot move through inside the configuration sapce, we willl called it $\mathcal{C}_{obs}$. We will form a path from the start position to the goal position, which must be a collision free path *e.g.* the path must not intersect with obstacles $\mathcal{C}_{obs}$. The free area that the path can be generated inside the configuration space $\mathcal{C}$, denoted as $\mathcal{C}_{free}$.

There are many renditions of probabilistic roadmap algorithm but the core concept is the same [77–80]. The probabilistic roadmap algorithm samples the free configuration space area $\mathcal{C}_{free}$ as nodes, and connects these nodes to form a roadmap of possible motions.

In the free space $\mathcal{C}_{free}$, a graph is formed from these nodes as $G = (V, E)$. The algorithm will try to connect nodes of the graph with each other with conditions such as distance between nodes, the weight factor, etc. Traditionally, the connection between nodes is a straight line and collision free. Fig. 5.20 shows the concept of probabilistic roadmap algorithm using nodes and graph.

After the graph is formed inside the configuration space $\mathcal{C}$, it can now be used to do the motion planning. The goal is to find the best path inside the graph that connects from the starting point (the robot position) to the

Method	Average travel distance	Position error	Intensity error
Single robot	581.41m	0.06m	0.57%
3 robots with 1m comm.	300.62m	0.05m	0.70%
3 robots with 2m comm.	265.54m	0.06m	0.80%

Table 5.6: Comparison between different in communication range using real world map.

goal point (the estimated intensity location). There are several algorithms which can achieve such a result such as depth-first search, breath first search, bouncing motion, etc. Algorithm 5.1 shows how PRM algorithm constructs the graph.

Algorithm 5.1 Roadmap Construction

```
V ← ∅, E ← ∅
loop
  V ←samples of node c in C_free
  for Each c' ∈ V in order of increasing distance from c do
    if c and c' are not connected then
      if the distance of c and c' is less than Thres then
        if the planner find the path between c and c' then
          E ← (c, c')
        end if
      end if
    end if
  end for
end loop
```

In our case, the algorithm composed of a graph of possible paths, by considering free space, occupied space, and unknown space [81,82]. The nodes are generated semi-randomly in the free space of the map as in Fig. 5.22. Then, random connections are created between nodes. Finally, we can find the an obstacle free path by tracking the length of the edge between point A to point B. The frontier cells are generated on free space of the map. Then, we run the test if there is any frontier which is inaccessible and remove them. We test this environment with 3 robots. Fig. 5.24 shows the map and how those robots navigation inside the map.

5.8.3 Experimentation

In this experiment, we compare the effect of using the different communication range in the real map. We use the particle filters that is proposed in this work as a localization tool. The experiments was performed 60 times in the same environment. Table 5.24 shows the comparison between three cases, single robots, 3 robots with communication range of 1m, and 3 robots with communication range of 2 meters. The result shows that the increment in communication range does affect the overall performance of of the robots. The robots will have more chance to connect with each other if the communication range is bigger, since the communication happens by chance.

5.9 Simulation in a Geometric Environment with Wall Attenuation

Similar to the previous section, in reality, the radiation is blocked by the environment such as concrete, lead, metal, etc. However, some amount of radiation is able to pass through such materials with lower magnitude because the radiation atom will interact with matter. In our case, we consider gammar particles only, since the attenuation of beta and alpha particles is more complicated. The gamma particles that travel through substance will get absorbed. Fig. 5.25 shows the radiation intensity get decreased when pass through matter.

We have I_0 as an initial intensity on the left hand side. The final intensity on the right side I_x is the reduced through the absorber with thickness of x. The geiger counter will measure the radiation that pass through as number of particles/time. As you can see, when the absorber gets thicker, the $I(0)$ will be smaller because the radiation get absorbed more in the absorber. The approximation of the interation between gamma radiation and substance can be written as Eq. 5.10 [83–85]:

$$I(x) = I_0 e^{-\alpha x} \tag{5.10}$$

The amount of radiation that pass through the matter is decreased exponentially with thickness x. The equation is called Lambert's law. It is widely used for linear attenuation. α refers to the linear attenuation coefficient of the material. It is often in the unit of $distance^{-1}$. In general, x is in the centimeter (cm). Thus, the αx is usually unitless.

5.9.1 Environment Settings

We will use this information to calculate the amount of the radiation that can pass through the wall. In our case, we assume that the wall is a concrete wall with a linear attenuation of 0.0833. The wall will have thickness of 5cm. Fig. 5.26 shows the environment that we will use in this experiment. The environment is indoor. The robot cannot go outside the boundary and the robot knows the map as priori. The robot task is to localize a radiation source in the environment by measuring the radiation that passes through wall.

5.9.2 Experimentation

5.9.2.1 Gridmap and PRM Creation

First, the robot generate the occupancy grid map of the environment as in Fig.5.27 to understand the free and occupied area. It is essential step for the robot to do path planning using probabilistic roadmap. The green nodes is the cells that the robot can travel to. Some of the nodes are in the occupied area (black area), thus, those nodes are deleted to prevent the robot for traveling through walls.

The next step is to create the probabilistic roadmap. In this case, we can connect nodes to the nearby nodes. Fig. 5.28 shows the probabilistic roadmap created by the robot. After PRM is created, the robot can use the node to travel within free space of the environment and avoid wall as obstacles.

We create the intensity point at $(4.5, 6)$ which is inside the difficult accessible space. There is only one way to enter the area which is on the top right corner. The robot must be estimate the radiation from outside of the said area and generate the path to the inside of the area. The plot of the radiation map can be found in Fig. 5.29. Notice that the radiation is not distributed equally in all direction since it was distorted by the wall attenuation.

5.9.2.2 Revised Particle Filter Function

The particle filter's estimation and likelihood function must be changed to accomodate the wall attenuation calculation. From inverse square function Eq. 2.2, we add the exponential term to the equation as the linear attenuation factor. The equation becomes:

$$\lambda_k = \frac{Ie^{-\alpha x}}{(x_k - x_0)^2 + (y_k - y_0)^2 + 1} + \lambda_b \tag{5.11}$$

In this case, we use the multiple landmarks calculation as the intensity estimation tool. Eq. 3.11 becomes:

$$\frac{I^i e^{-\alpha x_k}}{d_{k-1}^2} + \lambda_b = z_k \tag{5.12}$$

$$\frac{I^i e^{-\alpha x_{k-1}}}{d_{k-2}^2} + \lambda_b = z_{k-1} \tag{5.13}$$

$$\frac{I^i e^{-\alpha x_{k-n}}}{d_{k-n}^2} + \lambda_b = z_{k-n} \tag{5.14}$$

combining those terms, we have:

$$\frac{I^i e^{-\alpha x_k}}{d_k^2} + \lambda_b + \frac{I^i e^{-\alpha x_{k-1}}}{d_{k-1}^2} + \lambda_b + \cdots + \frac{I^i e^{-\alpha x_{k-n}}}{d_{k-n}^2} + \lambda_b = z_k + z_{k-1} + \cdots + z_{k-n} \tag{5.15}$$

$$\frac{I^i e^{-\alpha x_k}}{d_k^2} + \lambda_b + \frac{I^i e^{-\alpha x_{k-1}}}{d_{k-1}^2} + \lambda_b + \cdots + \frac{I^i e^{-\alpha x_{k-n}}}{d_{k-n}^2} + \lambda_b = \sum_{j=0}^{n} (z_{k-j} - \lambda_b) \tag{5.16}$$

$$I^i \cdot (e^{-\alpha x_k} d_k^{-2} + e^{-\alpha x_{k-1}} d_{k-1}^{-2} + \cdots + e^{-\alpha x_{k-n}} d_{k-n}^{-2}) = \sum_{j=0}^{n} (z_j - \lambda_b) \tag{5.17}$$

$$I^i \cdot \sum_{j=0}^{n} e^{-\alpha x_{k-j}} d_{k-j}^{-2} = \sum_{j=0}^{n} (z_{k-j} - \lambda_b) \tag{5.18}$$

$$I^i = \frac{\sum_{j=0}^{n} (z_{k-j} - \lambda_b)}{\sum_{j=0}^{n} e^{-\alpha x_{k-j}} d_{k-j}^{-2}} \tag{5.19}$$

Since finding the thickness of the wall is a computational expensive due to the ray casting algorithm require a lot fo calculation, we only use up to 5 recent measurement points to calculate the estimated intensity. The rest of the particle filter stay intact.

5.9.2.3 Experiment Process

Fig. 5.30 to Fig. 5.34 shows the process of the algorithm to estimate the radiation source inside the difficult accessible area. In the end, the robot successfully localize the radiation souce inside the area using PRM path

planning to access the area. The error of the position is 0.084m and the error of the intensity is 1.66%.

Figure 5.21: Freiburg indoor building 079 as a test map.

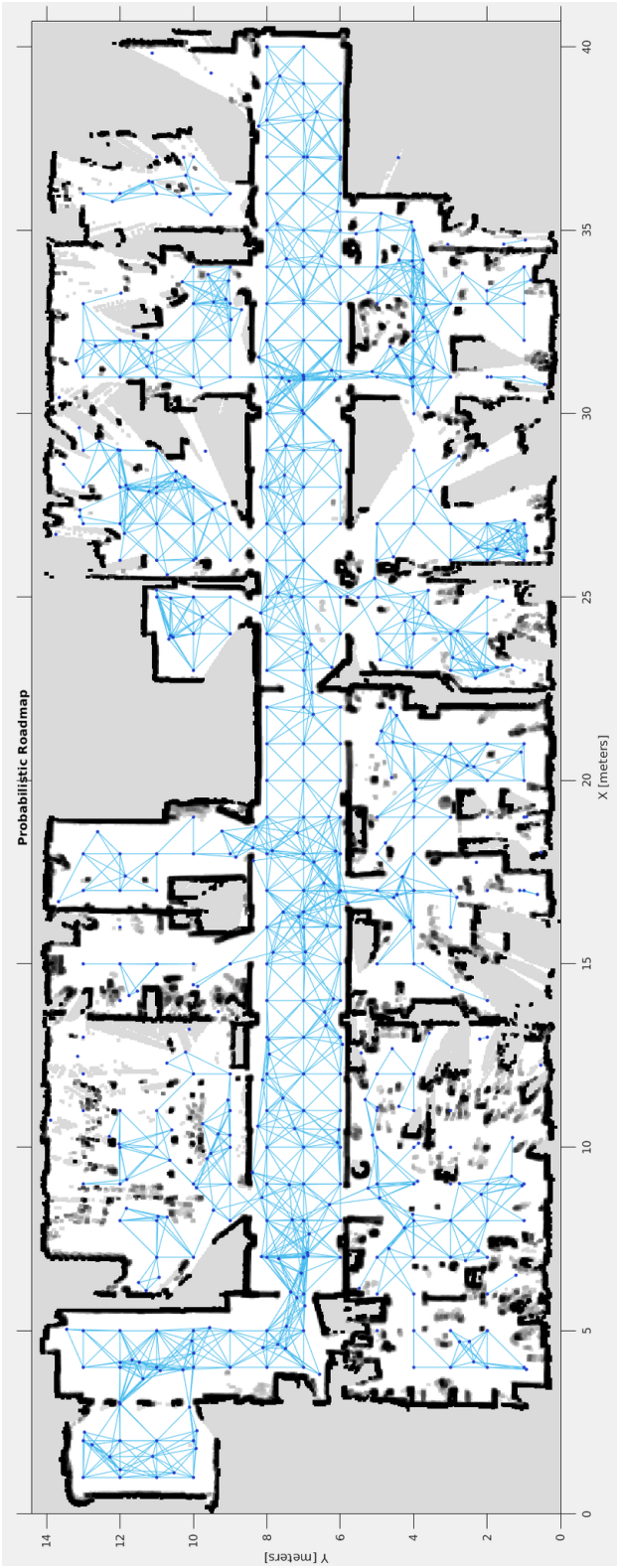

Figure 5.22: Node and edge generation of probabilistic roadmap over the map.

Figure 5.23: Frontier cells are generated on free space by removing those frontier cells which are out of bound.

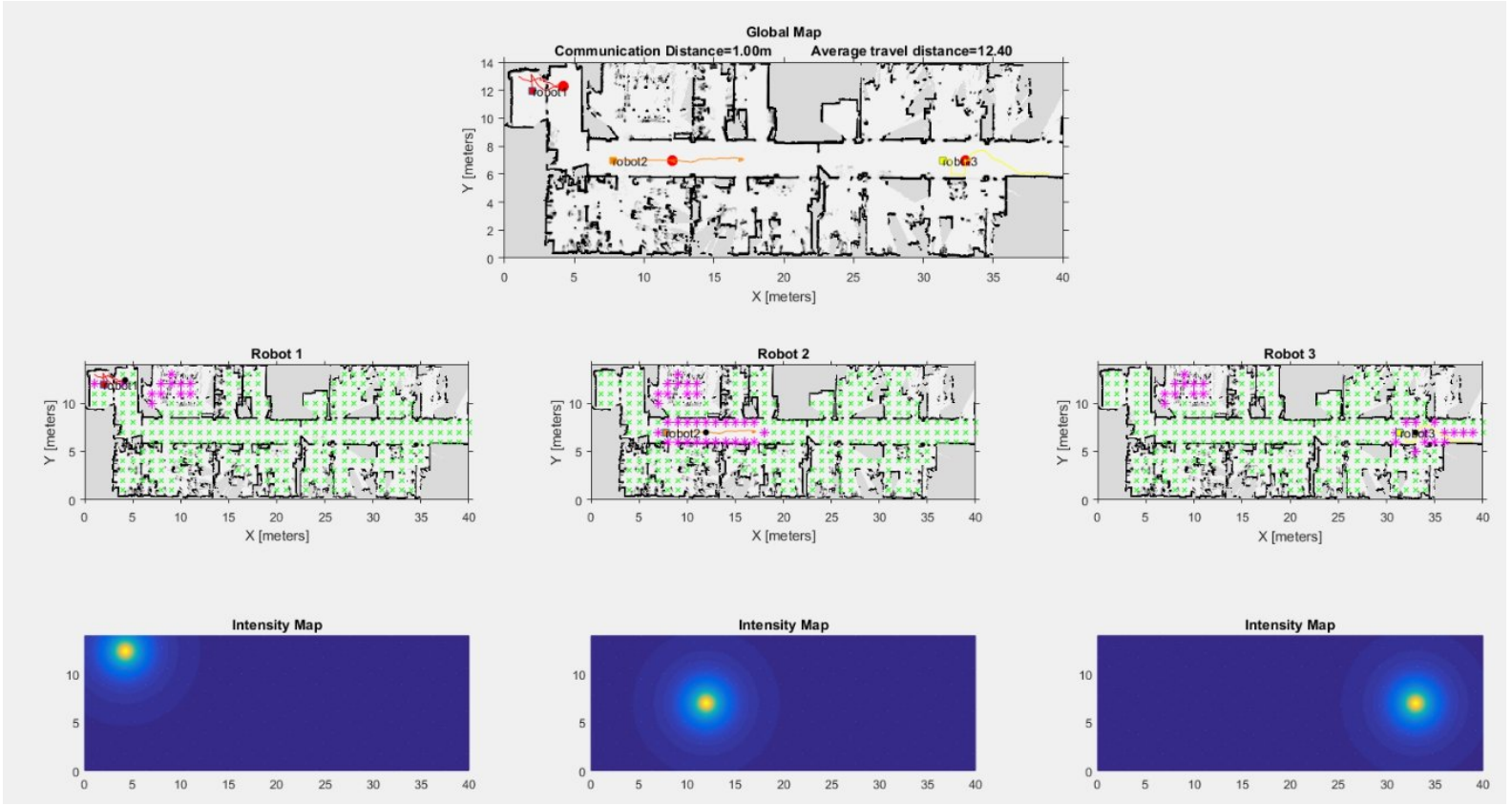

Figure 5.24: Three robots are deployed in the environment. The top figure is the global map of all robots. The middle maps are the visited (white space), unvisited (green dots) and frontier cells (magenta dots). The bottom maps are the estimated intensity map of each robot. When they are within the communication distance, they are able to share the information about the map *e.g.*frontier cells, visited and unvisted cells and radiation point.

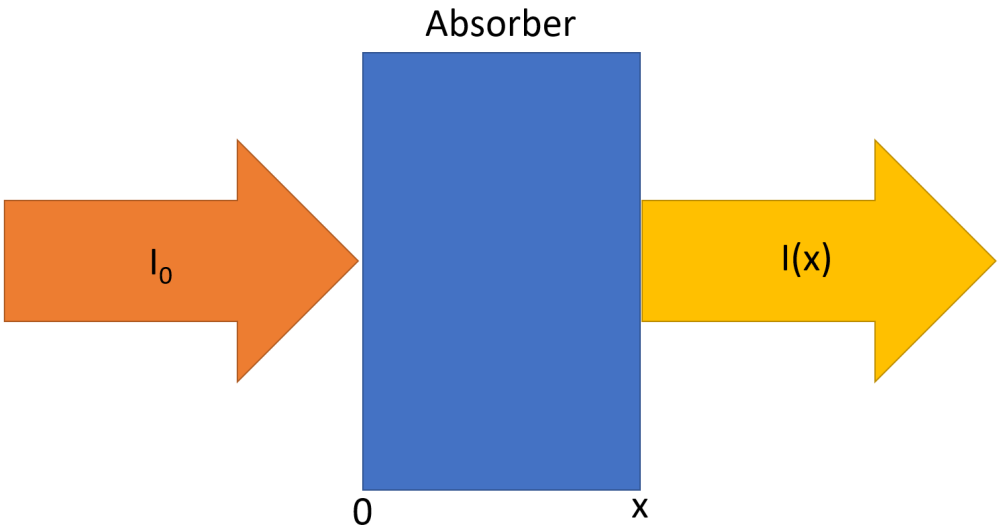

Figure 5.25: Assume that we have the absorber matter that has thickness of x, The initial radiation I_0 on the left hand side will pass through the substance and the reduced intensity $I(x)$ is on the right side as the result.

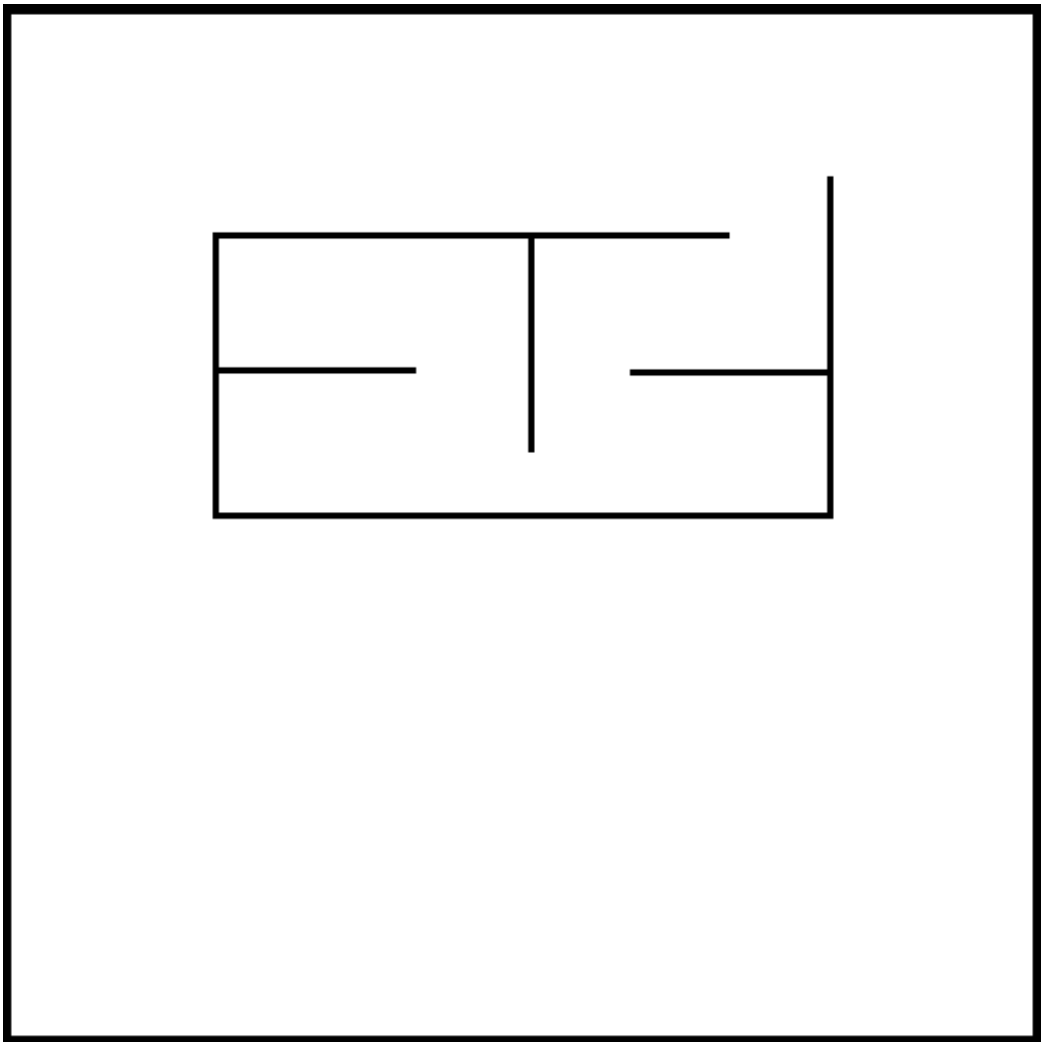

Figure 5.26: The environment is assume to be indoor with defined boundary. The robot can spawn anywhere in the environment, also the radiation point. The robot is forbidded to cross the wall.

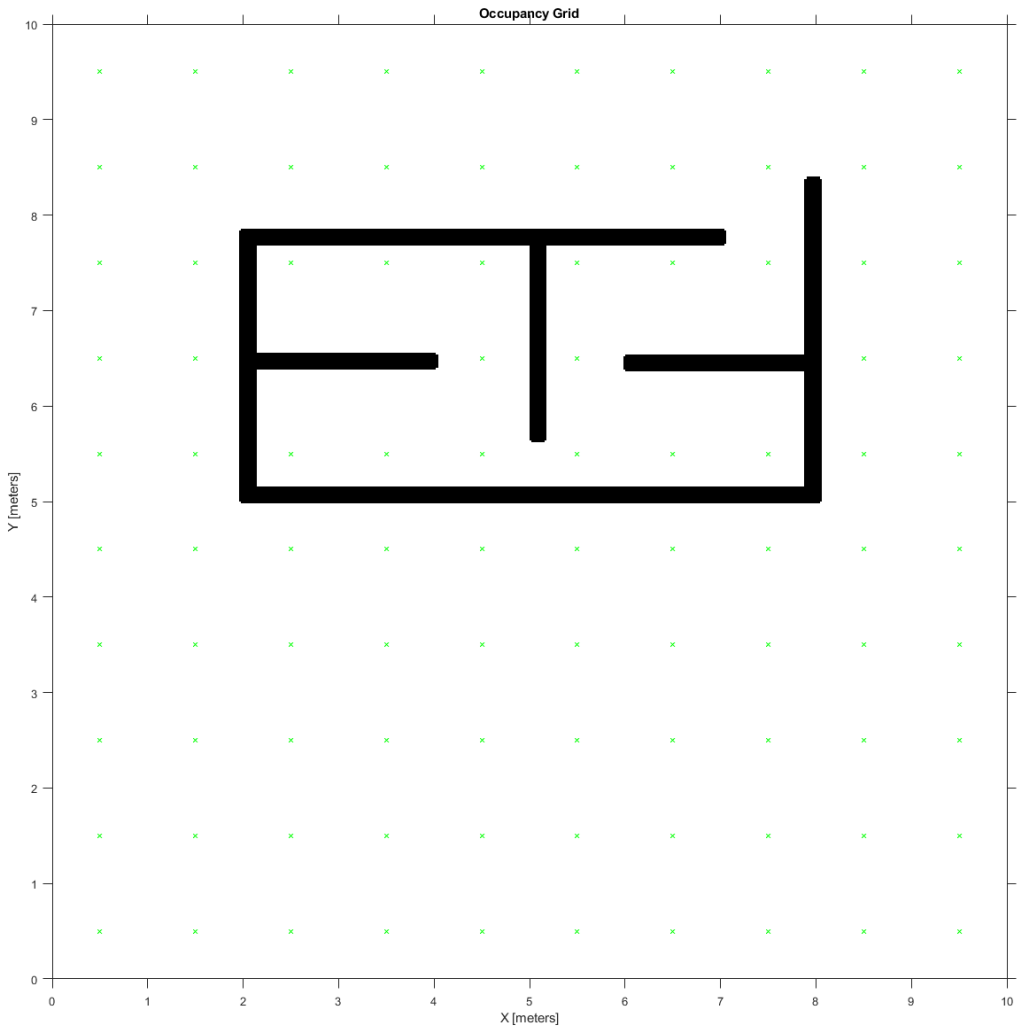

Figure 5.27: The grid map created by the robot in order to understand the free space and occupied area.

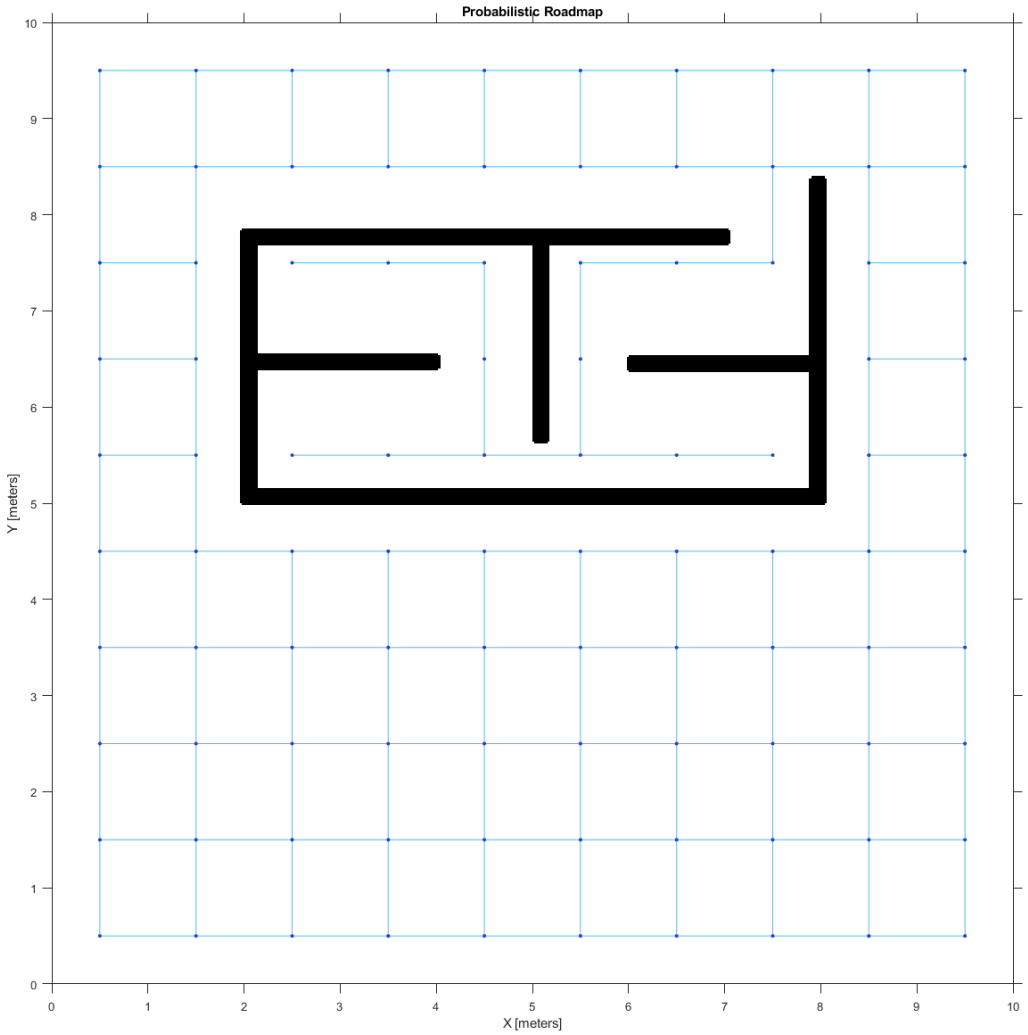

Figure 5.28: Probabilistic roadmap created by a robot as a tool to traverse inside the environment.

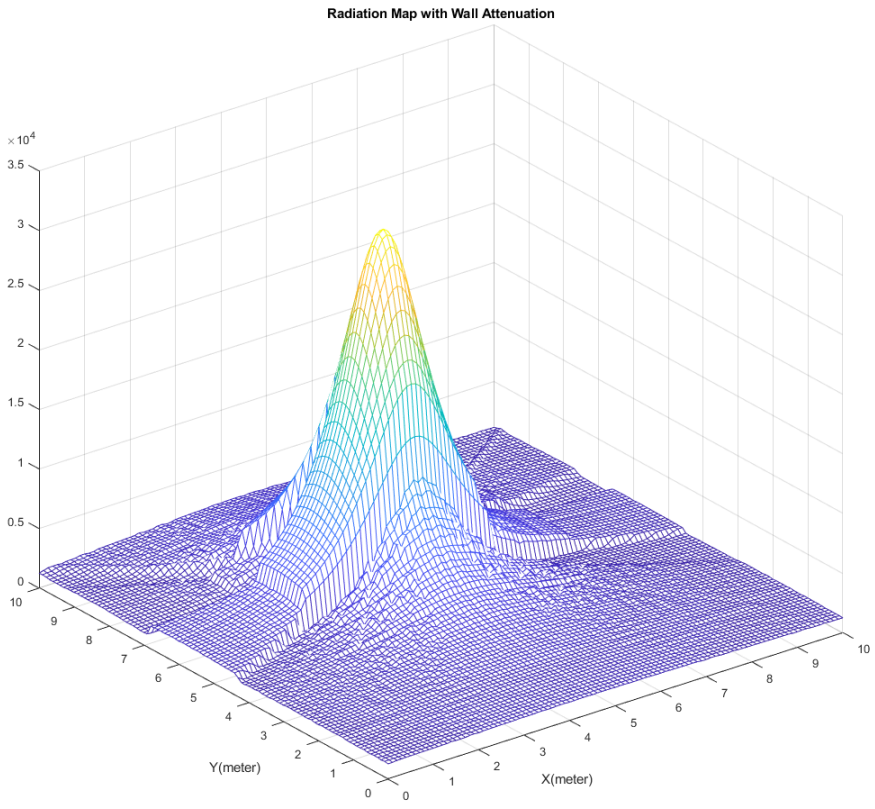

Figure 5.29: The plot of the radiation inside the difficult accessible area $(4.5, 6)$.

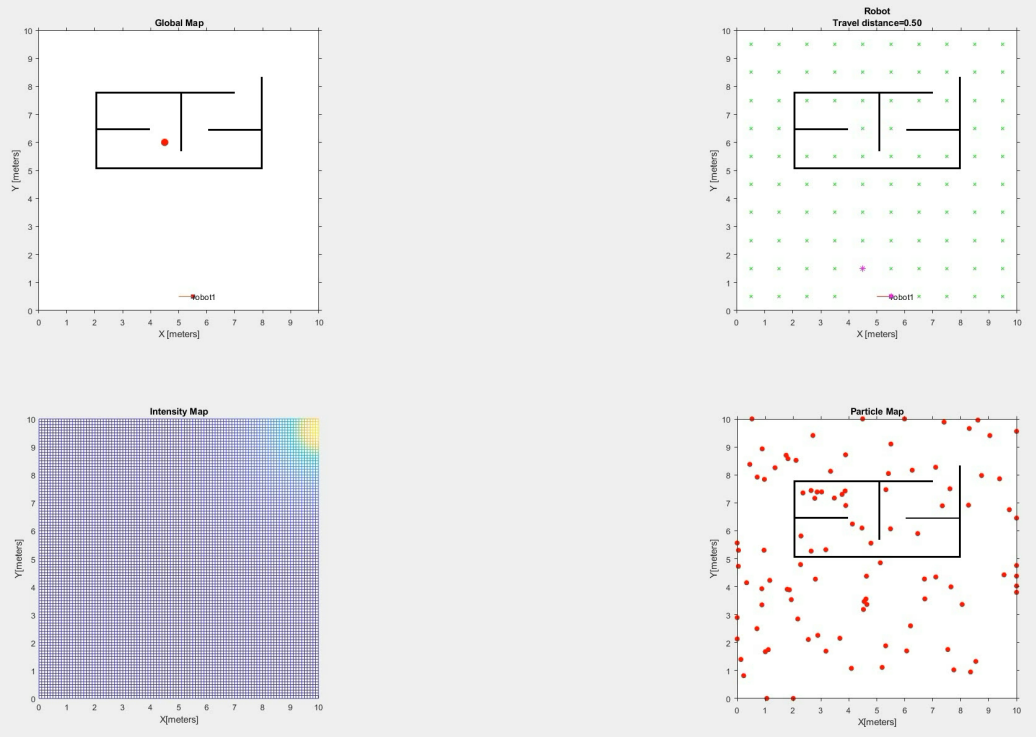

Figure 5.30: The initial step of the experiment. The robot is placed at the middle bottom of the environment so the robot will have the difficulty to reach the radiation source inside the difficult accesible space.

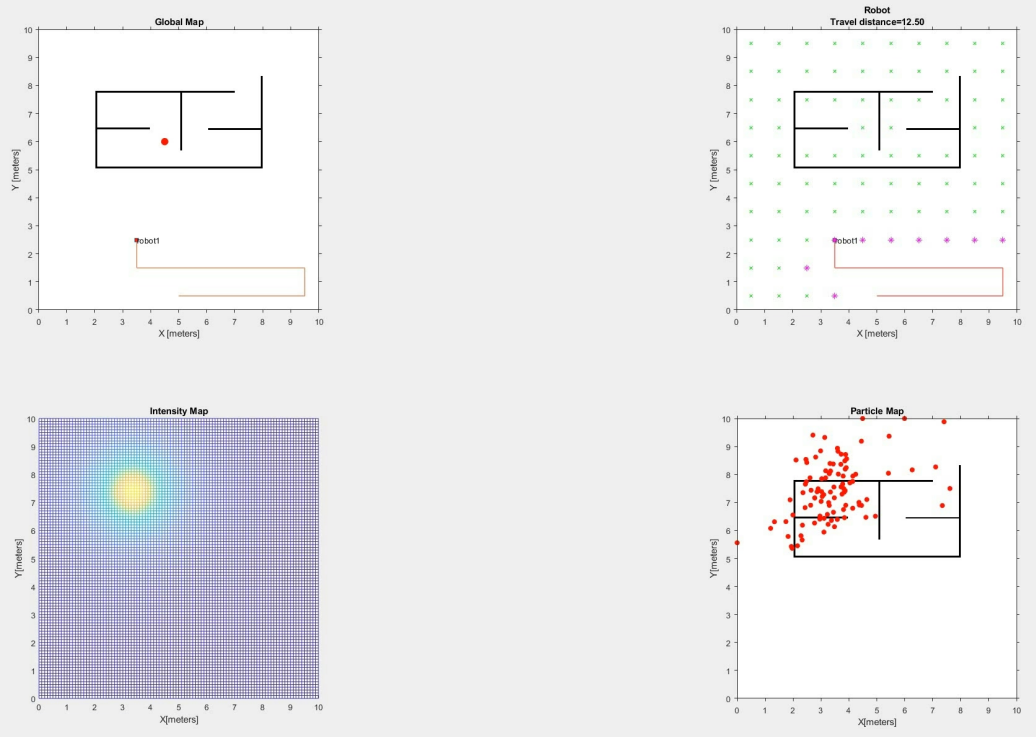

Figure 5.31: The robot will travel in the low intensity area and search for high intensity area.

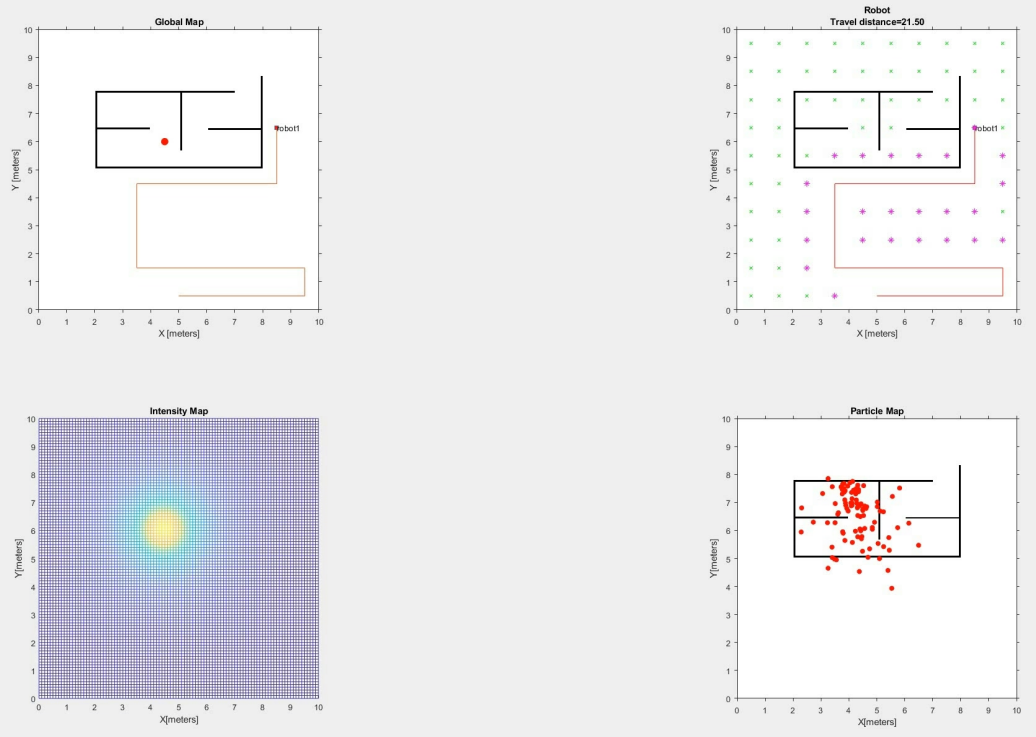

Figure 5.32: When the robot is in the high intensity area, it will generate a path to check the estimated intensity point that estimated by particle filter.

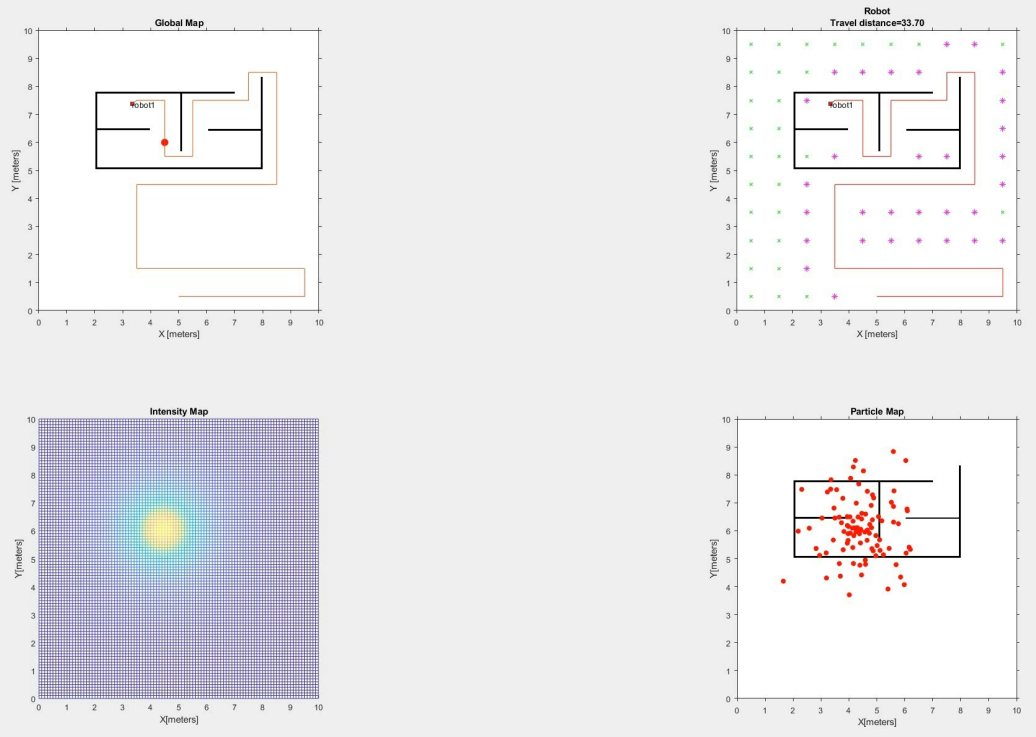

Figure 5.33: After the robot has arrived at the estimated area, it will follow the estimated point and measure the radiation near the estimated point in order to fine tune the estimated location and intensity of the source.

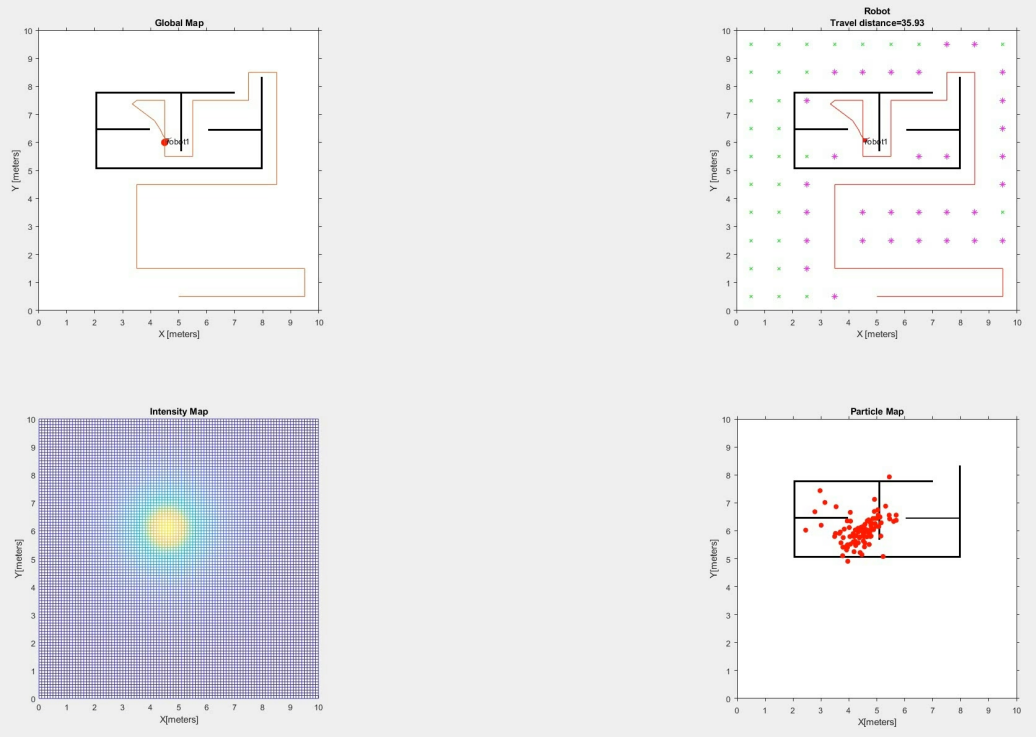

Figure 5.34: The robot will finish the process when the criteria is met. In this case, if there is no improvement in the result for 5 iteration and the robot has visited the estimated location, the algorithm will end.

Chapter 6

Conclusion

In this research, we have developed a search strategy for multiple sources of radioactive material using the robotic systems. The particle filter is employed to deal with the measurement uncertainty of a radioactive measuring instrument. The source separation strategy for mapping the multiple sources of radiation is developed. Frontier-based exploration is employed to help a robot navigate throughout the environment. The search strategy for multiple radiation sources by using the target point selection is utilized to help a robot choose an appropriate position, in order to reduce the exploration cost. The area pruning algorithms are introduced and greatly decrease the exploration time. The simulation is carried out in MATLAB using the radioactive source model in the ideal conditions, in which robot knows its position but no prior knowledge of the source. The indoor self-localization uncertainty was introduced and our algorithm can tolerate with an increase in the error of position and intensity. The proposed sources estimation and exploration algorithms outperform the traditional area coverage method using lawn mowing and spiral patterns, and frontier-based exploration using conventional target selection methods. Furthermore, the proposed method gives 95% sources intensity accuracy after applying sources separation algorithm and less than 0.1m in sources localization estimation error. In addition, both ideal geometric environment and indoor envinronment from the real building have been tested using our proposed algorithm in MATLAB simulation. Moreover, the effect of wall attenuation with the radiation is tested. The robot is successfully localize the radiation even there is some attenuation from the environment with precise accuracy.

Future work of this research may include the real environment testing using mobile robots, such as UAVs or ground robots. The cooperative algorithm between each robot can be included to reduce the redundancy of the exploration. The increment in uncertainty, such as low GPS accuracy, and false or loss in information can be quite a challenge. The mapping of radiation sources with disturbances from natural factors is also an interesting research topic.

References

[1] Wikipedia, "Radiation — Wikipedia, the free encyclopedia," 2015, [Online; accessed 27-July-2015]. [Online]. Available: https://en.wikipedia.org/wiki/Radiation

[2] ——, "Geiger counter — Wikipedia, the free encyclopedia," 2015, [Online; accessed 27-July-2015]. [Online]. Available: https://en.wikipedia.org/wiki/Geiger_counter

[3] A. Gunatilaka, B. Ristic, and R. Gailis, "On localisation of a radiological point source," in *Information, Decision and Control, 2007. IDC '07*, Feb 2007, pp. 236–241.

[4] E. T. Brewer, "Autonomous localization of $1/r^2$ sources using an aerial platform," Master's thesis, Faculty of the Virginia Polytechnic Instutite and State University, December 2009.

[5] W. K. H. Panofsky, "Nuclear proliferation risks, new and old," *Issues in Science and Technology*, vol. 19, 2003.

[6] R. Cortez, X. Papageorgiou, H. Tanner, A. Klimenko, K. Borozdin, and W. Priedhorsk, "Experimental implementation of robotic sequential nuclear search," in *2007 Mediterranean Conference on Control & Automation*. IEEE, 2007, pp. 1–6.

[7] P. Robins and P. Thomas, "Non-linear bayesian cbrn source term estimation," in *Information Fusion, 2005 8th International Conference on*, vol. 2, July 2005, pp. 8 pp.–.

[8] A. Kumar, H. G. Tanner, A. V. Klimenko, K. Borozdin, and W. C. Priedhorsky, "Automated sequential search for weak radiation sources," in *2006 14th Mediterranean Conference on Control and Automation*. IEEE, 2006, pp. 1–6.

[9] S. M. Brennan, A. M. Mielke, and D. C. Torney, "Radioactive source detection by sensor networks," *IEEE Transactions on Nuclear Science*, vol. 52, no. 3, pp. 813–819, 2005.

[10] B. Ristic, M. Morelande, A. Gunatilaka, and M. Rutten, "Search for a radioactive source: Coordinated multiple observers," in *2007 3rd International Conference on Intelligent Sensors, Sensor Networks and Information*. IEEE, 2007, pp. 239–244.

[11] A. Martin, *An introduction to radiation protection 6E*. CRC Press, 2012.

[12] N. Tsoulfanidis, *Measurement and detection of radiation*. CRC press, 2010.

[13] R. J. Nemzek, J. S. Dreicer, D. C. Torney, and T. T. Warnock, "Distributed sensor networks for detection of mobile radioactive sources," *IEEE Transactions on Nuclear Science*, vol. 51, no. 4, pp. 1693–1700, 2004.

[14] A. A. R. Newaz, S. Jeong, H. Lee, H. Ryu, and N. Y. Chong, "Uav-based multiple source localization and contour mapping of radiation fields," *Robotics and Autonomous Systems*, vol. 85, pp. 12 – 25, 2016.

[15] N. Pinkam, A. A. R. Newaz, S. Jeong, and N. Y. Chong, "Rapid coverage of regions of interest for environmental monitoring," *Intelligent Service Robotics*, vol. 12, no. 4, pp. 393–406, Oct 2019.

[16] D. L. Stephens and A. J. Peurrung, "Detection of moving radioactive sources using sensor networks," *IEEE Transactions on Nuclear Science*, vol. 51, no. 5, pp. 2273–2278, 2004.

[17] N. Pinkam, S. Jeong, and N. Y. Chong, "Exploration of a group of mobile robots for multiple radiation sources estimation," in *2016 IEEE International Symposium on Robotics and Intelligent Sensors (IRIS)*, Dec 2016, pp. 199–206.

[18] F. Caballero, L. Merino, I. Maza, and A. Ollero, "A particle filtering method for wireless sensor network localization with an aerial robot beacon," in *2008 IEEE International Conference on Robotics and Automation*. IEEE, 2008, pp. 596–601.

[19] Hyperphysics. (2015, July) Radioactivity. http://hyperphysics.phy-astr.gsu.edu/hbase/nuclear/radact.html.

[20] R. Finck, K. Liden, and R. Persson, "In situ measurements of environmental gamma radiation by the use of a ge (li)-spectrometer," *Nuclear Instruments and Methods*, vol. 135, no. 3, pp. 559–567, 1976.

[21] E. Yee, "Theory for reconstruction of an unknown number of contaminant sources using probabilistic inference," *Boundary-layer meteorology*, vol. 127, no. 3, pp. 359–394, 2008.

[22] P. A. Karam and B. Stein, *Radioactivity*, ser. Science foundations. Chelsea House, 2009. [Online]. Available: https://books.google.co.jp/books?id=AgWtxh7uv84C

[23] J. Towler, B. Krawiec, and K. Kochersberger, "Radiation mapping in post-disaster environments using an autonomous helicopter," *Remote Sensing*, vol. 4, no. 7, p. 1995, 2012.

[24] S. L. Cambell and J. M. G. Duarte, MIT Department of Physics, Oct 2009, Poisson Statistics of Radioactive Decay.

[25] A. Martin and S. A. Harbison, *An introduction to radiation protection; 1st ed.*, ser. Sci. Paperbacks. London: Chapman and Hall, 1972.

[26] A. A. R. Newaz, S. Jeong, and N. Y. Chong, "Online boundary estimation in partially observable environments using a uav," *Journal of Intelligent & Robotic Systems*, vol. 90, no. 3, pp. 505–514, Jun 2018.

[27] A. Gunatilaka, B. Ristic, and R. Gailis, "Radiological source localisation," Master's thesis, Defence Science and Technology Organisation, July 2007.

[28] M. Morelande, B. Ristic, and A. Gunatilaka, "Detection and parameter estimation of multiple radioactive sources," in *2007 10th International Conference on Information Fusion*, July 2007, pp. 1–7.

[29] J. Howse, L. Ticknor, and K. Muske, "Least squares estimation techniques for position tracking of radioactive sources," *Automatica*, vol. 37, pp. 1727–1737, 11 2001.

[30] H.-I. Lin and H. J. Tzeng, "Search strategy of a mobile robot for radiation sources in an unknown environment," in *Advanced Robotics and Intelligent Systems (ARIS), 2014 International Conference on*, June 2014, pp. 56–60.

[31] R. A. Cortez, H. G. Tanner, R. Lumia, and C. T. Abdallah, "Information surfing for radiation map building," *International Journal of Robotics and Automation*, vol. 26, no. 1, p. 4, 2011.

[32] K. Krishnanand, P. Amruth, M. Guruprasad, S. Bidargaddi, and D. Ghose, "Glowworm-inspired robot swarm for simultaneous taxis

towards multiple radiation sources," in *Robotics and Automation, 2006. ICRA 2006. Proceedings 2006 IEEE International Conference on*, May 2006, pp. 958–963.

[33] B. Yamauchi, "Frontier-based exploration using multiple robots," in *Proceedings of the Second International Conference on Autonomous Agents*, ser. AGENTS '98. New York, NY, USA: ACM, 1998, pp. 47–53.

[34] D. Holz, N. Basilico, F. Amigoni, and S. Behnke, "Evaluating the efficiency of frontier-based exploration strategies," *Isr/Robotik 2010*, 2010.

[35] B. Yamauchi, A. Schultz, and W. Adams, "Mobile robot exploration and map-building with continuous localization," in *Proceedings. 1998 IEEE International Conference on Robotics and Automation (Cat. No. 98CH36146)*, vol. 4. IEEE, 1998, pp. 3715–3720.

[36] J.-C. Chin, D. K. Yau, N. S. Rao, Y. Yang, C. Y. Ma, and M. Shankar, "Accurate localization of low-level radioactive source under noise and measurement errors," in *Proceedings of the 6th ACM conference on Embedded network sensor systems*, 2008, pp. 183–196.

[37] S. Särkkä, *Bayesian filtering and smoothing*. Cambridge University Press, 2013, vol. 3.

[38] X. Li, X. Wang, Q. Li, and H. Zhao, "Localization algorithm and error analysis for micro radio-localizer," in *Sixth International Symposium on Instrumentation and Control Technology: Signal Analysis, Measurement Theory, Photo-Electronic Technology, and Artificial Intelligence*, vol. 6357. International Society for Optics and Photonics, 2006, p. 63570W.

[39] J. Reed, "Approaches to multiple-source localization and signal classification," Ph.D. dissertation, Virginia Tech, 2009.

[40] S. F. Gull, "Bayesian inductive inference and maximum entropy," in *Maximum-entropy and Bayesian methods in science and engineering*. Springer, 1988, pp. 53–74.

[41] G. Kitagawa, "Monte carlo filter and smoother for non-gaussian nonlinear state space models," *Journal of computational and graphical statistics*, vol. 5, no. 1, pp. 1–25, 1996.

[42] R. P. Mahler, *Statistical multisource-multitarget information fusion*. Artech House Norwood, MA, 2007, vol. 685.

[43] G. Welch, G. Bishop *et al.*, "An introduction to the kalman filter," 1995.

[44] S. J. Julier and J. K. Uhlmann, "New extension of the kalman filter to nonlinear systems," in *Signal processing, sensor fusion, and target recognition VI*, vol. 3068. International Society for Optics and Photonics, 1997, pp. 182–193.

[45] Y. Huang, Y. Zhang, B. Xu, Z. Wu, and J. A. Chambers, "A new adaptive extended kalman filter for cooperative localization," *IEEE Transactions on Aerospace and Electronic Systems*, vol. 54, no. 1, pp. 353–368, 2017.

[46] T. Moore and D. Stouch, "A generalized extended kalman filter implementation for the robot operating system," in *Intelligent autonomous systems 13*. Springer, 2016, pp. 335–348.

[47] E. A. Wan and R. Van Der Merwe, "The unscented kalman filter for nonlinear estimation," in *Proceedings of the IEEE 2000 Adaptive Systems for Signal Processing, Communications, and Control Symposium (Cat. No. 00EX373)*. Ieee, 2000, pp. 153–158.

[48] S. Thrun, W. Burgard, and D. Fox, *Probabilistic Robotics*, ser. Intelligent robotics and autonomous agents. MIT Press, 2005. [Online]. Available: https://books.google.co.jp/books?id=2Zn6AQAAQBAJ

[49] M. Rubinstein, "Introduction to recursive bayesian filtering," 2018.

[50] T. Guan, L. Fang, W. Dong, Y. Hou, and C. Qiao, "Indoor localization with asymmetric grid-based filters in large areas utilizing smartphones," in *2017 IEEE International Conference on Communications (ICC)*. IEEE, 2017, pp. 1–6.

[51] T. Furukawa, H. F. Durrant-Whyte, and B. Lavis, "The element-based method-theory and its application to bayesian search and tracking," in *2007 IEEE/RSJ International Conference on Intelligent Robots and Systems*. IEEE, 2007, pp. 2807–2812.

[52] J. Skilling, *Maximum Entropy and Bayesian Methods: Cambridge, England, 1988*. Springer Science & Business Media, 2013, vol. 36.

[53] J. Poterjoy, "A localized particle filter for high-dimensional nonlinear systems," *Monthly Weather Review*, vol. 144, no. 1, pp. 59–76, 2016.

[54] Q.-b. Zhang, P. Wang, and Z.-h. Chen, "An improved particle filter for mobile robot localization based on particle swarm optimization," *Expert Systems with Applications*, vol. 135, pp. 181–193, 2019.

[55] A. Beskos, D. Crisan, A. Jasra, K. Kamatani, and Y. Zhou, "A stable particle filter for a class of high-dimensional state-space models," *Advances in Applied Probability*, vol. 49, no. 1, pp. 24–48, 2017.

[56] B. Arulampalam, *Beyond the Kalman Filter: Particle Filters for Tracking Applications*, 2004.

[57] C. Musso, N. Oudjane, and F. LeGland, "Improving regularised particle filters in sequential monte carlo methods in practice, eds: Doucet a., de freitas n., gordon n., statistics for engeering and information science," 2001.

[58] E. Yee, A. Gunatilaka, and B. Ristic, "Comparison of two approaches for detection and estimation of radioactive sources," *ISRN Applied Mathematics*, vol. 2011, 2011.

[59] M. R. Morelande and B. Ristic, "Radiological source detection and localisation using bayesian techniques," *IEEE Transactions on Signal Processing*, vol. 57, no. 11, pp. 4220–4231, 2009.

[60] A. Smith, *Sequential Monte Carlo methods in practice*. Springer Science & Business Media, 2013.

[61] J. D. Hol, T. B. Schon, and F. Gustafsson, "On resampling algorithms for particle filters," in *2006 IEEE nonlinear statistical signal processing workshop*. IEEE, 2006, pp. 79–82.

[62] M. Arulampalam, S. Maskell, N. Gordon, and T. Clapp, "A tutorial on particle filters for online nonlinear/non-gaussian bayesian tracking," *Signal Processing, IEEE Transactions on*, vol. 50, no. 2, pp. 174–188, Feb 2002.

[63] N. M. Kwok, G. Fang, and W. Zhou, "Evolutionary particle filter: re-sampling from the genetic algorithm perspective," in *2005 IEEE/RSJ International Conference on Intelligent Robots and Systems*, Aug 2005, pp. 2935–2940.

[64] M. Bolic, P. M. Djuric, and S. Hong, "Resampling algorithms and architectures for distributed particle filters," *IEEE Transactions on Signal Processing*, vol. 53, no. 7, pp. 2442–2450, 2005.

[65] T. Edlinger and E. von Puttkamer, "Exploration of an indoor-environment by an autonomous mobile robot," in *Proceedings of IEEE/RSJ International Conference on Intelligent Robots and Systems (IROS'94)*, vol. 2. IEEE, 1994, pp. 1278–1284.

[66] B. Yamauchi, A. Schultz, and W. Adams, "Integrating exploration and localization for mobile robots," *Adaptive Behavior*, vol. 7, no. 2, pp. 217–229, 1999.

[67] B. Yamauchi, "A frontier-based approach for autonomous exploration," in *Proceedings 1997 IEEE International Symposium on Computational Intelligence in Robotics and Automation CIRA'97.'Towards New Computational Principles for Robotics and Automation'.* IEEE, 1997, pp. 146–151.

[68] Y. Wang, A. Liang, and H. Guan, "Frontier-based multi-robot map exploration using particle swarm optimization," in *2011 IEEE symposium on Swarm intelligence.* IEEE, 2011, pp. 1–6.

[69] N. Mahdoui, V. Frémont, and E. Natalizio, "Cooperative frontier-based exploration strategy for multi-robot system," in *2018 13th Annual Conference on System of Systems Engineering (SoSE).* IEEE, 2018, pp. 203–210.

[70] W. Burgard, M. Moors, C. Stachniss, and F. E. Schneider, "Coordinated multi-robot exploration," *IEEE Transactions on Robotics*, vol. 21, no. 3, pp. 376–386, June 2005.

[71] A. Rényi, "On measures of entropy and information," in *Proceedings of the Fourth Berkeley Symposium on Mathematical Statistics and Probability, Volume 1: Contributions to the Theory of Statistics.* Berkeley, Calif.: University of California Press, 1961, pp. 547–561. [Online]. Available: https://projecteuclid.org/euclid.bsmsp/1200512181

[72] C. E. Shannon, "A mathematical theory of communication," *The Bell System Technical Journal*, vol. 27, no. 3, pp. 379–423, July 1948.

[73] C. Stachniss, G. Grisetti, and W. Burgard, "Information gain-based exploration using rao-blackwellized particle filters." in *Robotics: Science and Systems*, vol. 2, 2005, pp. 65–72.

[74] J. Taylor, "The cramer-rao estimation error lower bound computation for deterministic nonlinear systems," *IEEE Transactions on Automatic Control*, vol. 24, no. 2, pp. 343–344, 1979.

[75] Y. Chen, J. Tang, C. Jiang, L. Zhu, M. Lehtomäki, H. Kaartinen, R. Kaijaluoto, Y. Wang, J. Hyyppä, H. Hyyppä *et al.*, "The accuracy comparison of three simultaneous localization and mapping (slam)-based indoor mapping technologies," *Sensors*, vol. 18, no. 10, p. 3228, 2018.

[76] Y. Toda and N. Kubota, "Simultaneous localization and mapping based on (μ+1)-evolution strategy for mobile robots," in *Intelligent Robotics and Applications*, H. Liu, N. Kubota, X. Zhu, R. Dillmann, and D. Zhou, Eds. Cham: Springer International Publishing, 2015, pp. 62–69.

[77] L. E. Kavraki, M. N. Kolountzakis, and J.-C. Latombe, "Analysis of probabilistic roadmaps for path planning," *IEEE Transactions on Robotics and Automation*, vol. 14, no. 1, pp. 166–171, 1998.

[78] T. Siméon, J.-P. Laumond, J. Cortés, and A. Sahbani, "Manipulation planning with probabilistic roadmaps," *The International Journal of Robotics Research*, vol. 23, no. 7-8, pp. 729–746, 2004.

[79] S. M. LaValle, M. S. Branicky, and S. R. Lindemann, "On the relationship between classical grid search and probabilistic roadmaps," *The International Journal of Robotics Research*, vol. 23, no. 7-8, pp. 673–692, 2004.

[80] P. Svestka and M. H. Overmars, "Coordinated motion planning for multiple car-like robots using probabilistic roadmaps," in *Proceedings of 1995 IEEE International Conference on Robotics and Automation*, vol. 2. IEEE, 1995, pp. 1631–1636.

[81] L. E. Kavraki, P. Svestka, J. . Latombe, and M. H. Overmars, "Probabilistic roadmaps for path planning in high-dimensional configuration spaces," *IEEE Transactions on Robotics and Automation*, vol. 12, no. 4, pp. 566–580, Aug 1996.

[82] M. U. Farooq, Z. Ziyang, and M. Ejaz, "Quadrotor uavs flying formation reconfiguration with collision avoidance using probabilistic roadmap algorithm," in *2017 International Conference on Computer Systems, Electronics and Control (ICCSEC)*, Dec 2017, pp. 866–870.

[83] S. J. Stanković, R. Ilic, K. S. Janković, D. Bojovic, and B. B. Lončar, "Gamma radiation absorption characteristics of concrete with components of different type materials," *Acta Physica Polonica. Series A: General Physics, Physics of Condensed Matter, Optics and Quantum Electronics, Atomic and Molecular Physics, Applied Physics*, vol. 117, no. 5, pp. 812–816, 2010.

[84] A. El-Khayatt, "Radiation shielding of concretes containing different lime/silica ratios," *Annals of Nuclear Energy*, vol. 37, no. 7, pp. 991–995, 2010.

[85] D. R. Ochbelagh, S. Azimkhani, and H. G. Mosavinejad, "Effect of gamma and lead as an additive material on the resistance and strength of concrete," *Nuclear engineering and design*, vol. 241, no. 6, pp. 2359–2363, 2011.

Publications

Journal

[1] Pinkam, N., Newaz, A. A. R., Jeong, S., and Chong, N. Y. (2019). Rapid coverage of regions of interest for environmental monitoring. *Intelligent Service Robotics*, 12(4), 393-406.

Conference Paper

[2] N. Pinkam, A. Elibol and N. Y. Chong, "Informative mobile robot exploration for radiation source localization with a particle filter," 2020 *The 4th IEEE International Conference on Robotic Computing*, Taichung [Paper Accepted].

[3] N. Pinkam, S. Jeong and N. Y. Chong, "Exploration of a group of mobile robots for multiple radiation sources estimation," *I2016 IEEE International Symposium on Robotics and Intelligent Sensors (IRIS)*, Tokyo, 2016, pp. 199-206.

[4] Pinkam, N., Newaz, A. A. R., Jeong, S., and Chong, N. Y. , "Rapid coverage of regions of interest for environmental monitoring," *The 5th International Conference on Robot Intelligence Technology and Applications (RITA)*, Daejeon, 2017, pp. 195-209.

[5] N. Pinkam, F. Bonnet and N. Y. Chong, "Robot collaboration in warehouse," 2016 *16th International Conference on Control, Automation and Systems (ICCAS)*, Gyeongju, 2016, pp. 269-272.